Mechanisms of Microwave Induced Damage in Biologic Materials

Annual Report

January 1988

by

Vitreous State Laboratory

The Catholic University of America

Washington, D.C. 20064

2

Mechanisms of Microwave Induced Damage in Biologic Materials

Annual Report

January 1988

by

M. Mullins, M. Penafiel, R. Mohr, C. Montrose,

T. Litovitz and C. Grosse

Supported by

U. S. Army Medical Research and Development Command
Fort Detrick, Frederick, Maryland 21701-5012

Contract No. DAMD17-86-C-6260

Vitreous State Laboratory
Catholic University of America
620 Michigan Ave., N.E.
Washington, D.C. 20064

SECURITY CLASSIFICATION OF THIS PAGE

REPORT DOCUMENTATION PAGE

Form Approved
OMB No. 0704-0188

1a. REPORT SECURITY CLASSIFICATION Unclassified	1b. RESTRICTIVE MARKINGS
2a. SECURITY CLASSIFICATION AUTHORITY	3. DISTRIBUTION/AVAILABILITY OF REPORT Approved for public release; Distribution unlimited
2b. DECLASSIFICATION/DOWNGRADING SCHEDULE	
4. PERFORMING ORGANIZATION REPORT NUMBER(S)	5. MONITORING ORGANIZATION REPORT NUMBER(S)
6a. NAME OF PERFORMING ORGANIZATION Vitreous State Lab Catholic University of America 6b. OFFICE SYMBOL (If applicable)	7a. NAME OF MONITORING ORGANIZATION
6c. ADDRESS (City, State, and ZIP Code) 620 Michigan Ave., N.E. Washington D.C. 20064	7b. ADDRESS (City, State, and ZIP Code)
8a. NAME OF FUNDING/SPONSORING ORGANIZATION U.S. Army Medical Research and Development Command 8b. OFFICE SYMBOL (If applicable)	9. PROCUREMENT INSTRUMENT IDENTIFICATION NUMBER DAMD17-86-C-6260
8c. ADDRESS (City, State, and ZIP Code) Fort Detrick Frederick, Maryland 21701-5012	10. SOURCE OF FUNDING NUMBERS PROGRAM ELEMENT NO. 62777A; PROJECT NO. 3E1-6277A878; TASK NO. BB; WORK UNIT ACCESSION NO. 021

11. TITLE (Include Security Classification)

Mechanisms of Microwave Induced Damage in Biologic Materials

12. PERSONAL AUTHOR(S)

M.Mullins, M.Penafiel, R.Mohr, C.Montrose, T.Litovitz, and C.Grosse

13a. TYPE OF REPORT	13b. TIME COVERED	14. DATE OF REPORT (Year, Month, Day)	15. PAGE COUNT
Annual	FROM 09/22/86 TO 09/21/87	January 25, 1988	60

16. SUPPLEMENTARY NOTATION

17. COSATI CODES			18. SUBJECT TERMS (Continue on reverse if necessary and identify by block number)
FIELD	GROUP	SUB-GROUP	
06	03		Microwaves; Biological Damage; DNA; Absorption, RA 3
06	01		

19. ABSTRACT (Continue on reverse if necessary and identify by block number)

An interdisciplinary team of biologists, physicists, and electrical engineers was created to tackle the problem of microwave damage to biological systems. This report describes work in five purposely overlapping areas: (1) design and construction of microwave exposure chambers; (2) investigation of the effects of microwave irradiation on the metabolic activity of several cell lines and an interferon system; (3) investigation of the mechanisms of microwave absorption in DNA solutions; (4) Theoretical studies of the inhomogeneous deposition of microwave energy in the region of DNA and cells in suspension; and (5) molecular dynamic (MD) computer simulation of electric field effects on long chain (DNA-like) molecules.

20. DISTRIBUTION/AVAILABILITY OF ABSTRACT ☐ UNCLASSIFIED/UNLIMITED ☐ SAME AS RPT. ☐ DTIC USERS	21. ABSTRACT SECURITY CLASSIFICATION Unclassified
22a. NAME OF RESPONSIBLE INDIVIDUAL Mary Frances Bostian	22b. TELEPHONE (Include Area Code) 301-663-7325 22c. OFFICE SYMBOL SGRD-RMI-S

SECURITY CLASSIFICATION OF THIS PAGE

ABSTRACT

Microwave radiation is one of the most thoroughly studied of environmental hazards, yet fundamental questions are still being raised concerning the existence of hazards associated with low levels of microwave exposure. It is the purpose of this project to attempt to contribute to a definitive understanding of the mechanisms by which microwaves can interact athermally with biological systems and modify metabolic function.

An interdisciplinary team of biologists, physicists, and electrical engineers was created to tackle this problem. This report describes work in five purposely overlapping areas: (1) design and construction of microwave exposure chambers; (2) investigation of the effects of microwave irradiation on the metabolic activity of several cell lines and an interferon system; (3) investigation of the mechanisms of microwave absorption in DNA solutions; (4) Theoretical studies of the inhomogeneous deposition of microwave energy in the region of DNA and cells in suspension; and (5) molecular dynamic (MD) computer simulation of electric field effects on long chain (DNA-like) molecules.

The microwave exposure system we have used was designed to operate in the 2-4 GHz range using coaxial and rectangular waveguide components. Temperature control was implemented by a circulating lossless fluid. SAR measurements within the sample tube indicated some variations with position (≈25%).

Experiments were conducted to assess the effects of microwave exposure on mammalian cultured cells. Three cell lines were chosen for use. The murine fibroblast line L-929 was selected as a vigorously growing, aneuploid cell type. Diploid human cells, displaying slower growth rates and density dependent inhibition of growth were also used. Cells were removed from monolayer culture and placed into suspension for the time of irradiation. Temperature was controlled during microwave exposure. Irradiation was with 2.45 GHz continuous wave or 1.25 GHz pulsed microwaves at SARs ranging from 6mW/g to approximately 1700 mW/g. Exposure times ranged from 0.5 to 6 hr. Following microwave exposure control and experimental cultures were aliquoted for three assays: (1) for general viability immediately post-irradiation, (2) for plating efficiencies, and (3) proliferation rates. In no instance was there a consistent, discernable difference in any of these parameters that correlated with exposure to microwave irradiations. Irradiation of cells in suspension will continue during the second contract year, but will employ suspension adapted L cells that will proliferate in suspension.

An interferon system was chosen to investigate possible effects of microwave irradiation on transcription of specific gene sequences. Activities of the enzyme 2',5', oligoadenylate (2-5A) synthetase and the 2-5A dependent RNase, and RNase L, were

studied after microwave exposure. Very preliminary data indicate unchanged levels of (2-5A) Synthetase but a two fold increase in RNase L activity was observed. We plan to verify these preliminary results with additional experiments including exposure to viruses to activate the interferon system.

The major goal of the physics group in this project was to examine the interaction of microwave radiation with DNA molecules. The initial effort was directed toward verifying (if possible) the reported resonant absorption in plasmid DNA for microwaves in the 2 to 9 GHz region. We measured the microwave absorption in several DNA solutions and were unable to detect any DNA related resonances. We found that experimental artifacts contribute to what appear to be absorption resonances but are in fact due to spurious reflections in the measurement system. We did find that DNA solutions exhibit an excess absorption relative to water or to the buffered saline solvent alone. The magnitude of that absorption is much larger than for water when the DNA concentrations in the solutions are considered. The nature of the excess or enhanced absorption has not been fully characterized, but could be related to some relaxation process involving the DNA molecules and their associated counter ions in the solution. In addition to the DNA absorption measurements, we conducted investigations in two areas suggested by the DNA absorption work. In the first we irradiated several DNA samples with high power microwaves at 1.25 and 9.37 GHz to determine if any gross direct damage to the DNA could be observed due to the excess absorption. No measurable damage to the DNA samples was observed. In the second we examined the problem of DNA damage resulting from exposure to copper microwave probes. We found that copper dissolution was enhanced by the presence of microwaves and that copper dissolution involves the formation of hydrogen peroxide which is a biotoxin.

Data in the published literature have indicated that microwave absorption of solutions of E. coli DNA and DNase 1 was enhanced when the DNA was shortened by enzyme activity. The interpretation of these results was based on the assumption that DNA molecules could exhibit resonant type absorption whose amplitude and characteristic frequency depended upon chain length. This resonance based argument has been considerably weakened by our work described above and other published work which have not been able to find any resonance associated with DNA microwave absorption. An important problem does remain unsolved. What is the origin of the enhanced absorption in the E. coli experiment? An oft used explanation is that bound water causes this effect. We consider this explanation below and show that it is inconsistent with the reported data.

Other reports in the literature have attempted to explain the absorption of DNA solutions as being due to the additional ion brought into the electrolyte buffer by the DNA. Such an interpretation implies that the absorption is only a function of the total number of ions in solution, and does not depend upon how they interact with the biologic species. Because our prelim-

inary data described above does not agree with this hypothesis we have investigated this theoretically in our considerations below. Our results indicate a very important effect of the interaction of the ions with the DNA and suggest that the absorption per unit volume can be over 1000 times greater in the region of the DNA molecule than in the bulk buffer solution.

There is a question as to whether there exists any direct, i.e., non-thermal, absorption of microwave energy by biological macromolecule such as DNA. We have hypothesized that such absorption can occur by the non-resonant excitation of internal modes of motion of the molecules through interaction with the field induced motion of counter ions in the immediate neighborhood of the molecule. Making use of Molecular Dynamics (MD) computer simulation "experiments" we have attempted to test this hypothesis and thereby gain some insight into the nature of the response of a polymer electrolyte solution subjected to an external electric field.

To attempt to simulate the behavior of an ionic solution containing biological molecules is certainly beyond the scope of this work; however, testing the essence of the above hypothesis does not demand such a detailed mimicking of the situation. Rather by examining the behavior of the vibrational modes of an electrically charged short-chain polymer in an ionic solution following the sudden application of an electric field, it should be possible to establish whether these modes can be excited by coupling to the ionic atmosphere around the molecule. To ensure that any observed excitation of the molecular vibrations is not due simply to the modes re-equilibrating at a new higher temperature caused by heating the solvent with the ionic current, quasi-isothermal conditions are maintained by continually scaling the solvent atom velocities to maintain a constant total kinetic energy.

To date the results have not been conclusive. What has been established is that there is a coupling of energy between the field-driven motion in the ionic environment and the intramolecular vibrations. However it appears that under certain conditions the effect of the external field is to modify the ionic neighborhood of the polymer molecule such that the internal vibrational energy is actually decreased; under different conditions, the internal vibrations are enhanced.

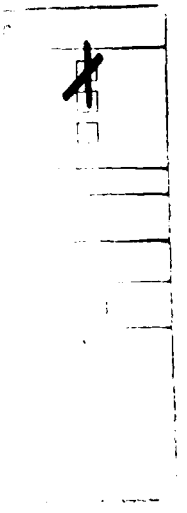

A-1

FOREWARD

Citations of commercial organizations and trade names in this report do not constitute an official Department of the Army endorsement or approval of the products or services of these organizations.

TABLE OF CONTENTS

CHAPTER FOUR
THEORY OF ENHANCED ABSORPTION OF DNA SOLUTIONS

CHAPTER FIVE
MOLECULAR DYNAMICS: RESPONSE OF A POLYMER ELECTROLYTE SOLUTION TO IMPRESSED ELECTRIC FIELDS

CHAPTER 1

DESIGN AND EVALUATION OF MICROWAVE IRRADIATION SYSTEMS

R. Meister and M. Penafiel

1.1 Summary

A wide range of microwave irradiation equipment has been used to study the effects of microwave radiation on animal tissues and animal cultured cells. Irradiation chambers for exposure of cultured cells have been generally selected according to the nature of the sample, that is, whether the cells were exposed in suspension or as monolayer cultures, the sample size, and the need for special provisions for control of critical experimental parameters such as temperature and pH. In many instances, anechoic chambers have been used for the exposure of large samples, however, for smaller samples, waveguide systems have been used which provide efficient energy coupling and good energy confinement for safe operation.

The system herein described was designed to operate in the 2-4 GHz range using coaxial and rectangular waveguide components for exposure with CW microwaves. The irradiation chamber called the applicator was constructed from a twelve inch section of WR284, S-band rectangular waveguide modified to accept a 1 cm OD, 2 ml sample tube. Temperature control was implemented by circulating a fluid of low dielectric constant and essentialy lossless through an enclosure included as part of the applicator which surrounds the sample tube within the waveguide. The sample tube was inserted vertically into the applicator.

SAR measurements within the sample tube filled with a cell suspension sample indicated some variations with position. Two configurations were used to measure the SAR, one using an appropriately modified waveguide, and the other using the applicator with thermal insulation for the sample provided in both cases. The SAR at the front of the sample, that is the side first exposed to the microwave radiation was in both cases considerably larger than that in other positions within the sample. Since results of measurements in the applicator are more representative of the irradiation conditions these were used to specify SAR as a function of the net power delivered to the sample. The following relation for the SAR was obtained SAR = $(0.61\ P_{net}) \pm 25\%$.

The adequacy of temperature control was tested by making temperature profile measurements at nominal SAR's of 10, 100, and 1000 mW/g for two nominal temperatures, 37°C and 43°C. Results of these measurements indicated good (±0.5°C) temperature uniformity at the two low SAR values, however, at the high SAR a large gradient from top to bottom of the sample was observed.

The system described was used for irradiation of both cells in suspension and monolayer cultures with CW microwaves primarily at 2.45 GHz. Aditionally, a facility at WRAIR was used for irradiation of cell suspensions with pulsed microwaves at 1.25 GHz. Temperature control for this arrangement was provided in a similar fashion as that described above. This facility and another one (X-band) also available at WRAIR were also used for irradiation of DNA solutions with pulsed microwaves.

Irradiations of yeast cell suspensions with CW microwaves at 2.45 GHz were carried out to investigate the possibility of microwave induced genetic damage. Results from this study indicate no effect on genetic variability with exposure to microwaves at SAR's of the order of 100 mW/g.

Microwave induced changes in copper leaching in deionized water were studied with CW (2.45 GHz) and pulsed (1.25 GHz) microwaves. Various sample configurations were used. Some results were inconclusive, others demonstrate that the effect is solely thermal, however, in these situations, the electric field at the surface of the sample was zero, and therefore, these results do not negate the possibility of non thermal effects under conditions where the sample surface is for instance perpendicular to the electric field.

1.2 Microwave Irradiation System for Biological Cells in Aqueous Media.

1.2.1 System Description

The cell irradiation system used during this reporting period was designed to operate in the 2-4 GHz range using coaxial and rectangular waveguide components. A block diagram of the system is shown in Fig 1.1. Power from the Sweep Oscillator to the TWTA is adjusted with the aid of a coaxial attenuator to limit the output power from the TWTA to about 10 Watts. The isolator prevents possible damage to the TWTA due to reflections from mismatched loads. The Low Pass Filter is included to eliminate high frequency components from the output signal of the TWTA. Power delivered to the sample is adjusted using a variable Coaxial Attenuator. The incident power is measured at the output of the 20 dB Waveguide Coupler terminated in a Waveguide to Coax adapter followed by a sensor and Power Meter. Additionally, a 10 dB Coaxial Attenuator is included at power levels greater than 1 Watt. The output from the applicator is measured in a similar fashion. The term 'applicator' refers to the section of waveguide where the sample is loaded for irradiation. The applicator loaded with the sample tube containing the sample, consisting of an aqueous cell suspension, represents a substantial impedance mismatch in the line. A Slide Screw Tuner is used to match to the load impedance by appropriately adjusting the position and depth of the probe. The match condition is determined through VSWR measurements made using the Slotted Line and the Standing Wave Indicator shown in the system diagram.

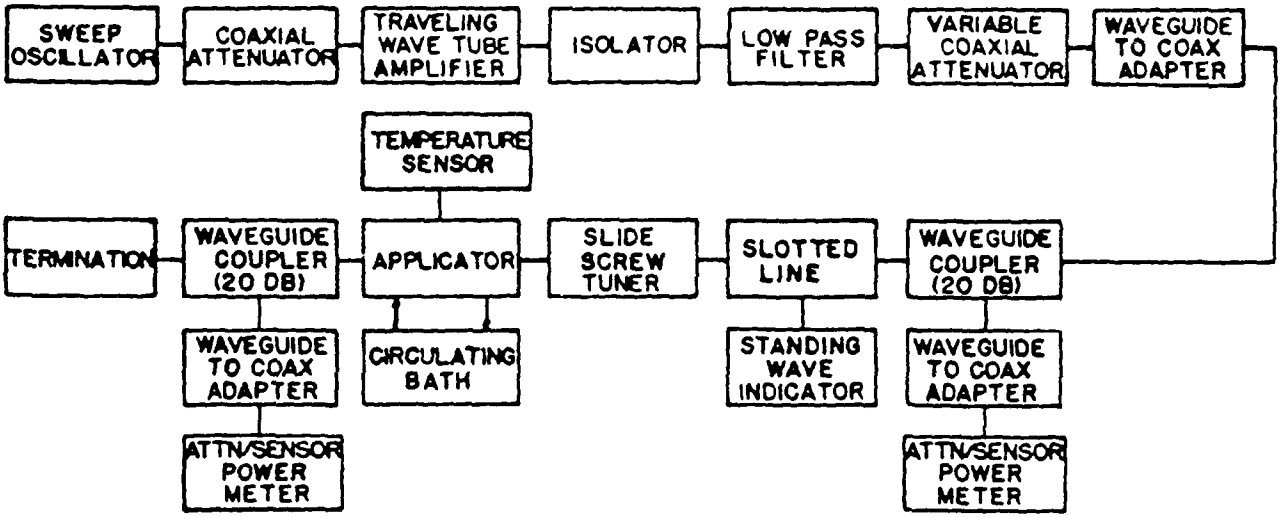

Fig 1.1: System block diagram.
Power propagating beyond the applicator is absorbed at the Waveguide Termination. Probing of the electric field within the loaded sample tube gave an estimate of the field uniformity. SAR and temperature profile measurements were carried out to attempt to study the field distribution within the sample. No theoretical calculations of the electric field distribution have been made.

1.2.2 Applicator Design

While an important consideration in the design of the applicator was to achieve field uniformity within the sample, it was also neccesary to take other factors into account such as size and shape of the sample container dictated by experimental and bioassay requirements for the irradiation and bioanalysis of the biological cell suspensions. Ease of sample insertion, ability to provide for sample cooling to minimize microwave heating, and ability to monitor the sample temperature all had to be taken into account. The applicator was developed around a 12 inch section of WR284, S-band copper rectangular waveguide. The rectangular waveguide was operated in the principal or TE_{01} mode. In this mode, the electric field in the empty rectangular waveguide is perpendicular to both the direction of wave propagation and to the broad sides of the guide, varying as a half sine transverse to the direction of propagation. To satisfy important experimental requirements for the cell irradiation experiments, including sample volume and the ability to maintain sample sterility, 1 cm O.D. x 0.8 cm I.D., 2 ml round tubes with

screw cap tops with silicone ring seals were selected as containers for the cell suspensions. Filling a container with 2 ml of sample made an aqueous cylinder approximately 2.5 cm in height.- The guide with the sample in position should behave somewhat like a two dielectric space. Since the center portion is filled with a post of high dielectric permittivity, the field should be largely concentrated within the post. A solution of a mathematical model roughly describing this configuration, that is, a dielectric post as an obstruction in a waveguide indicates that the field has a raised 3-D (sinx)/x form for the unmatched condition [1]. Although this model has not been directly applied to the present configuration it does indicate that a large fraction of the incident power can be coupled into the dielectric post.

Due to the large difference between the dielectric permitivity of water and air, insertion into the waveguide of a sample tube containing an aqueous cell suspension introduces a large impedance mismatch which causes most of the incident power intercepted by the sample to be reflected. Use of the Slide Screw Tuner allows a match with VSWR close to 1. To facilitate sample insertion, sample mixing and temperature monitoring, the applicator was designed to accept the sample tube through an aperture in the waveguide. Slots for sample insertion which minimally affect wave propagation may be cut in a rectangular waveguide along directions parallel to the current flow. Slots cut along the center line of the broad wall are particularly useful since at that position the current is a minimum and consequently, the mismatch introduced is minimal. In this case, the aperture chosen for sample insertion was circular and was drilled along the center line of one of the broad walls of the waveguide. Measurements of incident power, transmitted power and VSWR in an empty guide with such an aperture for sample insertion showed no measurable mismatch.

Sample cooling to minimize effects from microwave heating was provided by circulating a fluid around the sample tube. The container for the circulating fluid, hereafter called the sample bath, was placed within the waveguide so as to surround the sample tube. Insertion of the sample tube causes the container to seal with the aid of an O-ring seal to allow circulation of the cooling liquid. The cylindrical sample bath of 1 inch O.D. and 1/16 inch walls was constructed from plexiglass. Input and output lines for the circulating fluid were fed into the waveguide through holes drilled along the center of the broadwalls. Fig 1.2 shows a longitudinal cut along the center of the applicator. Fig 1.3 shows the applicator with the circulating bath and the plumbing necessary to empty the sample bath prior to sample withdrawal. A circulating fluid with low dielectric constant and essentialy lossless was chosen to have minimum effect on the mismatch. Freon 'TF' was initially used, however, because of its high vapor pressure it was not very satisfactory for continuous use. A nontoxic, chemically inert silicone fluid, DC200/5, was chosen as a replacement.

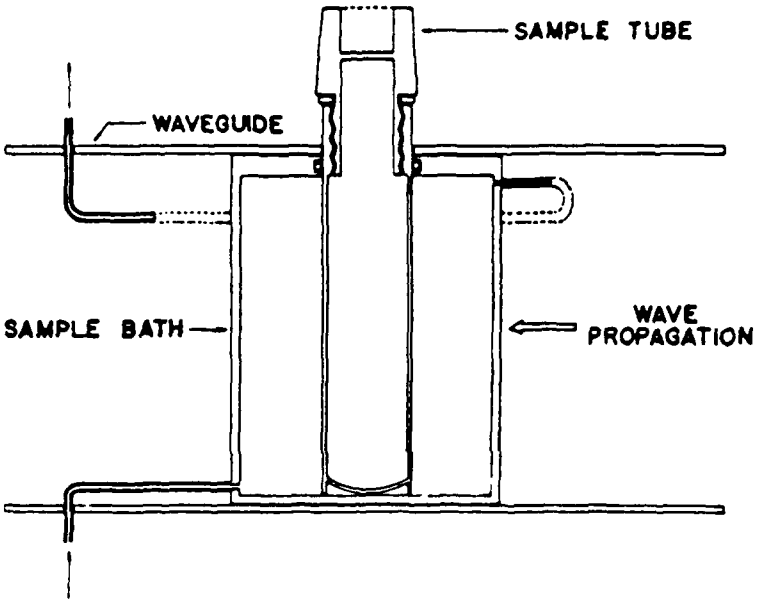

Fig 1.2: Longitudinal cut along applicator loaded with sample tube.

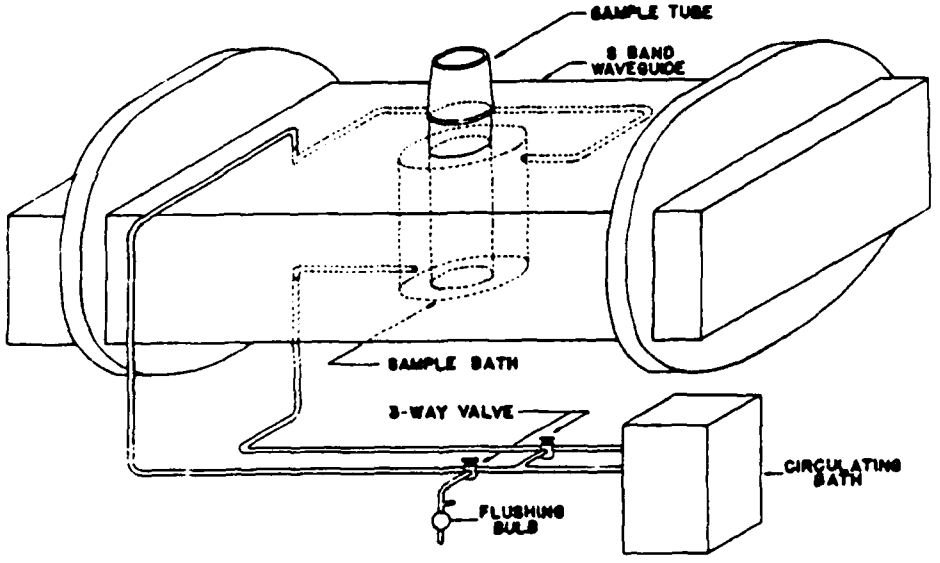

Fig 1.3: Applicator with circulating bath for temperature control.

1.2.3 SAR Measurements

The Specific Absorption Rate (SAR) is used to specify microwave energy deposition within a sample exposed to a microwave field. The SAR may be expressed as $SAR=(1/C_p)(dT/dt)$ where C_p is the specific heat of the irradiated sample and dT/dt is the rate of increase of temperature with time produced by microwave heating of the sample. To make the SAR measurement the sample should be thermally insulated with a non-microwave absorbing material to minimize heat losses during the measuring interval. SAR measurements were carried out in two different ways. For the first one, a 12 inch section of WR284 rectangular waveguide similar to that used for the applicator was filled with a styrofoam block cored to allow placement of the sample tube. To provide additional insulation, the cap of the tube was fitted with styrofoam plugs, and the section extending outside the waveguide was also surrounded with a styrofoam block. A Narda 8011B microwave transparent probe was used to perform the temperature measurements. All measurements were carried out with the probe at a depth approximately 1 cm below the liquid level in the sample tube. Measurements at this depth were made at five positions within the sample tube, in the center, and front, back, left, and right across the center relative to the direction of wave propagation looking at the sample tube in the applicator from above. The probe diameter was approximately 1.5 mm imposing a limitation on how close to the walls of the container measurements could be taken. The probe was flexible with a small curvature at the tip preventing very accurate positioning. A thin wall capillary tube was used to guide the probe for measurements along the center vertical axis of the sample tube, Fig 1.4a. For measurements along the walls of the container, the probe was held in position with adhesive tape, Fig 1.4b. Readings at various power levels were taken to obtain the expected linear relationship between the SAR and the net power (incident minus transmitted). The results of these measurements are shown in Fig 1.5. To obtain functional relations between the SAR and the net power delivered to the sample, least squares fits to a straight line $y = \underline{a}x$ were performed using the set of SAR measurements for each probe position. An average SAR was obtained by performing a simple arithmetic average of the $\underline{a}$ coefficients: $SAR = 0.69\ P_{net}$.

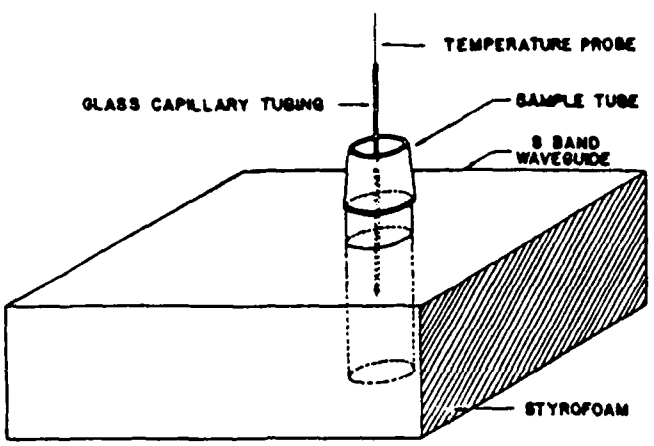

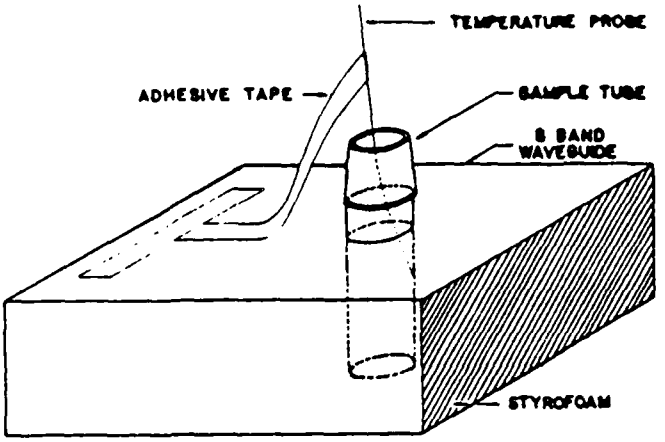

Fig 1.4a Fig 1.4b

Fig 1.4a: SAR measurement at center of sample tube.
Fig 1.4b: SAR measurements at wall of sample tube.

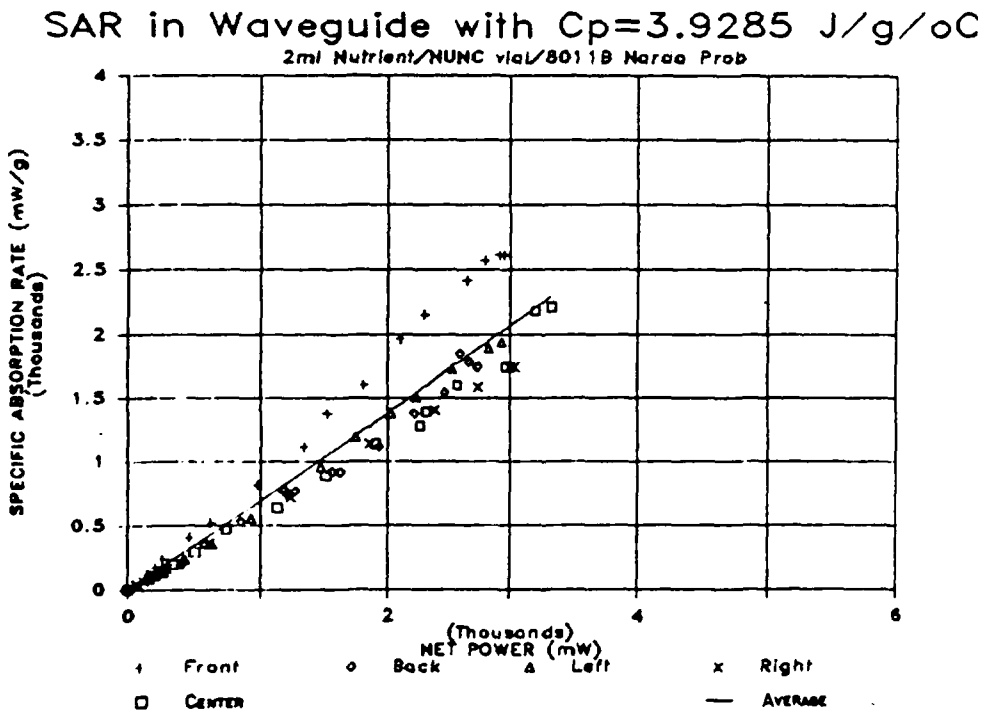

Fig 1.5: SAR vs. net power in waveguide configuration.

The above measurements of SAR were performed under conditions which minimize heat loss from the sample. During actual use, the applicator is surrounded by the sample bath filled with silicone cooling fluid which provides a path for heat dissipation. As explained earlier, the sample bath and the silicone fluid are of low dielectric permittivity and essentially lossless, however, they may cause small changes in the electric field affecting the SAR within the sample. To investigate this possibility, a second method was used to measure the SAR. In this case, measurements were carried out with the sample tube in the applicator insulating the sample bath and sample tube cap with styrofoam as in the previous measurements. The sample bath was filled with non-circulating fluid maintained at room temperature. As before, measurements were taken at five positions, center, front, back, right, and left at a depth of approximately 1 cm below the liquid level in the sample tube. Readings at various power levels were taken to obtain the expected linear relationship between incident power and SAR. The results of these measurements are shown in Fig 1.6. As before, to obtain functional relations between the SAR and the net power delivered to the sample, least squares fits to a straight line $y = \underline{a}x$ were performed using the set of SAR measurements for each probe position. An average SAR was obtained by performing a simple arithmetic average of the $\underline{a}$ coefficients: SAR = 0.61 P_{net}.

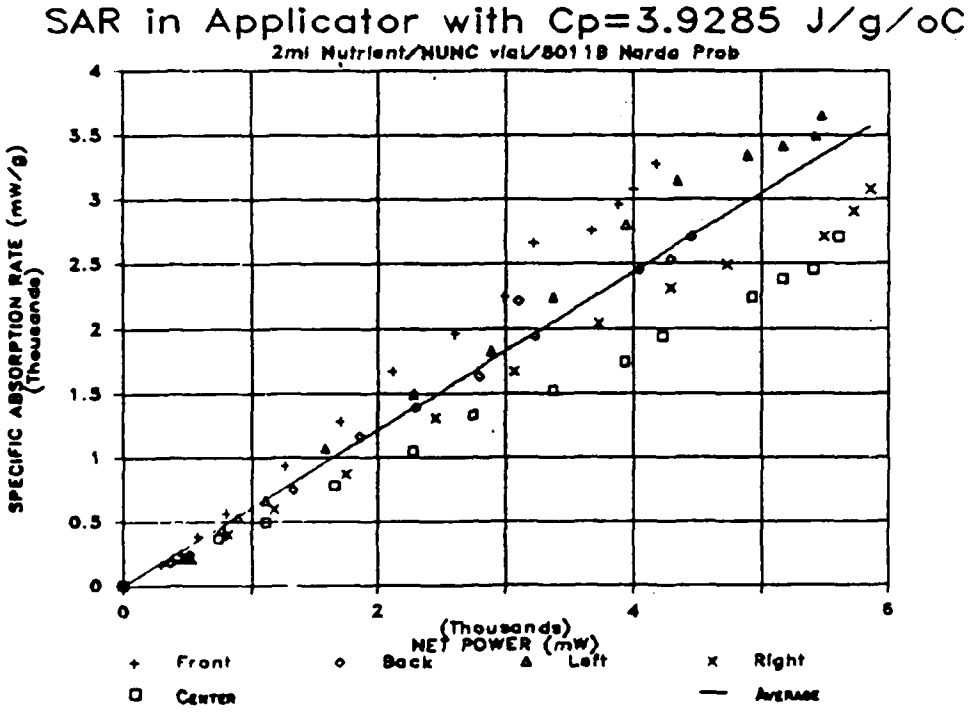

Fig 1.6: SAR vs. net power in applicator configuration.

TABLE 1.1
SAR = $\underline{a}$ * P_{net}

Position	In Waveguide	In Applicator
Center	0.63	0.46
Front	0.91	0.77
Back	0.64	0.61
Left	0.67	0.67
Right	0.58	0.52
Average	0.69 ± 0.12	0.61 ± 0.11

Slope $\underline{a}$ of curve SAR = $\underline{a}$ * P_{net}

The results of both methods of measurements are summarized in Table 1.1. The tabulated values correspond to the parameter $\underline{a}$ of the least squares fit calculation. The SAR values obtained from measurements in the insulated waveguide are generally larger than those obtained in the applicator. Since the second configuration is more representative of the actual experimental condition, we use the results of measurements in the applicator to specify the SAR of experiments carried out with this applicator. SAR values for biological experiments previously reported in the Quarterly Reports were based on single position SAR measurements plotted as a function of the input power. Since the sample was periodically mixed to prevent settling of the cell suspension, a better estimate of the SAR is obtained from the average values calculated above as a function of the net power. In this summary the reported SAR's are computed using the following relation: SAR = 0.61 P_{net}. These values represent average exposure doses with an estimated range of ± 25% about the mean.

1.2.4 Temperature Profile Measurements

A primary requirement of the applicator design was to allow microwave irradiation of mammalian cultured cells in an aqueous medium at a specified temperature. Due to sensivity of various physiological parameters to small temperature changes within the range of study, adequate temperature control was an important design consideration. Specification of the SAR in a situation where sample cooling is implemented does not give sufficient information to determine the temperature profile within the sample. This measurement is performed when temperature equilibrium is achieved. As might be expected, due to conditions at the boundaries between the sample tube and the cooling fluid the temperature profile shows a larger gradient as the SAR is increased requiring more cooling to counteract microwave heating of the sample. This is particularly true without continuous sample mixing. Temperature measurements were carried out with a Luxtron fiberoptic thermometer at nominal SAR's of 10, 100, and 1000 mW/g and nominal sample temperatures of 37°C and 43°C. Profile measurements provided details of the deviation from the temperature set at a position half way into the liquid in the

center axis of the tube, along planes intercepting at the center of the sample tube perpendicular and parallel to the direction of wave propagation. Results are summarized in tables 1.2 and 1.3. It is apparent from these results that adequate temperature control cannot be provided with this microwave applicator when irradiating at SAR's in the range of 1000 mW/g if a relatively uniform temperature distribution within the sample is desired.

TABLE 1.2

Nom. SAR (mW/g)	Perpendicular plane			Parallel plane		
	Bottom	Center	Top	Bottom	Center	Top
10	37.5	37.4	37.3	38.0	37.7	37.2
100	35.9	36.8	36.5	35.9	37.0	37.0
1000	18.8	33.5	39.6	18.6	35.0	40.0

Average readings over width of sample vial for Nom. Temp.= 37° C

TABLE 1.3

Nom. SAR (mW/g)	Perpendicular plane			Parallel plane		
	Bottom	Center	Top	Bottom	Center	Top
10	43.4	43.3	43.0	43.7	43.5	43.0
100	42.5	42.9	42.9	42.6	43.1	42.8
1000	26.0	40.0	45.2	26.0	40.0	44.6

Average readings over width of sample vial for Nom. Temp.= 43° C

Other measurements to investigate the effect of sample positioning on temperature profile were made along the center longitudinal axis of the sample tube. In this case no cooling was implemented, however, the tube was surrounded by non-circulating cooling fluid at room temperature. The SAR was approximately 500 mW/g. Two sets of measurements were carried out, one with the applicator positioned so that the sample tube was upright, and the other one with the applicator positioned so that the long axis of the tube lay in a horizontal position. The results of both sets of measurements are shown in Fig 1.7. This figure shows that the temperature gradient was essentially eliminated with the 90° reorientation of the sample vial. This suggests a significant effect on the temperature gradient along the vertical axis produced by convection currents arising from density variations along this axis. In view of these results a new microwave applicator which implements continuous sample mixing has been introduced for more recent studies.

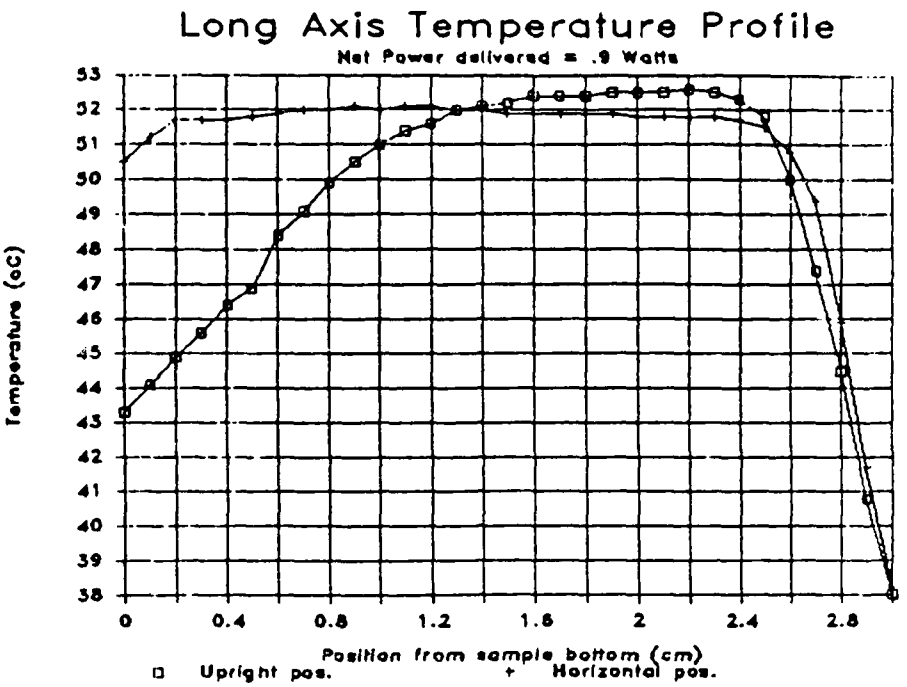

Fig 1.7: Temperature profile measurements within sample tube.

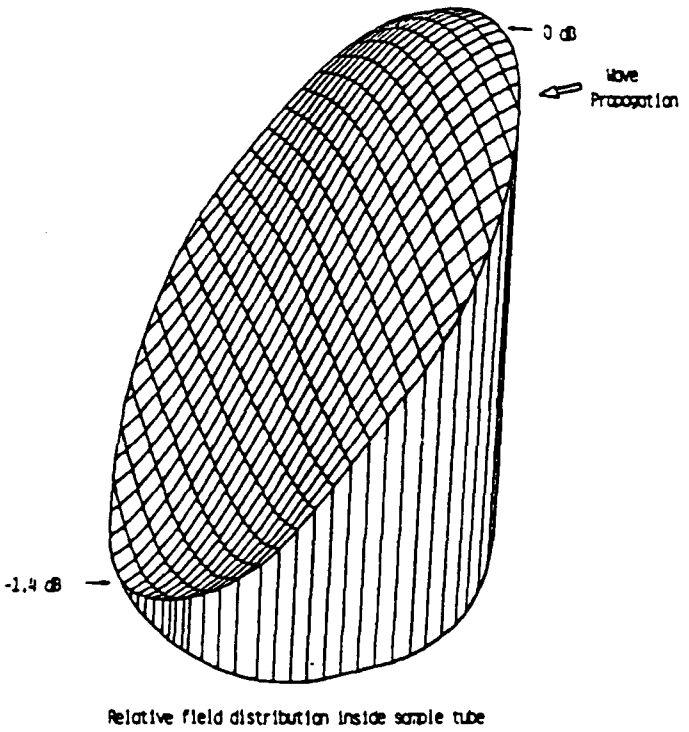

Fig 1.8: Relative field distribution. Readings are in dB below value at front face.

1.2.5 Standing Wave Measurements

To obtain a relative measure of the electric field variability within the sample, the relative magnitude of the field was measured across the sample tube on a plane parallel to the broad side of the waveguide. Measurements were made with a short 1 mm O.D. monopole antenna at 1 mm intervals on an imaginary grid with lines parallel and perpendicular to the direction of wave propagation. The results, shown in Fig 8, indicate that the relative electric field distribution is fairly uniform across the sample tube in the direction transverse to the direction of wave propagation, while measurements in the direction of wave propagation drop off slowly first and then more sharply from front to back of the sample.

1.3 Irradiation of Mammalian Cultured Cells with CW Microwaves

1.3.1 Cells in Suspension

During this reporting period, 38 microwave irradiation experiments of mammalian cultured cells in suspension including L929, IMR90, and XP cells were carried out in conjunction with the Biology Group. The objective of this work was to perform studies of cell survival, cell proliferation, and cell growth at normal (25°C-37°C) and elevated (>37°C) temperatures in the presence of CW microwave radiation. The conditions of each experiment are summarized in Table 1.4. Detailed experimental objectives, description of sample preparation procedures, bioanalysis procedures, and results are being reported in Chapter 2.

Prior to experiment ICS-31, the control sample was run immediately after the irradiated sample using the same hardware with the microwave source off. Starting with experiment ICS-31, a sham applicator was used identical to the one used for irradiation without the associated microwave hardware. This configuration allowed simultaneous treatment of the test sample and the sham, thus minimizing differences in treatment between the two samples other than microwave irradiation. However, the control sample was heated with circulating water rather than freon or silicone.

TABLE 1.4

Exp.I.	Freq (GHz)	Cell Type	Temp (°C)	P_{net} (Watts)	Time (hrs)	SAR (mW/g)	Method
ICS-1	3.0	L929	25	0.05	0.5	31	i
ICS-2	3.0	L929	25	0.05	0.5	31	ii
ICS-3	2.45	L929	30	0.40	0.5	244	iii
ICS-4	2.45	L929	30	0.04	2.0	24	iv
ICS-5	2.45	L929	30	0.05	4.0	31	iv
ICS-6	2.45	L929	30	0.05	6.0	31	iv
ICS-7	2.45	L929	30	0.05	6.0	31	v
ICS-8	2.45	L929	37	0.05	6.0	31	v
ICS-9	2.45	L929	30	0.05	24.0	31	iv
ICS-10	2.45	L929	30	2.36	2.0	1440	v
ICS-11	2.45	IMR90	30	2.31	1.0	1410	v
ICS-12	2.45	L929	30	2.42	1.5	1476	v
ICS-13	2.45	IMR90	30	2.45	2.0	1494	v
ICS-14	2.45	L929	30	2.54	2.0	1549	v
ICS-15	2.45	IMR90	30	2.55	1.5	1556	v
ICS-16	2.45	L929	30	3.67	1.0	2239	iv
ICS-17	2.45	L929	39	2.72	2.0	1659	v
ICS-18	2.45	IMR90	30	2.57	3.0	1568	v
ICS-23	2.45	IMR90	37	0.17	3.0	104	v
ICS-24	2.45	IMR90	37	0.19	3.0	116	v
ICS-25	2.45	XP	37	0.19	2.0	116	v
ICS-26	2.45	IMR90	35	1.92	2.0	1171	v
ICS-27	2.45	XP	35	1.91	2.0	1165	v
ICS-28	2.45	L929	45	0.02	2.0	12	v
ICS-29	2.45	L929	45	0.02	2.0	12	v
ICS-30	2.45	L929	47	0.02	2.0	12	v
ICS-31	2.45	L929	42	0.02	1.5	12	v
ICS-32	2.45	L929	43	0.02	1.0	12	v
ICS-33	2.45	L929	43	0.02	2.0	12	v
ICS-34	2.45	L929	43	0.25	2.0	152	v
ICS-35	2.45	L929	37	0.24	17.5	146	iv
ICS-37	2.45	L929	37	2.45	4.0	1495	iv
ICS-38	2.45	L929	43	0.28	2.0	171	v
ICS-40	2.45	L929	37	0.26	3.0	159	iv
ICS-41	2.45	L929	37	0.27	4.0	165	iv
ICS-42	2.45	L929	37	0.25	4.0	153	iv
ICS-43	2.45	L929	37	0.26	2.0	159	v

NOTES FOR TABLE 1.4

i: Irradiate sample tube filled with highly concentrated cell suspension, and sample tube filled with DI water to compare dT/dt for both samples. Results inconclusive due to poor sample insulation.

ii: Irradiate sample tube filled with cells in suspension, with nutrient medium, and with DI water at the same power level with circulating cooling fluid at a set temperature, to compare the increase in temperature from the set point for each sample. Results were similar in all cases.

iii: Irradiate cell suspensions at three power levels each separated from the next by an order of magnitude. Listing in table is for highest power level only.

iv: Irradiate at specified power level. Mix periodically by repeatedly drawing and discharging the cell suspension in the sample tube with a 200 µl pipetter.

v: Same as iv. periodically taking 200 µl aliquot and replacing with an equal volume of fresh nutrient medium.

1.3.2 Cells Attached to a Substrate

During this reporting period, thirteen (13) microwave irradiation experiments of cells attached to a substrate were carried out in conjunction with the Biology Group using L929 cells. The cells were grown on glass slides with approximate dimensions 2.5 cm x 0.9 cm x 0.02 cm. The slides were inserted into NUNC tubes similar to those used for irradiation of cell suspensions (one slide per tube) and filled with 2 ml of nutrient medium. The applicator was positioned to maintain the glass slides in the NUNC tubes parallel to the ground level. This configuration was chosen to minimize detachment of the cell layer which is more likely to occur if the slide is positioned vertically. The glass slides were arranged so that the surface supporting the cells would be perpendicular to and facing the direction of wave propagation, Fig 1.9. These experiments were carried out to perform a preliminary study of possible effects due to CW microwave radiation on the rate of Thymidine and Uridine uptake by cells attached to a substrate. Changes in these parameters would indicate changes in RNA and DNA synthesis. The conditions of each experiment are summarized in Table 1.5. Details about experimental objectives, sample preparation, and bioanalysis procedures are being reported in Chapter 2.

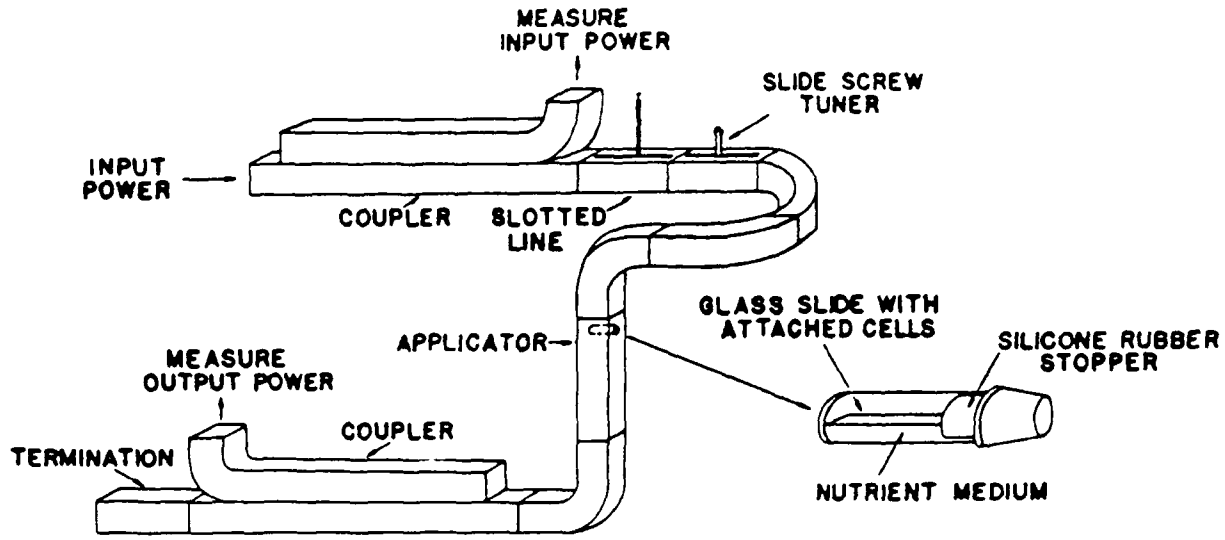

Fig 1.9: System configuration for irradiation of attached cells.

TABLE 1.5

Exp.ID	Freq (GHz)	Cell Type	Temp (°C)	P_{set} (Watts)	Time (hrs)	SAR (mW/g)	Method
IAC-1	2.45	L929	37.5	0.02	16.5	12	i
IAC-2	2.45	L929	37	0.02	17.5	12	i
IAC-3	2.45	L929	37	2.73	2.0	1665	ii
IAC-4	2.45	L929	45	2.40	2.0	1464	ii
IAC-5	2.45	L929	37	2.54	2.0	1550	iii
IAC-6	2.45	L929	45	2.54	2.0	1550	iii
IAC-7	2.45	L929	45	2.68	2.0	1635	ii
IAC-8	2.45	L929	45	2.68	2.0	1635	iii
IAC-9	2.45	L929	37	2.98	2.0	1818	iii
IAC-10a	2.45	L929	37	2.64	0.5	1610	iv
IAC-10b	2.45	L929	37	2.78	0.5	1696	v
IAC-10c	2.45	L929	45	2.90	0.5	1769	iv
IAC-10d	2.45	L929	45	2.85	0.5	1739	v

NOTES FOR TABLE 1.5

i: Irradiate sample with the specified incident power for the specified time.

ii: Irradiate sample for 105 minutes. Remove 0.2 ml aliquot of nutrient medium and replace with an equal volume of nutrient medium spiked with tritiated Thymidine. Continue irradiation for an additional 15 minutes.

iii: Irradiate sample for 90 minutes. Remove 0.2 ml aliquot of nutrient medium and replace with an equal volume of nutrient medium spiked with tritiated Uridine. Continue irradiation for an additional 30 minutes.

iv: Prior to irradiation, remove 0.2 ml aliquot of nutrient medium from sample vial and replace with an equal volume of nutrient medium spiked with tritiated Thymidine. Irradiate sample for 30 minutes.

v: Same as iv. spiking nutrient medium with tritiated Uridine.

1.4 Irradiation of Mammalian Cultured Cells in Suspension with Pulsed Microwaves.

During this reporting period four (4) microwave irradiation experiments of cells in suspension were performed with high peak power, low average power pulsed microwaves, using a microwave irradiation facility at the Department of Microwave Research of the Walter Reed Army Institute of Research (WRAIR). The applicator, provided by WRAIR, was constructed around a straight section of L-band rectangular waveguide. A 2 inch sample insertion port with an aluminum guiding sleeve was provided on one of the broadsides of the waveguide. An insulating styrofoam block with a 2 inch well cored out to accept a sample container was positioned directly below the sample insertion port filling part of the waveguide. To use this applicator, a sample bath was built of plexiglass to fit snugly into the styrofoam cavity. A 13 mm x 100 mm sample tube was chosen to hold the cell suspensions. The sample tube was filled with 3 ml of sample and positioned in the applicator such that the liquid level approximatelly coincided with the upper wall of the waveguide.
Insertion of the sample tube into the sample bath sealed this container with the aid of an O-ring seal to allow circulation of the cooling fluid, Fig 1.10. SAR measurements were performed at three positions along the vertical central axis of the sample tube, 0.2 cm, 1.7 cm, and 3.2 cm from the bottom of the tube. These measurements were made with non circulating cooling liquid (Freon TF) filling the sample bath. Results of these measurements are shown in Table 1.6. Values measured at the center (1.7 cm from the bottom) of the sample tube are used to calculate the reported experimental SAR's. The experiments were carried out at various peak power levels with pulses of 2 μsec and 10 μsec

widths adjusting the pulse repetition rate to maintain the average power low (SAR < 100 mW/g). Filtered air was bubbled into the sample on five minute intervals to mix the cell suspension. The conditions of each experiment are summarized in Table 1.7. Results of these experiments and analysis are being reported in Chapter 2.

TABLE 1.6
SAR measurements in WRAIR Applicator

Probe Pos.[a] (cm f bot.)	Net Power (Watts)	SAR (W/Kg)	SAR(NP(W))[b] (1/Kg)
0.2	24.0	1974	82.25
1.7	23.8	8740	367.23
3.2	23.0	5773	251.00

a: Probe position from bottom of sample tube.
b: Slope of SAR as function of net power delivered to sample.

TABLE 1.7

Exp.ID	Freq (GHz)	Cell Type	Temp (°C)	Pulse Width (μs)	Rep. Rate (Hz)	Peak Power (KW)	Time (hrs)	SAR Center (mW/g)
ICS-19-WR	1.25	L929	30	2.2	0.211	500	2.0	76.8
ICS-20-WR	1.25	L929	30	2.2	0.211	500	2.0	76.8
ICS-21-WR	1.25	L929	30	2.0	0.422	257	2.0	72.3
ICS-22-WR	1.25	L929	30	10.0	0.042	550	2.0	61.7

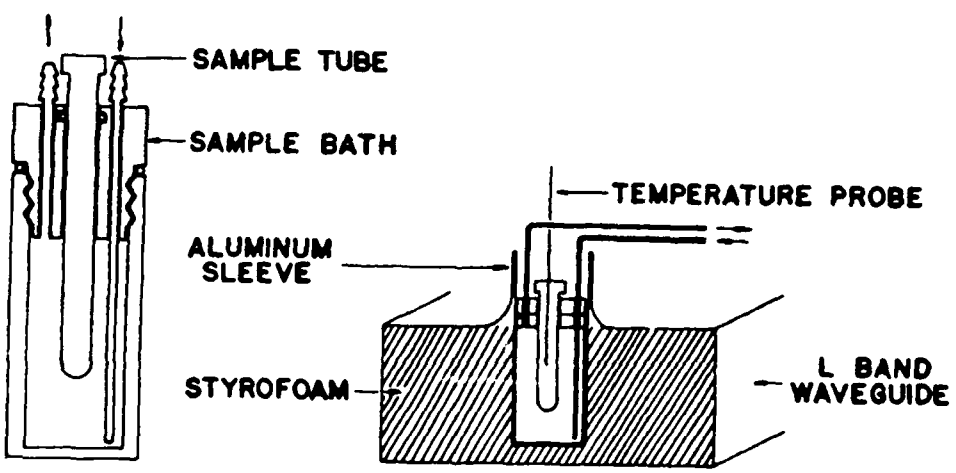

Fig 1.10: Cross section of sample bath and applicator for microwave irradiation experiments at WRAIR.

1.5 Irradiation of DNA solutions with Pulsed Microwaves

During this reporting period, two (2) microwave irradiation experiments of DNA solutions were carried out in conjunction with the Physics Group. One experiment, IDNA-1-WR, was performed using an X-band waveguide irradiation system available at WRAIR. The applicator, built around a section of X-band rectangular waveguide, was temperature controlled with circulating water. The sample holder was a reduced volume rectangular glass spectrophotometer cell. A 0.4 ml sample was used to perform the experiment. Temperature was monitored within the sample cell with an optical probe. No calibration SAR measurements were made in this experiment. The second experiment, IDNA-2-WR, was performed using the same experimental set up as that described in section 1.4. Experimental conditions are summarized in Table 1.8. Results and analysis are being reported in Chapter 3.

TABLE 1.8

Exp.ID	Freq (GHz)	DNA Type	Temp (°C)	Pulse Width (μs)	Rep. Rate (Hz)	Peak Power (KW)	Time (hrs)	SAR Center (mW/g)
IDNA-1-WR	9.37	Super-coiled	21.5	1	1	78	1.0	-
IDNA-2-WR	1.25	Super-coiled	25.0	15	0.06	200	1.0	67

1.6 Irradiation of Yeast Cells in Suspension with CW Microwaves

Genetic changes in higher eukaryotic cell cultures exposed to microwave radiation have been previously reported in the literature [2]. Searching for more insights in this area, we engaged in a cooperative effort to investigate the possibility of microwave induced damage in lower eukaryotic cells. A simplified and direct method for the study of genetic changes in yeast cells, saccharomyces serviciae one of the lower eukaryots, was developed over the past few years by Dr John Golin, a faculty member in the Biology Department at The Catholic University of America. Cells exposed to a potential mutation agent, such as microwave radiation, are appropriately treated and plated to allow formation of cell colonies easily observable with the naked eye. Colonies of mutant cells appear white as opposed to normal colonies which have a pink coloration. Spontaneous mutations amounting in general to less than 0.5% of the total number of colonies may occur and should be taken into account.

Seven microwave irradiation experiments of yeast cell suspensions were performed. The conditions of each experiment are summarized in Table 1.9. In all but one of the experiments, no significant differences in the percent of white colonies were observed between the irradiated samples and the controls. In experiment ICSY-3 the control showed a substantial number of mutations the cause of which is unknown and most likely a random occurrence. The evidence gathered from these experiments is sufficient to conclude that microwave radiation at SAR's of the order of 100 mW/g does not cause genetic variability on strain JG44 of saccharomyces cerviciae cells suspended in yeast extract peptone in dextrose (YPD) solution.

TABLE 1.9

Exp.ID	Freq (GHz)	Cell Type	Temp (°C)	P_{inc} (Watts)	Time (hrs)	SAR (mW/g)	S/C	Total Colon.	Whites
ICSY-1	2.45	JG44	25	0.37	2.0	104	sample	~100	0
							control	~100	0
ICSY-2	2.45	JG44	25	0.38	2.0	137	sample	~1000	0
							control	~1000	1
ICSY-3	2.45	JG44	25	0.39	2.0	106	sample	651	2
							control	406	99
ICSY-4	2.45	JG44	25	0.39	2.0	100	sample	aborted	
							control	aborted	
ICSY-5	2.45	JG44	25	0.39	2.0	100	sample	aborted	
							control	aborted	
ICSY-6	2.45	JG44	25	0.39	2.0	100	sample	957	0
							control	1410	0
ICSY-7	2.45	JG44	25	0.39	2.0	100	sample	35	0
							control	51	0

1.7 Irradiation of Copper in Deionized Water with CW and Pulsed Microwaves

During this reporting period, twelve (12) experiments were carried out to investigate the possibility of increased copper leaching in deionized water induced by microwave irradiation. Various experimental arrangements were used. One experiment was performed with high peak power pulsed microwaves using the experimental set up described in section 1.4. Experimental conditions are summarized in Table 1.10.

The results of the coaxial copper probe experiments (ICU-6, ICU-7, ICU-8) showed small changes in copper leaching with input power, which appear to increase linearly at first with the square root of the input power leveling off at around 1.6 (Watts) , Fig 1.11. No temperature data were taken during these runs to separate temperature effects.

The results of experiments performed with the copper disk positioned such that its flat surface is parallel to the E-field (ICU-9, ICU-10) showed a linear relation between copper concentration in the leachant and the square root of the input power. In this case, a linear relation is also obtained plotting the copper concentration in the leachant as a function of the equilibrium temperature. Thus, it is apparent that the increase in leaching is at least partially due to the temperature rise caused by microwave heating. To separate these effects a constant temperature experiment (ICU-12) was performed using a cooling bath to control the sample temperature. The results from this experiment indicated that there was no significant difference in leaching with changes in input power, Fig 1.12. In this case, these results showing no electric field effect are predictable since the field is zero at the disk surface. The results of experiment ICU-11-WR carried out with a similar configuration using high peak power pulsed microwaves were inconclusive.

The results of experiment ICU-4 carried out with the copper disk positioned flat at the bottom of the sample tube with its flat surface perpendicular to the E-field were inconclusive.

TABLE 1.10

Exp.ID	Freq. (GHz)	Temp control	Time (mins)	Max Power (Watts)	Method
ICU-1	2.45	RT	20	0.015	i
ICU-2	2.45	32° C	20	10.3	ii
ICU-3	2.45	RT	30	10.6	iii
ICU-4	2.45	RT	30	9.0	iv
ICU-5	2.45	RT	60	6.9	v
ICU-6	2.45	RT	60	6.9	vi
ICU-7	2.45	RT	64	6.9	vi
ICU-8	2.45	RT	60	6.9	vi
ICU-9	2.45	RT	60	6.9	v
ICU-10	2.45	RT	60	6.9	v
ICU-11-WR	1.25	RT	60	523K peak	vii
ICU-12	2.45	RT	60	5.2	v

i: Immerse coaxial copper probe 2 mm into a 10 ml sample of DI water. Irradiate at various power levels for specified time.

ii: Immerse coaxial copper probe with 5 mm of exposed length into a 1.8 ml sample of DI water. Irradiate at various power levels for the specified time.

iii: Immerse coaxial copper probe with 4 mm of exposed length into a 10 ml sample of DI water. Irradiate at various power levels for the specified time.

iv: Immerse a thin copper disk (.35 in D x .034 in W) into a 1.8 ml sample of DI water contained in a NUNC sample tube, position it at the bottom of the tube such that the E-field is perpendicular to the disk face. Irradiate in the microwave applicator used for cell irradiation work at various power levels starting from 0 to the maximum power level shown in Table 1.10 for the specified time interval.

v: Same as i. with copper disk positioned in the sample tube such that when placed in the microwave applicator the flat surface of the disk is parallel to the E-field and perpendicular to the direction of wave propagation.

vi: Immerse coaxial copper probe with 4 mm of exposed surface into a 1.8 ml sample of DI water contained in a NUNC tube. Irradiate at various power levels starting from 0 to the maximum power level shown in Table 1.10 for the specified time interval.

vii Immerse a thin copper disk (0.35 in D x 0.035 in W) into a 3 ml sample of DI water contained in a 10 ml sample tube. Place the disk in the tube such that the flat surface of the disk is parallel to the E-field. In this experiment an irradiation facility at WRAIR was used.

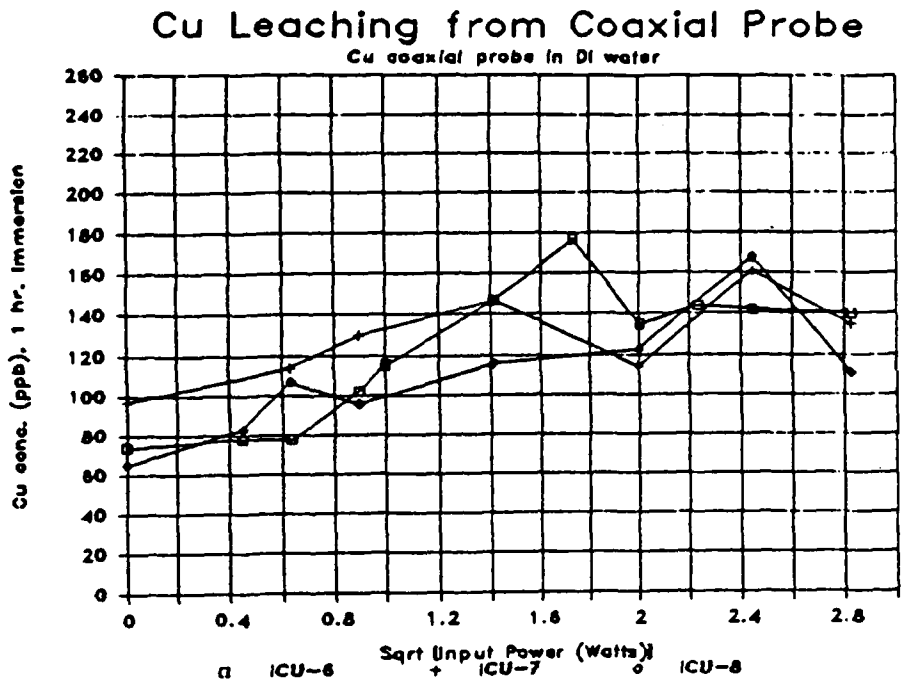

Fig 1.11: Copper (Cu) leaching from Cu coaxial probe. Concentration in leachant (deionized water) vs. square root of input power.

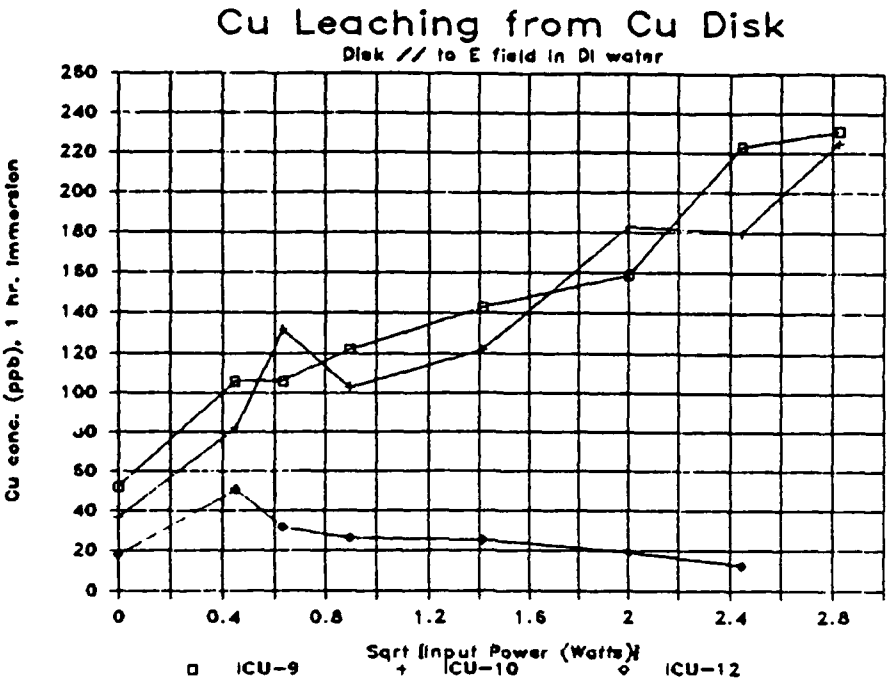

Fig 1.12: Copper (Cu) leaching from Cu disk. Concentration of Cu in leachant (deionized water) vs. square root of input power.

1.8 References for Chapter 1

[1] Y. Leviatan, G. S. Sheaffer, "Analysis of Inductive Dielectric Post in Rectangular Waveguide," IEEE Trans. Microwave Theory Tech., Vol. MTT-35, pp. 48-59 (Jan., 1987).

[2] J. Saffer, Abstracts for 9th Annual BEMS Meeting, June 21-25, 1987.

1.9 List of Tables for Chapter 1

1.10 List of Figures for Chapter 1

CHAPTER 2

EFFECTS OF MICROWAVE IRRADIATION OF CULTURED MAMMALIAN CELLS

J. Brent, D. Krause, M. Mullins, R. Nardone, and L. Shonk

Experiments were conducted to assess the effects of microwave exposure on mammalian cultured cells. Three cell lines were chosen for use. The murine fibroblast line L-929 was selected as a vigorously growing, aneuploid cell type. Diploid human cells, displaying slower growth rates and density dependent inhibition of growth were also used.

Cells were removed from monolayer culture and placed into suspension for the time of irradiation. Temperature was controlled during microwave exposure by use of a circulating bath outside the tube containing the cells. Irradiation was with 2.45 GHz continuous wave, or 1.25 GHz pulsed microwaves at SARs ranging from 6 to approximately 1700 mW/g. Exposure times ranged from 0.5 to 6 hr. Control cell cultures were maintained at the temperature of the irradiated cultures by a circulating water bath.

Following microwave exposure control and experimental cultures were aliquoted for three assays. Cells were processed for trypan blue dye exclusion as a test for general viability immediately post-irradiation. Ability of cells to function in culture after microwave irradiation was assayed by plating efficiencies, and growth curves to determine proliferation rates. In no instance was there a consistent, discernable difference in any of these parameters that correlated with exposure to microwave irradiations.

Additional experiments were initiated to assess the effects of microwave irradiation on efflux of fluorescein from L-929 and HeLa cells. Efflux corresponding to published reports was observed at temperatures of 23° or less, but physiological temperatures resulted in progressive cell death. As a result these experiments were terminated.

Irradiation of cells in suspension will continue during the second contract year, but will employ suspension adapted L cells that will proliferate in suspension, thus allowing irradiations to be conducted for periods of several days or longer. Cultures will be assayed for cell density, as a measure of cell proliferation, and for progression through the cell cycle by means of flow cytometry. Metabolic activities will be assessed by incorporation of radiolabeled precursors for DNA, RNA and protein. Two dimensional gel electrophoresis will be used to compare expression of proteins by irradiated and control cultures. Cultures will also be assayed for variabilities in expression of enzymes of the interferon system that may be produced by irradiation. An additional set of experiments will be conducted using the LLC-PK$_1$ line of epithelial cells; these cells will allow assay for the establishment and maintenance of specific differentiated function under conditions of microwave exposure.

2.1 Introduction

Assessing the biological effects of microwave irradiation through experiments based on whole animal irradiations has proven difficult. Problems arise in determining dosimetry for different parts of an animal, and in distinguishing thermal from athermal effects. Experiments employing irradiation of cultured cells provide an experimental situation in which dosimetry and rises in temperature may be more rigorously handled and controlled. Further, the large number of mammalian cultured cell lines available provides a wide variety of experimental subjects, ranging from transformed, aneuploid cell lines to diploid, senescing lines, and lines that express specific, inducible patterns of differentiation.

The types of microwave irradiation equipment used for experiments with cultured cells place limitations on experimental design. Waveguides have been used in most reported experiments. The physical restrictions of the waveguide cross section, particularly with microwave frequencies above 2.45 GHz, prohibit the use of large, monolayer cultures. Thus, experiments involving incorporation of labeled precursors for nucleic acids, proteins or other cell components must be done using autoradiographic techniques for cells grown on cover slips, and use of assays such as plating efficiency will be difficult or impossible. The use of suspension cultures, whether of suspension-adapted cell lines or cells released from monolayer and placed temporarily in suspension for purposes of irradiation, allows greater numbers of cells to be placed into a waveguide system, and so gives greater flexibility in experimental design. Suspension cells, however, will not exhibit the development of the cytoskeleton characteristic of monolayer cultures; further, cells placed into temporary suspension from monolayer will not proliferate during suspension, and may show alterations in other aspects of their behavior. Anechoic chambers and horn antennas have been employed in irradiation systems. Such setups have allowed the use of large culture flasks during irradiations, so that larger numbers of cells can be employed in assays following irradiation. Such designs, however, may lack the flexibility of waveguide systems for alteration in experimental design, or for temperature control.

Results from published reports on microwave irradiations of cultured mammalian cells have come from use of both monolayer cultures (1,2,4,8,15,20,22,23) and of monolayer cells placed into suspension for irradiation (5,12,17). Conditions for these irradiations have varied widely, with exposures ranging from 15 min. (4) to as long as 1 week or more (22,23), and specific absorption rates (SARs) from 0.05 mW/g (8) to 1200 mW/g (12) where SARs were reported. Microwave frequencies from 434 MHz (18) to 74 GHz (4,15,19) have been employed. Of these reports, some (1,3,4,5-,8,12,15,17,19) have made provisions for control of temperature of the cultures so as to prevent thermal effects arising from microwave heating.

the cultures so as to prevent thermal effects arising from microwave heating.

Microwave irradiations of cell cultures were reported to cause no athermal changes in cell survival, viability or growth (12,17,1-8), and no changes in synthesis of DNA, RNA (15) and protein (4), or alterations of general ultrastructure (19). Additionally, lack of irradiation effects were noted for in vitro differentiation of erythroid leukemic cells (3). However, reports also claim what were judged to be athermal effects of microwave irradiation. Decreased growth rate and increased incidence of chromosomal breaks were reported for rat kangaroo cells cultured under conditions of continuous irradiation in microwave ovens, with irradiation serving to maintain temperature at approx. 37° (22,23), but without rigorous monitoring and control for possible temperature fluctuations. Lower growth rate and changes in morphology were reported after irradiation of Chinese Hamster cells (5). Lowered plating efficiencies were noted for HeLa cells after microwave irradiation, as well as enhanced transformation by a tumor promotor (1); these results have been called into question, however, since they are no longer repeatable in the original laboratory (E.K. Balcer-Kubiczek, personal communication). Other reported effects include alterations in the lymphoblastoid transformation of lymphocytes in vitro (20), and enhanced efflux of Ca^{++} from neuroblastoma cells (8), the latter effect reported to occur only at specific SARs. Additionally, ultrastructural studies of neuroblastoma cells have revealed membrane breaks and alterations of the cristae of mitochondria after exposure to microwaves (21). This assessment came from comparisons of microwaved samples with control samples heated to equivalent temperatures in water baths, and so may be subject to interpretation depending on accuracy of temperature measurements and controls.

Given the scattering of techniques, irradiation conditions and results, and the variations in temperature controls that have been reported, we proposed a systematic study in which cultured cells would be assayed for a variety of endpoints during, and following, irradiation, with temperature control and measurement of SAR being conducted through a collaborative effort with an electrical engineering group. The first data from this work are detailed in the sections below, and include results of viability, plating efficiency, and growth studies following irradiations (2.45 GHz, continuous wave, 0.5 to 6 hr.) of 3 mammalian cell lines removed from monolayer and placed temporarily into suspension for the time of irradiation. Results from this initial series of experiments show no consistent variation which can be correlated with exposure to microwaves for any of the assayed parameters. Additional experiments attempted for assessment of efflux of materials through the cell membrane are reported, although results were found not to be applicable to the study.

2.2 METHODS

2.2.1 Cell Cultures and Maintenance

Three established mammalian cell lines were chosen for irradiation. The aneuploid murine fibroblast line L-929 was selected as a general, rapidly growing cell type. Additionally, two human fibroblast lines were selected. Diploid IMR-90 cells display density-dependent inhibition of growth in culture, and are of additional interest in that they display senescence after multiple population doublings (14). Fibroblasts of Clone 12 BE, derived from a patient with the disease xeroderma pigmentosum, were also employed. The xeroderma pigmentosum (XP) cells are deficient in DNA repair (6), a genetic defect which produced the disease condition in the donor.

Each cell line was maintained in monolayer culture using Eagle's Minimum Essential Medium (EMEM), supplemented with 20mM HEPES buffer and 10% fetal bovine serum. Cells were removed from culture flasks, for subculturing or experimentation, by application of a standard trypsin-EDTA stripping solution; a timed procedure was used to minimize excessive exposure of cells to this solution. Except for conditions during actual irradiations, cultures were maintained at 37° in a humidified atmosphere of 5% CO_2, 95% air.

2.2.2 Culture Conditions for Irradiation

Cells were prepared for irradiation by release from the growth surface with trypsin-EDTA solution, followed by resuspension in serum-free EMEM at a concentration of $5x10^6$ cells per ml. Two ml of this cell suspension were placed in a polypropylene, cryogenic tube for insertion into the irradiation device or into a control chamber. During the time of irradiation, both experimental and control cells were maintained in suspension by either (1) gentle bubbling of filtered 5% CO_2/95% air through a slotted glass capillary tube, or (2) resuspension by careful hand pipetting at 15-30 min. intervals. Hand pipetting was used for most of the work since bubbling, even in the absence of serum, produced progressive foaming of the culture medium. Foaming could be controlled by addition of filter-sterilized anti-foam agent, but this additive interfered with viability testing by trypan blue exclusion.

Irradiation was done at 2.45 GHz, continuous wave (CW), with SARs ranging from 6 to 2239 mW/g. Some cultures were also irradiated using facilities at the Walter Reed Army Institute of Research; these cultures were irradiated with 1.25 GHz microwaves, using peak powers of 250 and 500 kilowatts, pulsed to give average SARs of 39 to 49 mW/g. Culture temperatures were maintained at 30° or 37° C during irradiation. Irradiations at 30° were done with the expectation that any heating of "micro-domains" which might go undetected by the "macro level" temperature sensors would be unlikely to produce local temperatures above the normal growth temperature of 37°.

2.2.3 Post-Irradiation Handling of Cell Cultures

At the completion of chosen irradiation intervals cells were aseptically transferred from the cryogenic vials and aliquoted for each of 3 assays.

(1) Cell Viability: Determination of cell viability was done immediately post-irradiation using the trypan blue dye exclusion test. Cell counts were done on a hemocytometer. Viability data were used as an indication of the overall health of experimental and control cultures after the irradiation period, and were also used to correct the electronic cell counts used for setting up and analyzing growth curves and plating efficiencies.

(2) Growth Curves: Cell proliferation after irradiation was determined by plating $5x10^4$ viable cells per 60mm diameter petri dish, and then removing cells from individual dishes with trypsin-EDTA solution at one day intervals to determine cell numbers. For the more rapidly proliferating L-929 cells counts were terminated after 5-6 days. The more slowly proliferating IMR-90 and XP cultures were followed for 8-10 days. Population doubling times were calculated from the slopes of the straight line portions of the resultant semi-log plots.

(3) Plating Efficiencies: After irradiation 100 viable cells were plated into each of 10, 60mm petri dishes. Cells were allowed to settle and to grow for 7-10 days, at which time cultures were fixed and stained with geimsa. Stained colonies, representing progeny derived primarily from single cells, were counted to determine plating efficiency. Average plating efficiencies were much lower for the IMR-90 and XP cultures than for L-929.

2.2.4 Efflux Experiments with L929 Cells

Membrane efflux experiments were conducted according to modifications of the methods of Prosperi et al (16). L929 cells were removed from monolayer with trypsin-EDTA, washed with PBS, and resuspended in PBS containing 2.4×10^{-6} M fluorescein diacetate. Following a 3 min. incubation at 23° C, the cells were pelleted and resuspended in PBS or serum free medium containing 2-10 mM KCN. At desired time points sample tubes were immersed in ice water to halt appreciable further efflux of the fluorescein created by esterase activity on the fluorescein diacetate within the cell (It was empirically determined that holding of samples on ice produced no appreciable change in intracellular fluorescence.) Samples were analyzed by flow cytometry with average fluorescence determined by mean peak channel for each sample.

2.3 RESULTS

Results were interpreted with the expectation that any effects of microwave irradiation on the parameters assayed should vary consistently with SAR and time of exposure. Thus, increased SARs or exposure times should be expected to yield increasingly detectable differences in effects between control and microwave irradiated cells.

2.3.1 L-929 Irradiations

Results of viability, plating efficiency and growth studies of L929 cultures following irradiation are presented in tabular form (Tables 2.1 and 2.2), with some of these data arranged in graphs (Figures 2.1-2.5).

Continuous wave irradiations were performed with SARs ranging from 16 to 1676 mW/g, and exposure times from 30 min. to 6 hr. (24 hr. for one experiment). For irradiation times up to 6 hr. the data show no consistent variations that correlate with exposure to microwaves. Individual time points in a given experiment show variation between microwave and control samples. Such variation was primarily for results of plating efficiency where differences in the mean PE varied as much as 13% between control and irradiated samples (example: 31 mW/g, 37°, 4hr. exposure). Given the possibility of minor errors in diluting cultures to obtain 100 cells per plate, PE is the most susceptible of the assays to variation. In no case, however, was such variation a consistent feature that related to dosimetry such that an interpretable pattern was evident. Further, in most cases the mean data points for experimental and control cultures fell within each other's standard deviations, or the standard deviations overlapped.

Figure 2.1 displays results of an early experiment in which viabilities and PEs were compared after 30 min. microwave irradiations at SARs of 6, 18 and 244 mW/g. No changes which correlate with SAR are evident in either parameter . The low plating efficiency of the control samples in this experiment is anomalous, and cannot be attributed to a general raising of PE by irradiation as can be seen from other results of Table 2.1.
Figures 2.2, 2.3 and 2.4 display viabilities and PEs for experiments in which exposures ranged to 6 hr. with SARs from 31 to 1676 mW/g. These graphs illustrate the range of variation observed from time point to time point in a given experiment, and show the lack of any dosimetry-related correlations to microwave exposure. Consistency of cell proliferation after 2 hr. exposure to either relatively low (31 mW/g) or high (1676 mW/g) SARs is illustrated in Figure 2.5.

Results of L929 CW irradiations thus indicate no detectable perturbation of cell function after irradiation. The possible exception to this observation is seen in the results of the

24 hr. irradiation at an SAR of 31 mW/g. After irradiation both viabilities and PEs were significantly different, being approximately 10% lower in the microwaved samples; population doubling time, however, was unaffected. Since only a single experiment was performed, no definite conclusion can be drawn from these data. The drastic lowering of cell viability in control cultures over the 24 hr. period suggests the data be interpreted with caution. Due to this progressive drop in viability, longer exposures of cultures to microwaves were postponed until an adequate system for irradiation of suspension-adapted, proliferating cells could be put in place. This system is now in use with suspension-adapted L929 cultures, and will allow irradiations to be conducted for periods of several days with a proliferating cell population which will not decline in viability.

In addition to the irradiations cited above, L929 cultures were also exposed to 1.25 GHz microwaves, pulsed to give peak powers of 250 or 500 KW, and SARs of 39-49 mW/g. These conditions allowed moderate SARs, but high field strengths. Results of these experiments are presented in Table 2.2. In 3 of the 4 experiments PEs were higher in microwaved cultures, although mean PEs for a given time point fell within each other's standard deviations. Results, thus, probably are consistent with those from the CW irradiations. The pulse experiments were not continued due to lack of availability of the irradiation facility. It is possible that the need to transport cells to and from the irradiation site may have added to experimental error. Pulse experiments are now scheduled at our facility, where an appropriate pulse generation system is in place. Continuation of this work will also be done with proliferating, suspension-adapted cells, so that long term irradiations will be no problem.

2.3.2 IMR-90 Irradiations

The absence of detectable effects on viability, PE and cell growth after irradiation of L929 cells led to irradiations of the human, diploid fibroblast line IMR90 (14). In contrast to L929, IMR-90 does not display the unrestrained and rapid proliferation characteristic of an aneuploid, transformed cell type. Rather, IMR-90 cells grow more slowly (doubling time of 35-40 hr. vs. approx. 22 hr. for L929), and display density dependent inhibition of growth. It was reasoned that if the robust proliferative abilities of L929 served to mask effects of microwave irradiation, then such effects might be detected in IMR-90.

Results of a series of irradiations of IMR-90 are presented in Table 2.3, and in Figures 2.6 and 2.7. Population doubling rates post-irradiation were unaffected, even after 180 min. exposure at SARs of approximately 1500 mW/g (Figure 2.6). Viabilities and PEs, with the exceptions of a few, individual data points (for example, Figure 2.7a, viability, 3 hr. exposure) were also remarkably consistent between microwaved and control samples. These results thus support the conclusions drawn from the L929 irradiations that

with the use of a temperature control system to eliminate thermal effects, cell viability, PE and growth are unaffected after exposures of 0.5 to 6 hr., and SARs as high as 1500-1600 mW/g.

2.3.3 Xeroderma Pigmentosum (Clone 12BE) Irradiations

To supplement the CW data on IMR-90 an additional set of irradiations was done using the 12BE clone of a human, xeroderma pigmentosum (XP) fibroblast line. The XP cell line is characterized by defects in excision repair of DNA (6). This deficiency has been of use in the study of carcinogenic and mutagenic compounds, since it results in a more pronounced effect of such agents upon cell populations (13). The rationale for choosing the XP cells was based on the hypothesis that microwave-induced damage might be readily repaired by a cell with a functioning, normal complement of repair enzymes, while damage (in this case to the DNA) in a repair-deficient cell line might be revealed.

Results from 2 experiments in which XP cells were irradiated for 2 hr. at SARs of 116 or 1165 mW/g are presented in Table 2.4. As for the IMR-90 data, no consistent variation in assayed parameters is found in microwaved vs. control samples. The growth curves obtained from control and experimental cultures after 2 hr. irradiation at 1165 mW/g are presented in Figure 2.8.

2.3.4 CW Irradiations at Elevated Temperatures

In the experiments cited above thermal effects were avoided by use of the temperature control system assembled by the Electrical Engineering group. Since no microwave-dependent effects were observed within the limitations of the conditions assayed, it was felt that before proceeding with new experimental conditions irradiations should be conducted at temperatures elevated above the normal 37° optimum of mammalian cultured cells. Such conditions would ascertain the temperature limits of our cell lines, which would provide useful information for analyzing possible thermal effects. Also, it was felt that the effects of microwave-induced damage (or microwave-induced protection) might be more evident in a situation in which cells were subjected to environmental stress. A series of irradiations of L929 cells was conducted to see if this idea were true.

Figure 2.9 displays mean PEs obtained from a series of 60 min. irradiations at temperatures ranging from 30° to 47° C. SARs ranged from approximately 12 to 1700 mW/g for different samples, but since no changes in PE correlated with SAR, this was not taken into account in plotting the graph. The graph shows an obvious drop in PE from 39°to 45° C, but no differences that correlate with exposure to microwaves.

Results from specific experiments are presented in Figure 2.10. Viabilities and plating efficiencies, averaged from 2

separate experiments done at 43° C, are plotted against time of exposure to microwaves (average SAR, 162 mW/g). Both viability and PE are seen to drop progressively with exposure to the higher temperature, but no change in this drop appears due to microwave exposure.

The deleterious effects of thermal stress were ,thus, not accelerated or inhibited through addition of CW microwave irradiation.

2.3.5 MEMBRANE/EFFLUX EXPERIMENTS

Initial experiments measuring fluorescein efflux after incubation of L929 cells in PBS/fluorescein diacetate confirmed the basic features of efflux determined by Prosperi et al (16). As shown in Figure 11, efflux could be followed by diminishment of cellular fluorescence with time after incubation. Further, apparent active transport of fluorescein out of the cell was inhibited by the addition of KCN to the PBS used as the efflux buffer after incubation of cells with fluorescein diacetate. Figure 11 compares the efflux occurring at 23° C for PBS and PBS-10 mM KCN, showing the dramatic slowing of efflux with KCN present. Figure 12 illustrates the variation in efflux rates produced by varying the KCN concentration.

With these data in hand experiments were conducted to determine a phase transition temperature for the L929 membrane. These experiments were conducted by incubating cells in PBS-fluorescein diacetate at 23°, and then resuspending cells in PBS-KCN at the temperatures of interest. It became apparent quickly that higher temperatures accelerated the efflux of fluorescein across the cell membrane. By measuring rates of efflux and comparing rates for different temperatures it should have been possible to find temperatures at which the efflux rate exhibited a more pronouced change between temperatures, and so identify the phase transition temperature. Microwave irradiations would then be conducted at this temperature to see if efflux rates would increase.

Two factors prevented an accurate measurement of the phase transition temperature. First, despite attempts to control temperature carefully for fluorescein diacetate incubation with accurate water bath/circulators, considerable variation was found in the initial level of cellular fluorescence from experiment to experiment, and so for efflux rates at the same temperature. Despite this fact it was decided that by doing each experiment at three different efflux temperatures (e.g. 28, 30 and 32°) a definite break in rate difference could be determined. The second factor, however, resulted in termination of these experiments.

Initial experiments at 23° C (the temperature used by Prosperi et al (14)) showed some slowing of data accumulation in the flow cytometer with data points beyond 10 min. With higher temperatures, especially in the physiological range above 30°, this slowing became pronounced. Microscopic examination of the cells indicated that with incubation times beyond 5-10 min. progressive cell death was occurring in all samples, but especially at temperatures above approximately 23°. After efflux intervals of 20 min. over 50% of a cell population was determined to have died at temperatures of 32-36°. This fact probably accounted for the erratic efflux data that were obtained for such higher temperatures. Efforts to prevent cell damage and death during efflux included (1) use of varying concentrations of KCN, (2) use of serum free EMEM instead of PBS, (3) use of metabolic inhibitors other than KCN, (4) use of HeLa cells instead of L929, and (5) use of suspension-adapted L929 cells instead of cells removed from monolayer culture. Since none of these factors produced any significant improvement in cell viability during efflux conditions, further experiments were not conducted.

As an additional set of membrane studies the possibility of microwave-induced protein shedding from L929 membranes was examined by collecting culture medium after irradiations, precipitating the proteins with cold acetone, and examining the protein composition by SDS PAGE. Although cells were washed with serum free EMEM prior to irradiation, and maintained in serum free EMEM during irradiation, the protein bands present in all samples, experimental and control, were those characteristic of fetal bovine serum. Sufficient serum remained adsorbed to cells, to be released during suspension, and to obscure detection of any possible microwave-specific shedding of membrane proteins.

2.3.6 Interferon Experiments

The interferon system was chosen to investigate possible effects of microwave irradiation on transcription of specific gene sequences. Specifically, activities of the enzymes 2',5' - oligoadenylate (2-5A) synthetase and the 2-5A dependent RNase, RNase L, were studied in both microwave exposed and control samples. L-292 cells were irradiated in suspension and then placed into monolayer culture for 24 hrs. Cells were subsequently pelleted and then frozen for later analysis.

Results of the first two experiments indicated unchanged levels of the 2-5A synthetase, but an approximately two fold increase in RNase L activity in the microwave exposed cells. These preliminary results will be verified with additional experiments, including exposure to virus so as to activate the interferon system.

In conjunction with this work an additional series of assays has been planned using two dimensional gel electrophoresis to examine the pattern of polypeptides expressed in both microwave and control suspension cultures of L-929 cells. The two dimensional system employing isoelectric focusing and SDS polyacrylamide gel

electrophoresis can resolve over 1400 different polypeptides from whole cell preparations of HeLa cells (24). Comparison of the two dimensional polypeptide patterns from irradiated and control cultures should provide a means of assessing general variation in gene expression as the result of microwave exposure.

2.4 DISCUSSION

The results presented demonstrate no alterations in cell viability immediately post-irradiation, or for plating efficiency or population growth following irradiation of L929, IMR-90 and XP clone BE12 cells. These results thus provide more extensive data which are in agreement with earlier published reports (12,17,18) in which cultured cells, placed into suspension for irradiation, were observed to show no decrease in survivability/viability, or growth; the exception is the study of Chen and Lin (5) which reported both lowered growth rate and alterations in morphology in post-irradiation cultures of Chinese Hamster cells. It should be noted that no alterations were observed in the morphology of the 3 cell lines employed by us during the course of this study.

The conditions utilized for the work reported here involved removing the cells from monolayer and placing them into suspension for the period of irradiation. Only the cell viability assay was done immediately at the completion of irradiation, with PE and growth determinations requiring the cells to be placed into monolayer culture for several days before completion. Our PE and growth results thus show that there were no observable continuing effects of microwaves after irradiation was completed and the cells were returned to their normal culture conditions. It is possible, however, that effects were occurring during exposure to microwaves, but were not so severe as to impair recovery and subsequent normal growth once irradiation was ceased. Assessment of this possibility will require that assays be incorporated into the experiments so that cells can be removed immediately from the exposure system and tested. Also, the maximum exposure time employed for this work was 6 hr. (excluding the 24 hr. exposures which, as discussed in the Results section, are inconclusive). It may require more prolonged exposures to microwaves, or alterations in the irradiation conditions (different frequencies, pulsed exposures at higher fields) before any effects will become evident.

Results from experiments with IMR-90 and XP cells serve to confirm the results obtained with L929, and to assure that those results were not simply due to the high proliferative rate and aneuploid nature of the L929 transformed cell type. Both cell types are diploid and show slower rates of growth as well as density dependent inhibition of growth. Although microwave irradiations of bacteria have been correlated with mutation (2), our work with XP cells shows no diminishment in the ability of those cells to survive after irradiation, despite their limited

ability to recover from damage to their DNA (6). It may be that microwaves are capable of causing damage to DNA in ways that are not linked to the XP cells' limited repair capabilitities, but XP cells have been shown to be far more susceptible to the effects of carcinogens and mutagens than have cells with full repair capacity (13), suggesting they should also be sensitive to other conditions which might induce mutation.

To gain a better assessment of microwave effects that may be detectable only during irradiation, or after prolonged irradiation, will require a system which will allow several million cells to be maintained in a proliferating state during irradiation. Such a system should provide for periodic withdrawal of a significant fraction of the culture for assay, and provide cells which are undergoing normal activities during the course of irradiation. With these goals in mind we have adapted the L-929 cells for suspension culture and have begun irradiations with them. Initial radiations have employed the previous endpoints of viability, PE and growth, so that results may be related to those reported above. (The suspension L929 cells retain the ability to grow as monolayers when placed into appropriate culture conditions, allowing PE to be retained as an assay where desired.) Subsequent experiments, however, will involve the use of flow cytometry and cell synchronization techniques to analyze any cell cycle variation resulting from microwave exposure, and incorporation of labeled precursors to assess the metabolic capabilities of irradiated cells. Use of a suspension-adapted culture system should allow irradiations to be conducted for periods of several days so long as cell density is monitored and cultures are kept from overgrowth and stagnation.

2.5 REFERENCES

1. Balcer-Kubiczek, E.K. & G.H. Harrison. 1985. Carcinogenesis, 6:859-864.
2. Blevins, R.D., R.C. Crenshaw, Jr., A.E. Hougland & C.E. Clark. 1980. Radiation Res., 82:511-517.
3. Brown, R.F. & S.V. Marshall. 1986. Radiation Res., 108:12-22.
4. Bush, L.G., D.W. Hill, A. Riazi, L.J. Stensaas, L.M. Partlow & O.P. Gandhi. 1981. Bioelectromagnetics, 2:151-159.
5. Chen, K.C. & C.J. Lin. 1978. J. Microwave Power, 13:251-256.
6. Cleaver, J.E. 1969. Nature, 213:252-256.
7. Dardalhon, M., C. More, D. Averbeck & A.J. Berteaud. 1984. Bioelectromagnetics, 5:247-261.
8. Dutta, S.K., A. Subramoniam, B. Ghosh & R. Parshad. 1984. Bioelectromagnetics, 5:71-78.
9. Liburdy, R.P. 1985. Radiation Res., 103:266-275.
10. Liburdy, R.P. & P.F. Vanek, Jr. 1985. Radiation Res., 102:190-205.
11. Liburdy, R.P. & P.F. Vanek, Jr. 1987. Radiation Res., 109:382-395.
12. Lin, J.C. & W.D. Peterson. 1977. Bioengineering, 1:471-478.
13. McCormick, J.J. & V.M. Maher. 1977. pp. 251-278 in Short Term in vitro Testing for Carcinogenesis, Mutagenesis and Toxicity. The Franklin Institute Press, Philadelphia.
14. Nichols, W.W., D.G. Murphy, V.J. Cristofalo, L.H. Toji, A.E. Greene & S.A. Dwight. 1976. Science, 196:60-63.
15. Partlow, L.M., L.G. Bush, L.J. Stensaas, D.W. Hill, A. Riazi & O.P. Gandhi. 1981. Bioelectromagnetics, 2:123-140.
16. Prosperi, E., A.C. Croce, G. Bottiroli & R. Supino. 1986. Cytometry, 7:70-75.
17. Robinson, J.E., D. McCulloch, G.H. Harrison & A.Y. Cheung. 1982. Bioelectromagnetics, 3:237-245.
18. Sapareto, S.A., G.C. Li, K.A. White & G.M. Hahn. 1982. Radiation Res., 89:124-133.
19. Stensaas, L.J., L.M. Partlow, L.G. Bush, P.L. Iversen, D.W. Hill, M.J. Hagmann & O.P. Gandhi. 1981. Bioelectromagnetics, 2: 141-150.
20. Stodolnik-Baranska, W. 1967. Nature, 214:102-103.
21. Webber, M.M., F.S. Barnes, L.A. Seltzer, T.R. Bouldin, & K.N. Prasad. 1980. J. Ultrastructure Res., 71:321-330.
22. Yao, K.T.S. 1982. J. of Heredity, 73: 133-138.
23. Yao, K.T.S. & M.M. Jiles. 1970. in Biological Effects and Health Implications of Microwave Irradiation, S.F. Cleary, Ed., USDHEW, Rockville, MD.
24. Celis, J.E. et al. Expression of cellular proteins in normal and transformed human cultured cells and tumors: two-dimensional gel electrophoresis as a tool to study neoplastic transformation and cancer. In Two-Dimensional Gel Electrophoresis of Proteins, J.E. Celis and R. Bravo, Eds., Academic Press, New York.

2.6 LIST OF FIGURES FOR CHAPTER 2

Figure 2.1: Viability and plating efficiency plotted against SARs for L-929 cells exposed to 2.45 GHz, CW, at SARs of 0, 6, 16 and 244 mw/g. Exposures were for 30 min. at 30° C.

Figure 2.2: Viabilities (2a) and plating efficiencies (2b) of L-929 cells plotted against time of exposure to CW, 2.45 GHz irradiation at ar SAR of 31 mw/g. Exposures were for 0, 2, 4 and 6 hr. at 30° C. Average of 2 experiments.

Figure 2.3: Conditions as for Figure 2, except that the temperature during irradiation was 37°.

Figure 2.4: Viabilities (4a) and plating efficiencies (4b) of L-929 cells plotted against time of exposure to CW, 2.45 GHz irradiation at an SAR of 1676 mw/g. Exposures were for 0, 30, 60 and 120 min. at a temperature of 30°. Average of 4 experiments.

Figure 2.5: Representative growth curves of control and irradiated L-929 cells. Cells were irradiated at 2.45 GHz, CW, for 2 hr. at 30°. SARs were 31 mW/g (triangles) and 1442 mW/g (circles).

Figure 2.6: Representative growth curves of control and irradiated IMR-90 cells. Cells were irradiated at 2.45 GHz CW, at an SAR = 1500 mW/g for 2 hr at 37°.

Figure 2.7: Viabilities (7a) and plating efficiencies (7b) of IMR-90 cells plotted against time of exposure to CW, 2.45 GHz irradiation at an SAR of 110 mW/g. Exposures were for 0, 1, 2 and 3 hr at 37°. Similar results were obtained after exposure to an SAR of 1,000 mw/g.

Figure 2.8: Representative growth curves for control and irradiated XP cells. Cells were irradiated at 2.45 GHz CW, at an SAR = 1165 mW/g for 2 hr. at 37°.

Figure 2.9: Irradiation of L-929 cells at elevated temperatures. Averaged plating efficiencies vs. the temperature maintained during irradiation for temperatures from 30° to 47° C. SARs varied from 12 to 1659 mW/g; this variation was not considered in plotting the data.

Figure 2.10: Viabilities (10a) and plating efficiencies (10b) for a series of exposures of L-929 cells to microwave irradiation at 43° C. Exposures were from 0 to 120 min. at an average SAR of 162 mW/g. Results represent the averages of 4 separate experiments.

Figure 2.11: Efflux of fluorescein from L-929 cells following incubation of the cells in fluorescein diacetate containing buffer. Graph illustrates the reduced rate of efflux produced when 10 mM KCN (open circles) is included in the efflux buffer as contrasted to buffer without KCN (closed circles).

Figure 2.12: Variations in the rate of fluorescein efflux produced in 3 fractions of the same culture depending on the concentration of KCN in the efflux buffer.

TABLE 2.1
L929 IRRADIATIONS
2.45 GHZ, CONTINUOUS WAVE

SAR (mw/g)	TEMP. (°c)	EXP. TIME	% VIABILITY		% PLATING EFFICIENCY		DOUBLING RATE(hr)	
			Cont.	MW	Cont.	MW	Cont.	MW
0	30	30m	80		59±6.3		31.7	
6	30	30m		78		71±7.9		36.7
18	30	30m		84		76±4.7		31.6
244	30	30m		79		71±8.8		28.5
31*	30	0h	84±5.4	84±5.4	72±6.5	72±6.5	22.8	22.8
31*	30	2h	81±11	82±9.2	68±20	73±29	22.7±2.4	23.1±0.7
31*	30	4h	81±0.7	81±1.4	49±5.4	59±15	22.2±0.6	21.9±1.1
31*	30	6h	79±2.1	81±2.1	39±27	37±20	20.9±3.5	20.9±4.4
31	37	0h	96	96	91±8.6	91±8.6	17.4	17.4
31	37	2h	89	86	98±5.8	85±10	20.7	22.0
31	37	4h	81	85	80±7.7	67±6.3	22.4	17.7
31	37	6h	84	81	50±5.1	51±3.3	23.7	22.4
31	30	0h	97	97	83±6.1	83±6.1	22.8	22.8
31	30	24h	24	14	58±5.1	47±2.2	26.0	26.1
1676**	30	0m	96±0.8	96±0.8	88±6.6	88±6.6	18.3	18.3
1676**	30	30m	92±5.5	93±1.0	------	------	20.0	----
1676**	30	60m	92±4.1	94±1.0	59±16	67±22	18.2	----
1676**	30	90m	94±1.3	91±1.5	-----	-----	20.7	----
1676**	30	120m	93±2.8	93±0.0	52±11	59±8.8	18.5	19.1

* Average of 2 Experiments, ** Average of 4 Exp

TABLE 2.2

L929 IRRADIATIONS
1.25GHZ, PULSED

SAR (mw/g)	PEAK POWER (KW)	PULSE WIDTH (μ sec)	REPITITION RATE (Hz)	EXP. TIME (min)	% VIABILITY		% PLATING EFFICIENCY		DOUBLING RATE	
					Cont.	MW	Cont.	MW	Cont.	MW
				0	90	90	86±13	86±13	24.2	24.2
49	500	2.2	0.211	120	64	45	24±6.3	78±8.4	26.8	23.8
				0	85	85	62±16	62±16	22.7	22.7
49	500	2.2	0.211	120	66	74	77±12	92±17	22.1	22.8
				0	81	81	79±15	79±15	20.7	20.7
46	250	2.0	0.422	120	76	66	79±13	79±15	19.4	19.5
				0	74	74	83±14	83±14	18.5	18.5
39	500	10	0.042	120	72	65	66±7.0	86±22	19.6	19.5

TABLE 2.3
IMR-90 IRRADIATIONS
2.45 GHZ, CONTINUOUS WAVE

SAR (mw/g)	TEMP. (°c)	EXP. TIME	% VIABILITY		% PLATING EFFICIENCY		DOUBLING RATE(hr)	
			Cont.	MW	Cont.	MW	Cont.	MW
	30	0m	92	92	4.3±1.5	4.3±1.5	39.6	39.6
1410	30	20m	92	88	-------	7.2±2.9	----	37.9
1410	30	40m	91	89	-------	6.6±0.9	----	39.8
1410	30	60m	91	91	7.2±2.6	7.6±2.2	38.2	39.8
	30	0m	96	96	7.0±3.5	7.0±3.5	45.9	45.9
1494	30	60m	90	91	6.8±3.0	8.8±0.8	45.0	44.1
1494	30	120m	95	94	5.4±2.8	3.6±0.6	44.9	46.0
	30	0m	89	89	4.0±2.5	4.0±2.5	44.3	44.3
1556	30	30m	--	89	-------	-------	----	42.0
1556	30	60m	--	85	-------	5.8±1.5	----	51.1
1556	30	90m	--	90	-------	2.6±0.6	----	43.4
1556	30	120m	90	--	3.0±2.6	-------	42.8	----
	30	0m	92	92				
1568	30	30m	--	92				
1568	30	60m	87	85				
1568	30	120m	91	90				
1568	30	180m	91	85				
	37	0m	95	95	7.0±3.0	7.0±3.0	39.2	39.2
104	37	60m	92	95	4.8±1.6	11.7±4.1	39.2	38.5
104	37	120m	88	80	10±2.5	9.1±1.9	39.2	39.2
104	37	180m	70	89	8.6±3.1	8.0±2.6	37.2	38.0
	37	0m	95	95	10.1±2.2	10.1±2.2	30.9	30.9
116	37	60m	90	95	11.2±2.1	10.2±2.9	28.7	30.0
116	37	120m	89	86	12.1±3.3	10.1±2.0	27.3	30.0
116	37	180m	77	89	11.6±3.0	9.4±2.6	27.2	27.0
	37	0m	97	97	3.9±1.4	3.9±1.4	37.1	37.1
117	37	60m	91	88	7.4±2.6	5.9±2.0	35.3	35.3
117	37	120m	83	90	7.0±2.2	7.1±2.1	32.8	34.2
*	37	0m	95±0	95±0	8.6±2.2	8.6±2.2	35.1±5.9	35.1±5.9
110*	37	60m	91±1.4	95±0	8.0±4.5	11.0±1.1	34.0±7.4	34.3±6.0
110*	37	120m	89±0.7	83±4.2	11.1±1.5	9.6±0.7	33.3±8.4	34.6±6.5
110*	37	180m	74±5.0	89±0.0	10.1±2.1	8.7±1.0	32.2±7.1	32.5±7.8
**	30	0m	93±3.3	93±3.3	4.8±1.5	4.8±1.5	41.7±4.1	41.7±4.1
1442**	30	60m	90±1.9	88±3.0	7.1±0.3	7.0±1.4	39.5±5.0	42.6±6.7
1442**	30	120m	90±5.0	91±2.3	5.1±2.0	5.4±2.5	40.2±6.5	40.1±8.3
1442**	30	180m	91	85				

* Average of 2 low SAR experiments
** Average of 5 high SAR experiments

TABLE 2.4
XP CLONE 12BE IRRADIATIONS
2.45 GHZ, CONTINUOUS WAVE

SAR (mw/g)	TEMP. (°c)	EXP. TIME	% VIABILITY		% PLATING EFFICIENCY		DOUBLING RATE(hr)	
			Cont.	MW	Cont.	MW	Cont.	MW
	37	0m	97	97	5.6±3.0	5.6±3.0	42.4	42.4
116	37	60m	94	94	5.3±1.3	3.8±1.6	42.4	46.2
116	37	120m	80	86	4.9±1.5	5.9±1.7	44.9	43.6
	37	0m	85	85	24.2±3.3	24.2±3.3	40.4	40.4
1165	37	60m	75	80	12.1±2.3	14.4±3.1	43.6	41.3
1165	37	120m	83	83	19.8±3.3	14.9±2.8	36.5	40.4

Fig. 2.1

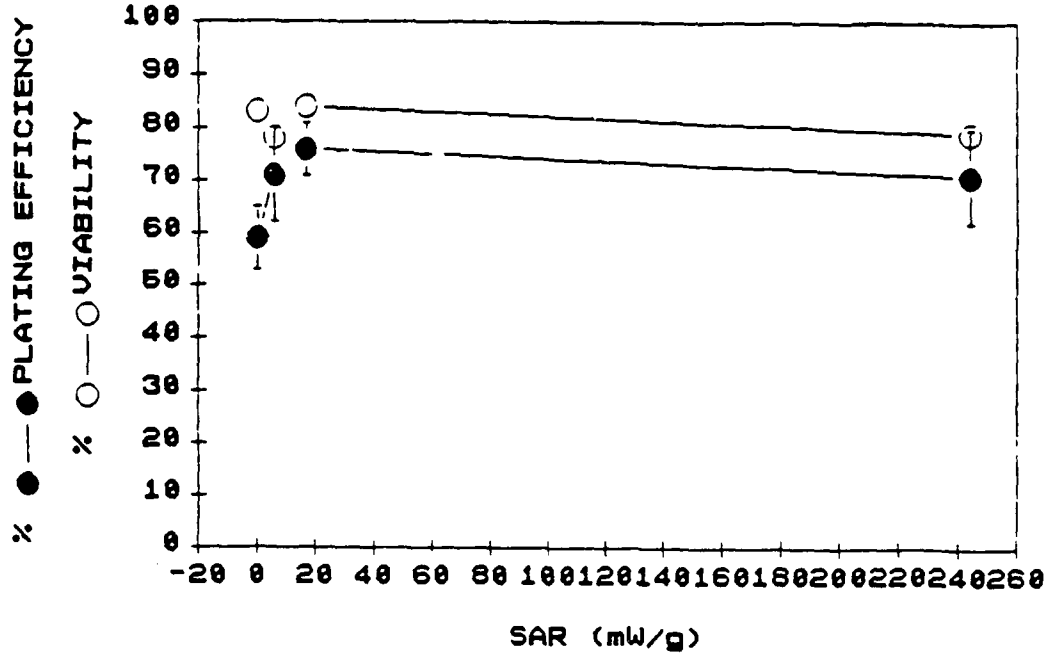

L929, Viability and Plating Efficiency with Varied SAR

Fig. 2.2a

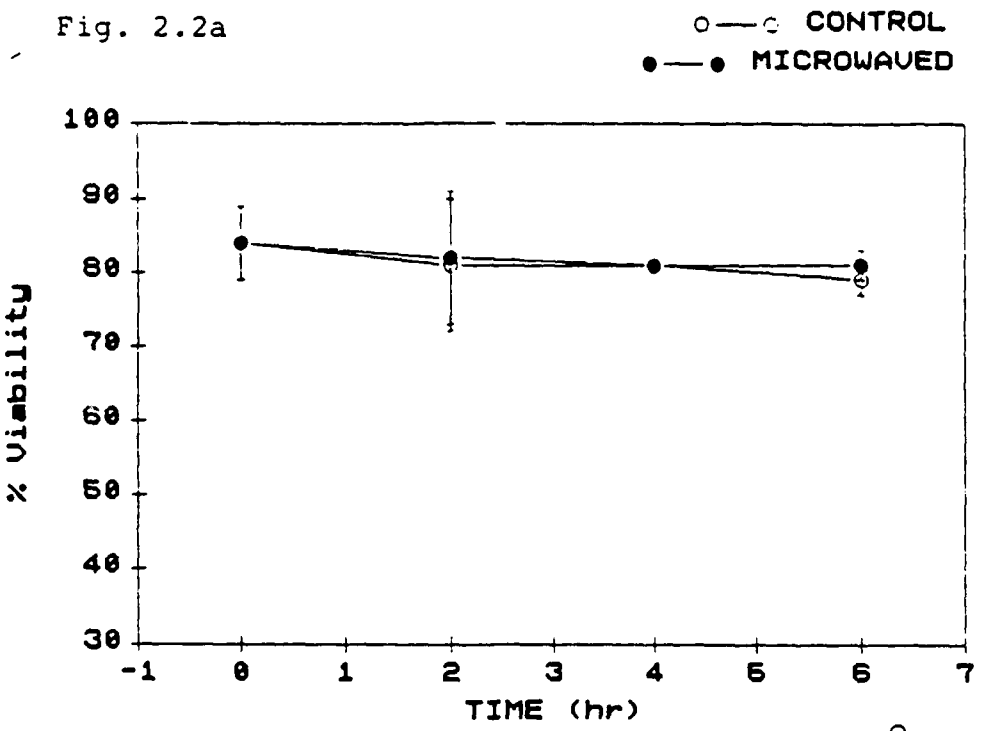

L929, Viability After Varied Irradiation Time, 30°, 31mW/g.

Fig. 2.2b

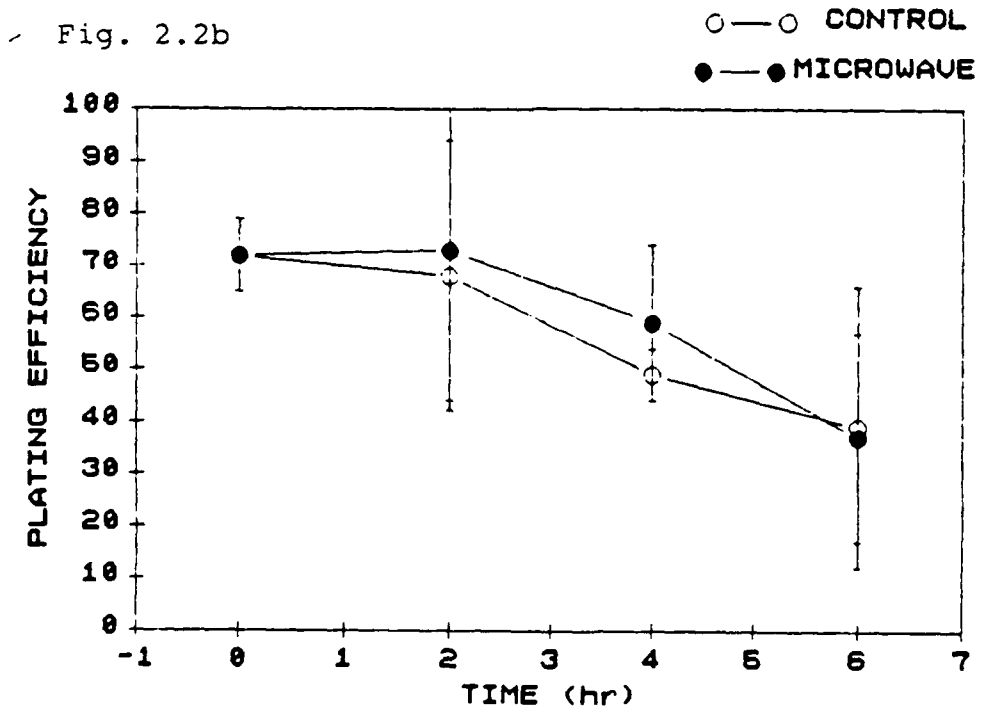

L929, Plating Efficiency After Varied Irradiation Time, 30°, 31mW/g.

Fig. 2.3a

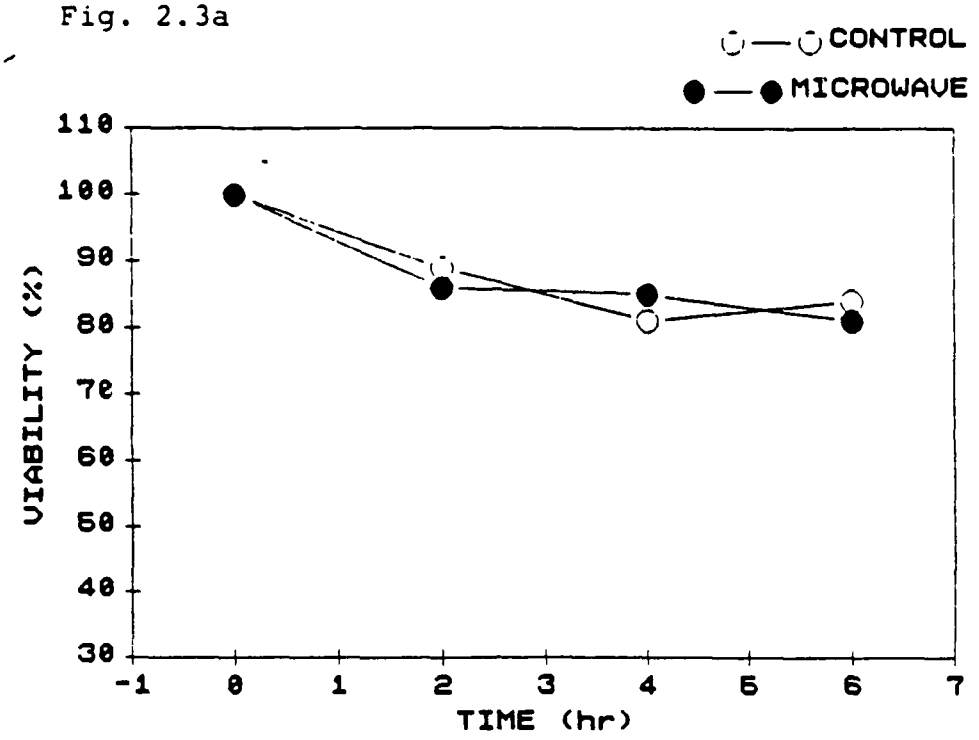

L929, Viability After Varied Irradiation Time, 37°, 31mW/g.

Fig. 2.3b

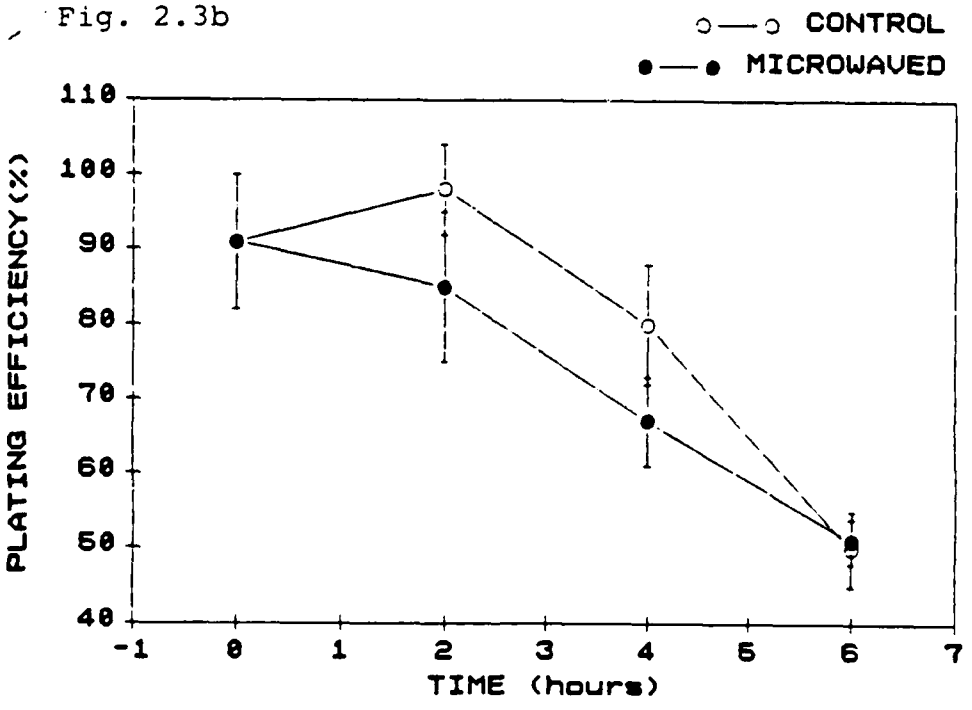

L929 Plating Efficiency After Varried Irradiation Time, 37°, 31mW/g.

Fig. 2.4a

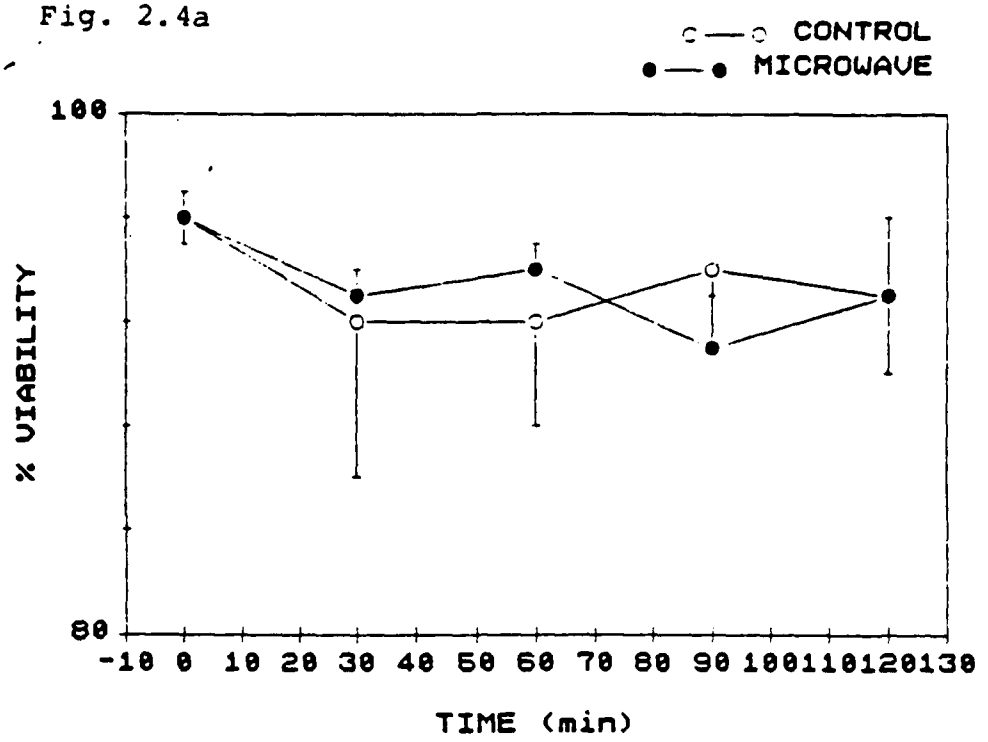

L929, Viability After Varied Irradiation Time, 1676mW/g.

Fig. 2.4b

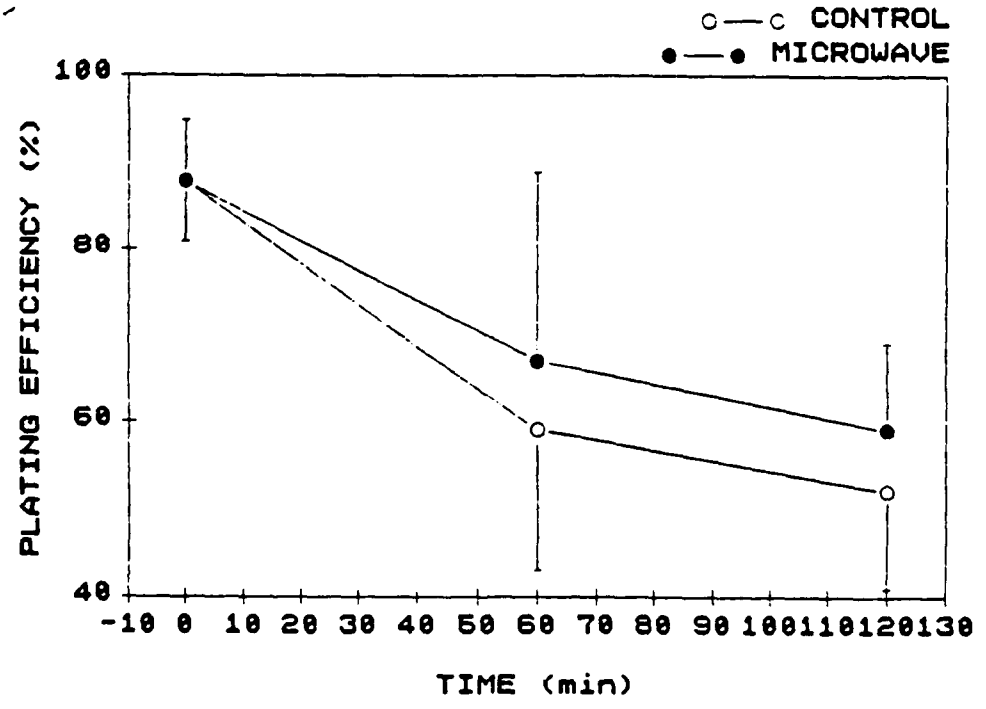

L929, Plating Efficiency After Varied Irradiation Time, 1676mW/g.

Fig. 2.5

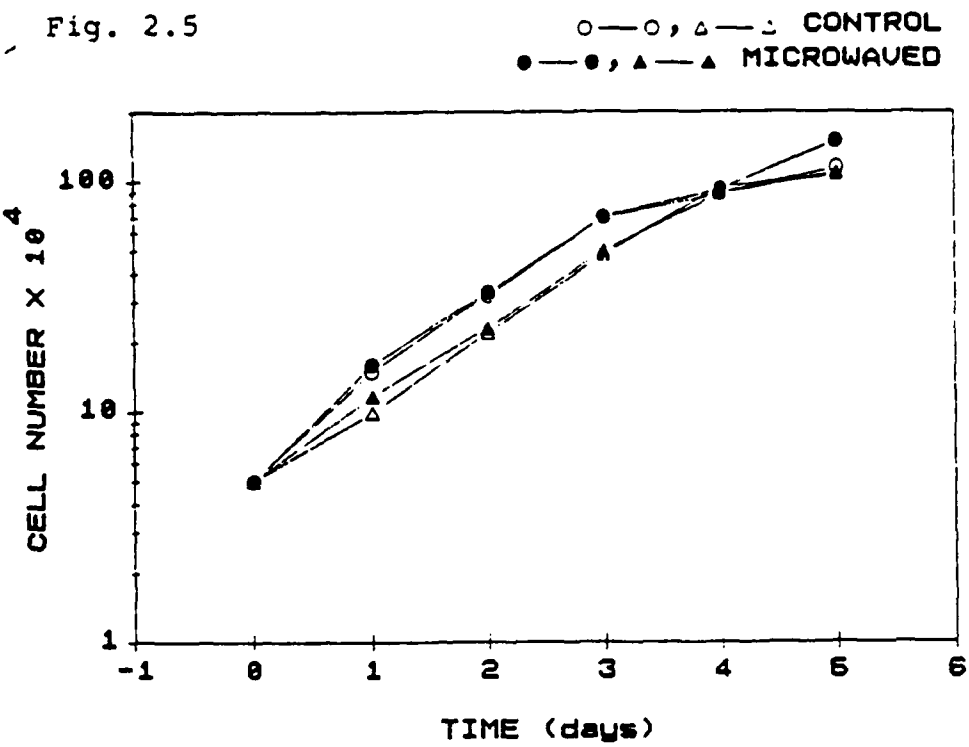

L929, Growth Curves After Irradiation,31 and 1442mW/g.

Fig. 2.6

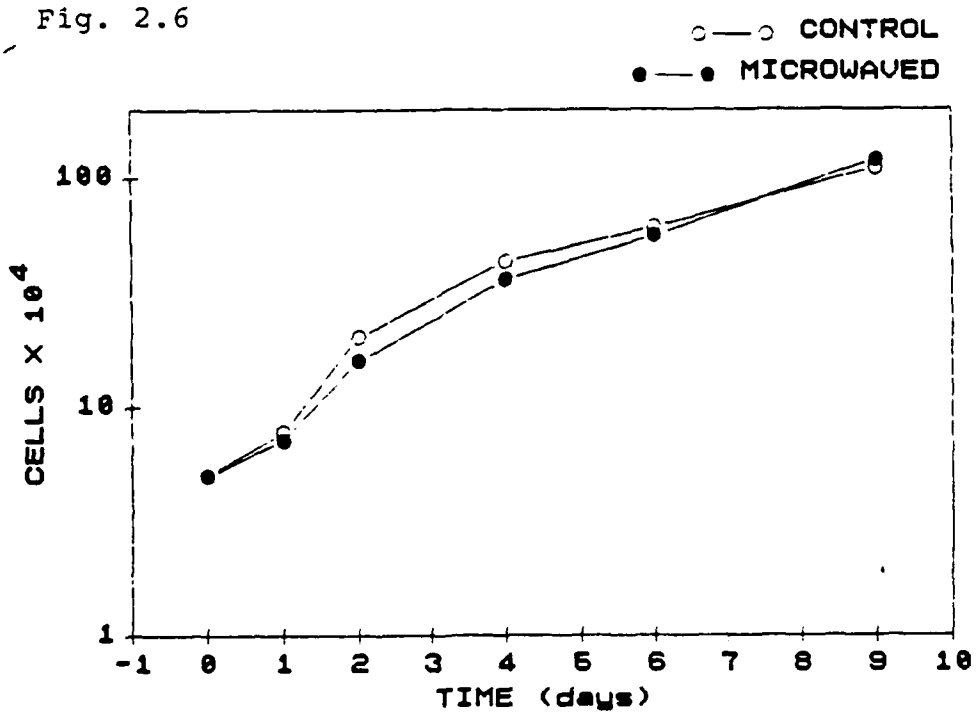

IMR90, Growth Curves After Irradiation, 1500mW/g.

Fig. 2.7a

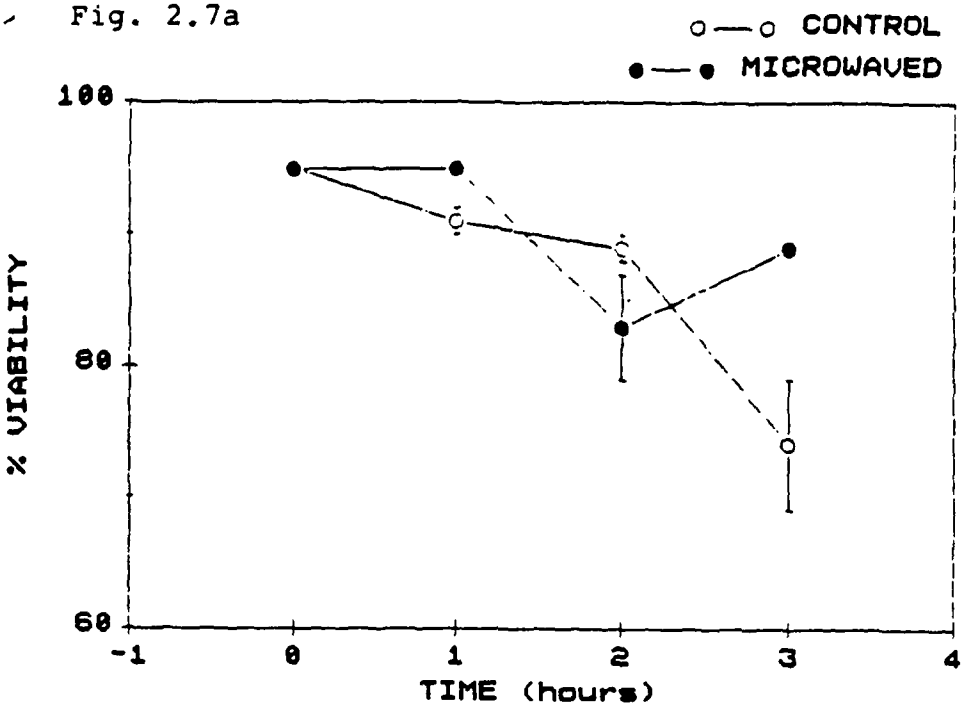

IMR90, Viability After Varied Irradiation Time, 110mW/g.

Fig. 2.7b

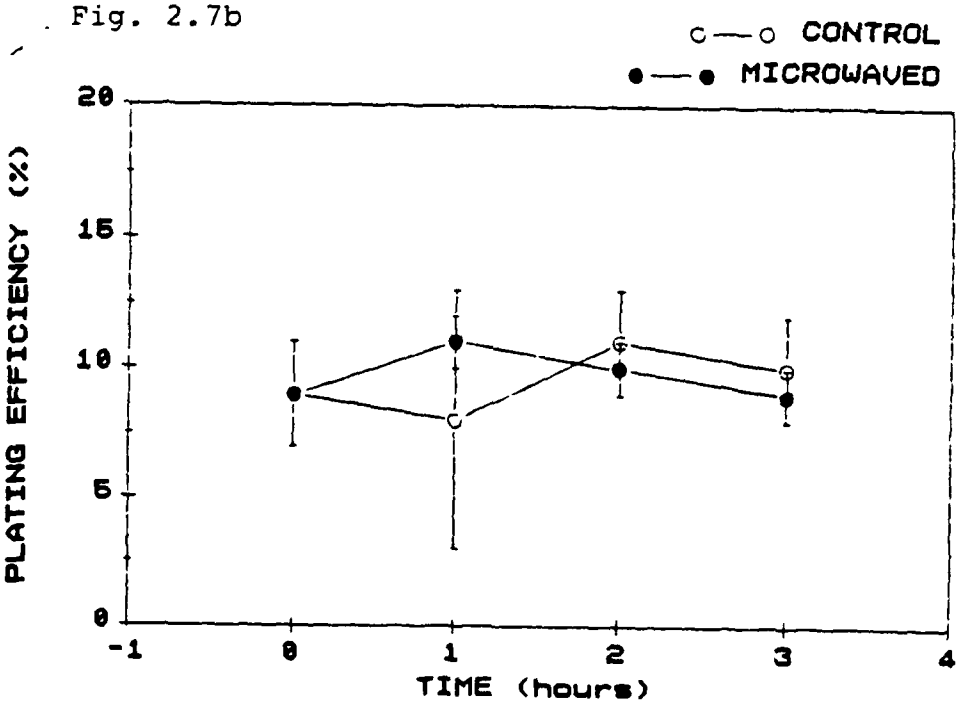

IMR90, Plating Efficiency After Varied Irradiation Time, 110mW/g.

Fig. 2.8

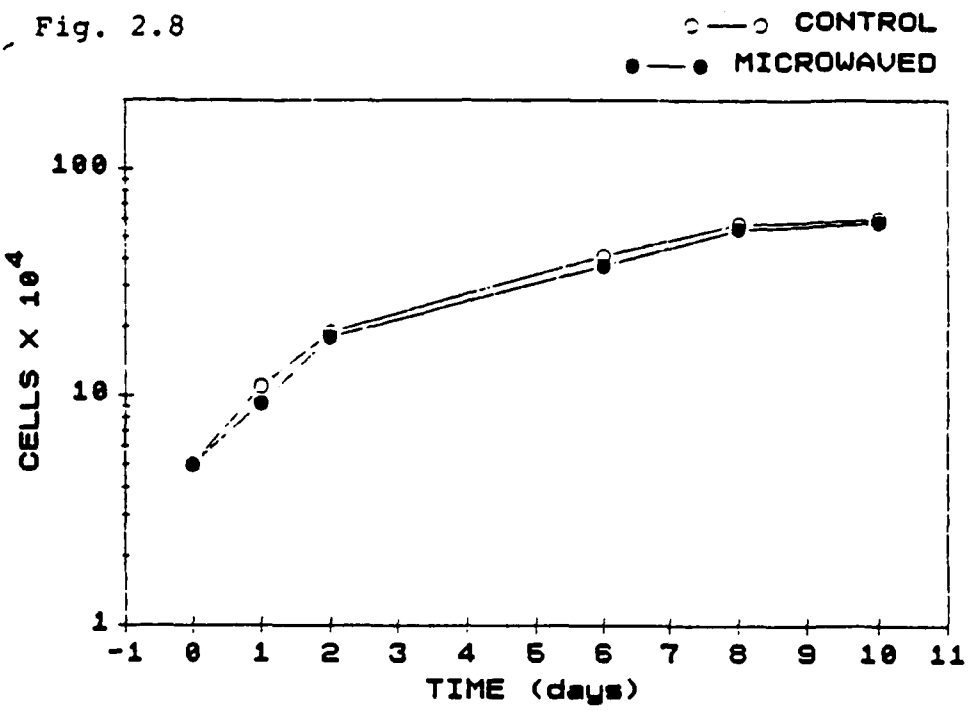

XP Cells, Growth Curve After Irradiation, 1165mW/g.

Fig. 2.9

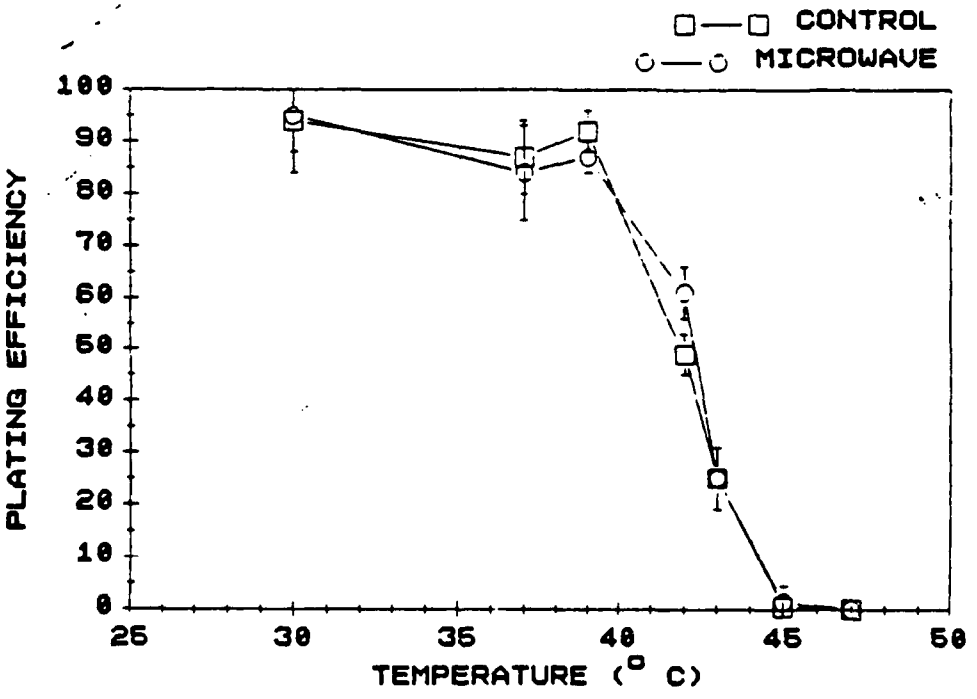

L929, Plating Efficiencies with Elevated Temperatures, Varied SARs.

Fig. 2.10a

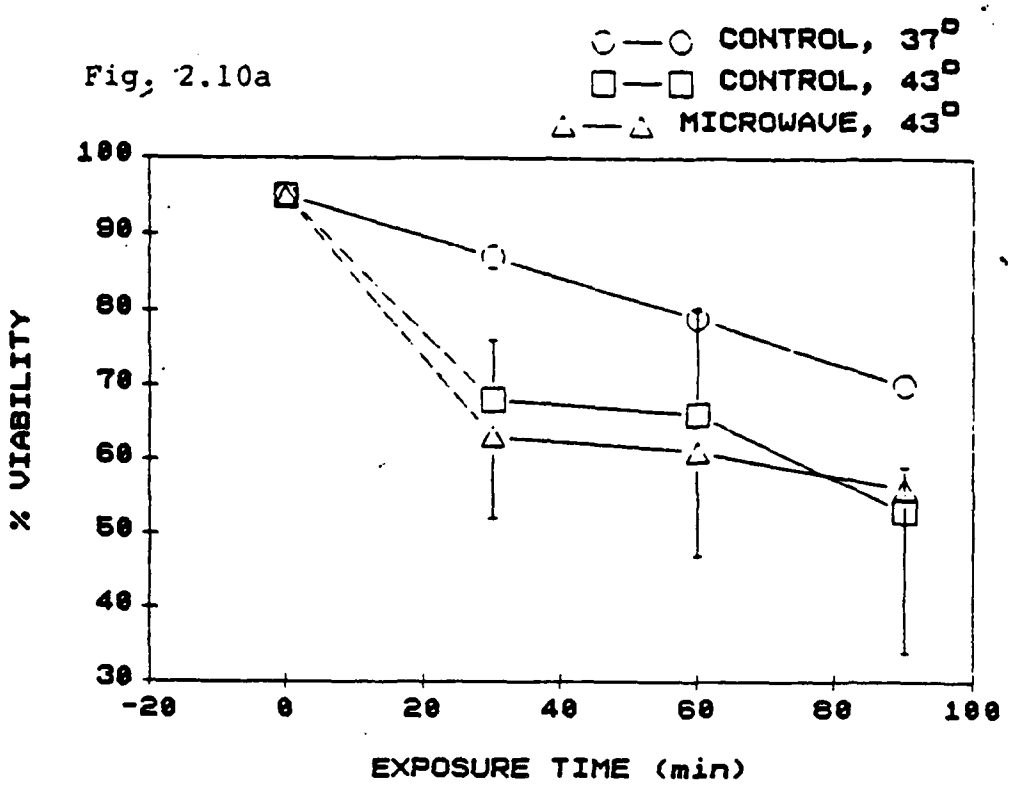

L929, Viability, 43°, Varried Irradiation Times.

Fig. 2.10b

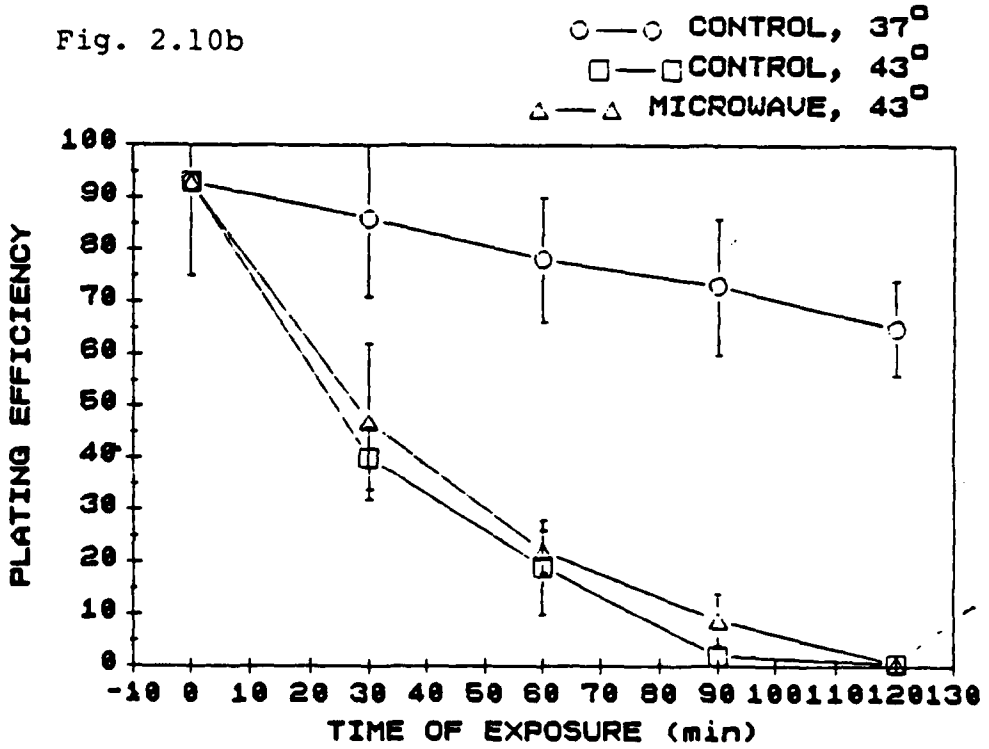

L929 Plating Efficiency 43°, Varied Irradiation Times.

Fig. 2.11

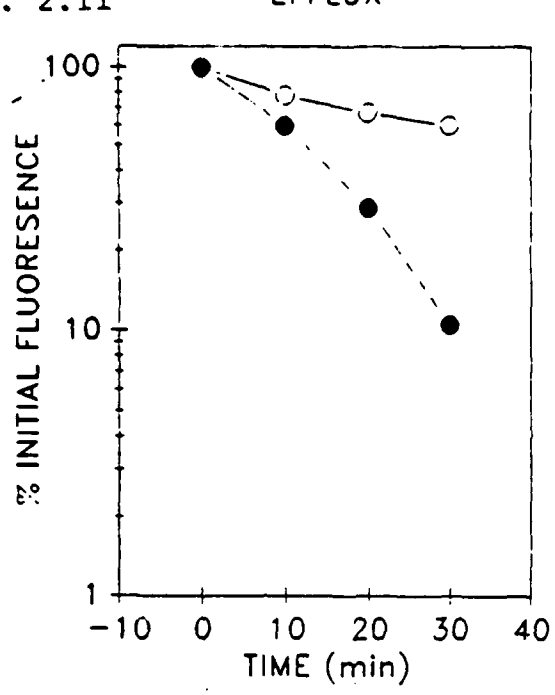

L929, Fluorescein Efflux With and Without KCN Present.

Fig. 2.12

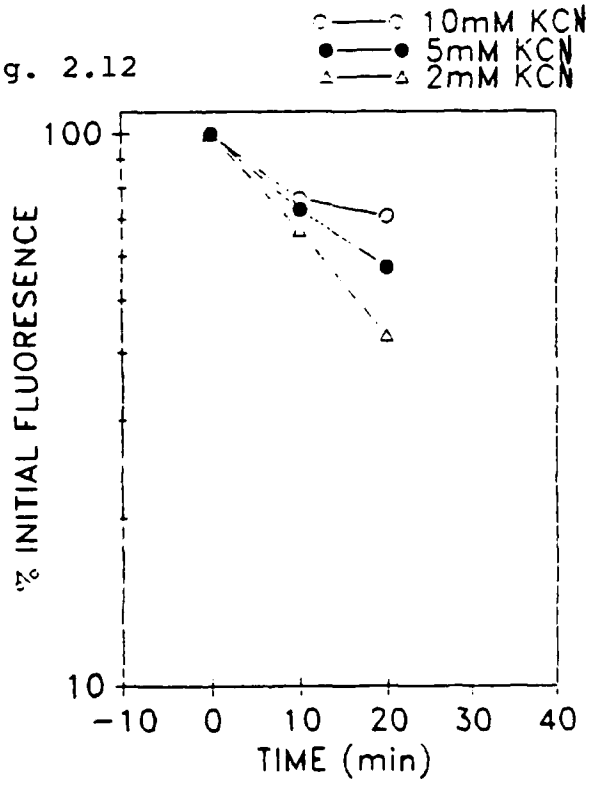

L929, Fluorescein Efflux With Varied KCN Concentration.

CHAPTER 3

MECHANISM OF MICROWAVE ABSORPTION OF DNA

R. K. Mohr, B. Saif, and T. A. Litovitz

The major goal of the physics group in this project was to examine the interaction of microwave radiation with DNA molecules. The initial effort was directed toward verifying if possible the reported resonant absorption in plasmid DNA for microwaves in the 2 to 9 GHz region. We measured the microwave absorption in several DNA solutions and were unable to detect any DNA related resonances. We found that experimental artifacts contribute to what appear to be absorption resonances but are in fact due to spurious reflections in the measurement system. We did find that DNA solutions exhibit an excess absorption relative to water or to the buffered saline solvent alone. The magnitude of that absorption is much larger than for water when the DNA concentrations in the solutions are considered. The nature of the excess absorption has not been fully characterized but could be related to some relaxation process involving the DNA molecules and their associated counter ions in the solution.

In addition to the DNA absorption measurements we conducted limited investigations in two areas suggested by the DNA absorption work. In the first we irradiated several DNA samples with high power microwaves at 1.25 and 9.37 GHz to determine if any gross direct damage to the DNA could be observed due to the excess absorption. No large scale damage to the DNA samples was observed. In the second we examined the problem of DNA damage resulting from exposure to copper microwave probes. We found both that copper dissolution is enhanced by microwave irradiation, and that copper dissolution involves the formation of hydrogen peroxide which is a biotoxin.

3.1 Introduction

The substance of the work being reported here is a study of the interaction of microwave radiation with DNA molecules. The goal of this study is the characterization and understanding of that interaction with particular sensitivity to mechanisms that could contribute to or result in damage to DNA or its functions. The initial motivation for this effort came from published experimental [1,2] and theoretical [3] work which indicated that resonant absorption could occur in DNA molecules. If this were the case it might be expected that relatively low levels of radiation could deposit sufficient energy into a DNA molecule to cause breakage or other damage.

Since the observation of resonant absorption in DNA was not expected and was somewhat controversial the first step in our research was to attempt to duplicate the observations reported by Edwards et.al. [1,2]. In order to do this we had to obtain a source of purified monodisperse DNA and establish the microwave techniques required to measure absorption in the DNA samples. We found that purified DNA could be prepared in fairly routine fashion using HPLC (high performance liquid chromatography) techniques. We obtained an HP 8510 automatic network analyzer (ANA) to perform the microwave absorption measurements. This instrument is similar to that used by Edwards but is a more modern design and has greater sensitivity. The results of our measurements on several DNA samples are that we observe an excess absorption associated with the DNA which is relatively frequency independent below about 9 GHz. We do not observe any resonances associated with the DNA. In our examination of the experimental technique used to measure the DNA absorption (open ended coaxial probe) we found that, when measuring moderately absorbing liquids, reflections from sample containers and liquid air interfaces cause what appear to be resonances. We suspect that the "resonances" observed by Edwards were due to some similar artifact.

In addition to the DNA absorption measurements, we have conducted limited investigations in several related areas which were suggested by the DNA work. The first investigation took advantage of the high power irradiation setup at the Walter Reed Army Institute for Research being used by our Engineering-Biology group. High power irradiations at two frequencies were performed on DNA samples. The samples were subsequently examined for damage with no significant damage being found. A second investigation was suggested by work conducted at the FDA [4] in which DNA was irradiated using a copper probe. Damage was observed and ultimately related to copper being dissolved from the probe. We initiated a study to determine the relationship between the copper probe, DNA, and microwave radiation. A potential outcome of the study is a microwave dosimeter.

3.2 Microwave Absorption in DNA

3.2.1. DNA Preparation

Our initial objective in this work was to duplicate if possible the observations by Edwards et. al [1,2] of resonant absorption in DNA. They claimed that certain conditions had to be met in order to observe the resonances. Specifically the DNA had to be monodisperse and free of contamination from proteins or other biological molecules. To place the resonances in the 1 to 10 GHz range required a molecule having on the order of a few thousand base pairs. Their work was done with pUC8.c2 and restriction fragments derived from it. Their initial reports specified the molecule as having 2740 base pairs. It has been subsequently reported [3] that the molecule used was actually a dimer of the 2740 bp molecule and thus had 5480 base pairs.

We acquired the assistance of Dr. John Golin of the CUA biology department in the preparation and purification of DNA. He attempted to follow the general method indicated by Edwards in the DNA preparation. Samples produced by these methods with what Golin considered normal care produced DNA which had unacceptably high levels of contamination from proteins. Protein contamination is indicated by a low 260/280 optical density ratio. Edwards has indicated that this ratio should be greater than 1.7. It was concluded that without a greatly increased time commitment from Golin the traditional preparation route would not be successful.

The biologists in our group suggested to us that recent work [5,6] indicated that HPLC could be employed to produce purified DNA in relatively large quantities in routine fashion. In these preparation methods the DNA is produced by normal techniques such as growth in E. coli and given preliminary standard purification and concentration treatments. The final purification which is quite difficult using traditional methods is made quite simple using HPLC. The DNA is injected onto a prepared column which holds it until it is eluted by the appropriate eluent concentration. By employing a gradual gradient in the eluent not only can protein and RNA contamination be removed but the various configurations (linear, circular, supercoiled) of the DNA may be separated and collected.

We purchased a silica gel based anion exchange column designed for plasmid DNA purification. The eluent for this column are buffered high concentration salt solutions. Preliminary work with the column indicated that it was capable of good resolution for the plasmid DNA. In Figure 1 we show a trace of the HPLC detector output which shows a single DNA peak separated in time from the nearest contamination peak by about thirty minutes. The trace was obtained from an analytical run sized injection of a moderately pure plasmid DNA sample. The solution represented by the DNA peak

was collected and the presence of purified DNA was confirmed by gel electrophoresis. We found, however, that the column did not perform consistently. Further we found that because of their corrosive effects high salt eluents were not compatible with the HPLC instrument available to us. Dr. Nardone brought to our attention a series of review articles by Dr. John A. Thompson of the NIH. One of those articles [7] involved the purification of plasmid DNA using a polymer based HPLC column and noncorrosive organic solvents.

We contacted Thompson and he confirmed our experiences with the silica based column. His own experience with that column type was that its performance was inconsistent and that it had a very short useful life. The column that he uses routinely for DNA purifications is not marketed commercially but the materials for its preparation are available. We obtained the materials for a preparative column and packed a column. In our discussions with Thompson he became interested in our efforts and offered to prepare several samples of purified plasmid DNA for us.

Thompson routinely works with a 2668 bp plasmid which he has named PSASAS. This plasmid is well characterized and can be readily modified. If we were to observe any resonances it was hoped that we could make modifications to the DNA structure and observe any changes in the resonances. The HPLC and gel electrophoresis traces for a sample of supercoiled PSASAS prepared for us by Thompson is shown in Figure 2. This sample was highly concentrated (1.72 g/l) and was relatively free of protein contamination as indicated by its 260/280 ratio of 1.8. The DNA was in an aqueous buffer having 5mM NaCl, 10mM Tris-HCl and 0.1 mM EDTA. This sample as well as several others prepared for us by Thompson have been the subject of our microwave experiments.

3.2.2 Absorption Measurements

There are a number of techniques available for the measurement of microwave absorption. The particular method selected is dictated by the particular experimental requirements such as frequency range, required accuracy, sample size and measurement speed. The automatic network analyzer used to make transmission or reflection measurements offers an excellent choice in the measurement of small liquid samples such as suspensions of biological molecules, e.g., DNA. Stuchly and co-workers [8] have been major proponents of a method employing the ANA with a simple probe consisting of an open ended coaxial line. This combination has the capability of rapid relatively accurate broad band measurements of sample volumes as small as a few hundred microliters. This method has been our method of choice and was the method employed by Edwards in his measurements.

The instrument used in our measurements was an HP 8510B network analyzer system consisting of an HP 8340A synthesized

sweeper, an HP 8515A test set and an HP 8510B detector, control and display unit. The sweeper provides a high accuracy phase locked frequency source providing up to 801 arbitrary frequency points between 45 MHz and 26.5 GHz. The test set directs the signal to the device under test or in our case the probe and provides test and reference signals to the detector section. After detection the signals are processed by the control and display unit which can display the data in a variety of formats or send it on to an independent computer for further analysis. The probe we used was made with standard 0.141" diameter semi-rigid coaxial cable with a precision 7 mm connector on one end. The cable consists of a copper cylinder and concentric center conductor separated by teflon insulation. The end of the probe was ground flat and gold plated. The samples were contained in standard microcentrifuge tubes which were temperature controlled using a circulating water jacket for the tubes. In the case of the open ended probe method of dielectric measurement one measures the S_{11} parameter which is the reflection coefficient for signals incident at the probe end from the test set port 1. That reflection coefficient can in turn be related to the dielectric properties of the media surrounding the probe tip.

The method relies on the assumption that one can model the discontinuity represented by the probe end as a lumped impedance consisting of a pair of shunt capacitors and a shunt resistance as shown in Figure 3. C_f represents the capacitance due to fringing fields extending into the teflon of the coax cable at its end. $C_o \varepsilon^*$ is the capacitance due to the fields extending into the external dielectric i.e. the sample with complex dielectric ε^*. R is a resistance added to account for radiation conductance. In the simplest cases R can be ignored and C_o and C_f can be considered to be constants independent of frequency and sample dielectric. In the present study we have been concerned primarily with determining the excess absorption due to DNA in a buffer solution. By a proper choice of calibration conditions some implicit correction is made for C_o and C_f variation as well as radiation loss. In our case of measuring small absorption differences the implicit corrections are sufficient to permit the use of the simplified circuit model for the probe.

In the case of the open ended probe the network analyzer measures the complex reflection resulting from the discontinuity at the end of the probe. In general an impedance discontinuity will cause a reflection coefficient given by:

$$S_{11} = \frac{Z - Z_o}{Z + Z_o} \qquad (1)$$

where Z is the impedance at the probe end and Z_o is the characteristic impedance of the coaxial cable. In the case where we assume C_o and C_f are constants and that radiation may be ignored this equation may be rewritten as:

$$S_{11} = \frac{1 - j Z_0 (C_0\epsilon^* + C_f)}{1 + j Z_0 (C_0\epsilon^* + C_f)} \quad (2)$$

where $j = \sqrt{-1}$. This expression may be solved for $\epsilon^* = \epsilon' - j\epsilon''$ to give:

$$\epsilon' = \frac{2|S_{11}| \sin(-\theta)}{\omega Z_0 C_0 [1 + 2|S_{11}| \cos\theta + |S_{11}|^2]} - \frac{C_f}{C_0} \quad (3)$$

$$\epsilon'' = \frac{1 - |S_{11}|^2}{\omega Z_0 C_0 [1 + 2|S_{11}| \cos\theta + |S_{11}|^2]} \quad (4)$$

where w is angular frequency and Θ is the phase. Finally, microwave absorption is given by:

$$\alpha = \sqrt{2\epsilon'} (\omega/c) \sqrt{\sqrt{1 + (\epsilon''/\epsilon')^2} - 1} \quad (5)$$

where c is the speed of light in vacuum.

The ANA is designed primarily for the testing of microwave devices and the standard calibration procedures must be modified or replaced in order to use the instrument for dielectric measurements. In any electrical network there are spurious signals due to a variety of causes. The source of these spurious signals is not of major concern as long as their effects can be eliminated by a calibration procedure. In the case of reflection measurements the network analyzer circuit may be modeled in such a way that there are three sources of measurement error. The measurement of reflection coefficients of three carefully chosen and well characterized standards will supply the data required to obtain error coefficients which will correct for these major sources of error.

In the standard calibration procedure one calibrates at the test port of the test set or at the end of a test cable attached to the test port. The calibration is accomplished by measuring a short, an open and a 50 ohm load. Internal routines supplied with the ANA automatically compute the error coefficients and store them in the instrument memory. With the correction turned on the signals are corrected so that the effects of spurious signals and other errors are removed up to the calibration plane represented by the test port or cable end whichever is appropriate. The corrected reflection coefficient will represent the true reflection coefficient at the calibration plane.

In our case the probe consisting of a connector and a length of semi-rigid coaxial cable is connected to the test port. The

standard calibration procedure corrects errors only up to the port connector but does not account for reflections from the probe connector or from probe coax flaws nor does it account for losses and phase shifts in the probe coax. There are several ways to get around this problem. One can shift the reference point of the calibration by adding the proper phase shift due to the distance from the test port to the probe tip. In addition, most spurious reflections due to the probe connector can be eliminated by a gating procedure available with the HP 8510. The control unit lets you observe the signal in a simulated time domain mode obtained by fourier transforming the signal. By placing a gate in time around the response of the probe tip one can eliminate spurious responses due to sources such as the connector. The remaining signal is then reverse transformed back to frequency mode and one has the response only due to what was inside the gate. In principle this method is very attractive but we found that it has several flaws for quantitative results. It does not account for any losses in the probe coax and it is possible to distort the signal in ways not easy to predict. A second method of shifting the calibration plane is to measure a short or open circuit with the probe. This data is then stored to be used to normalize any further measurements. This is equivalent to adding a response calibration to the standard calibration and is a useful method for quantitative measurements. This response calibration does not, however, correct for errors due to radiation conductance or to fringing capacitance variation. A third approach is to calibrate by measuring three standard conditions at the probe end itself. If one chooses as one of the calibration conditions a dielectric media with properties near to that of the unknown to be measured, there is some implicit correction for C_f variations and radiation losses since the correction procedure forces the ANA to yield the correct results for the calibration conditions. This last procedure is the primary calibration method that we have used.

The three standard conditions we have used are an open, a short and a saline solution. The open is easily achieved by measuring the probe with no material near its tip. The short is moderately difficult to achieve due to the problem of making a reproducible short at all frequencies. It has been suggested [9] that a piece of metal foil backed by a rubber block and pressed against the probe end will make a good short. In practice it is difficult to get reproducible results. We built a fixture, a sketch of which is shown in Figure 4, which clamps onto the end of the coax and which holds a gold plated grounding plate which can be driven against the probe end by a screw. One can easily determine when a good short has been achieved by simultaneously observing a stored spectrum of S_{11} for the open while observing the spectrum of the short. This can be done in real time using the ramp mode of the HP 8510 which provides spectra almost instantaneously. When a good short is obtained the spectra of the short will overlap that of the open except for frequency shifts in the noise.

In order to calculate the error correction coefficients it is necessary to be able to calculate the theoretical reflection coefficients corresponding to the three standard conditions. In the case of the short the reflection coefficient is simply -1. In the cases corresponding to the open and the saline solution we use equation 2. Values for C_o and C_f have been calculated and measured by Stuchly et. al. [10] for several standard sizes of coaxial cable including the size we have used (0.141' O.D.). ε^* for air is taken as equal to 1 and for saline solutions is calculated from formulas given by Stogryn [11]. Using the error model and corresponding equations given by Hewlett Packard for the network analyzer used in reflection mode we can solve for the complex correction coefficients at each measurement frequency. These coefficients are stored in the computer and are used to correct subsequent measurements. This correction procedure adequately corrects for errors introduced by the network analyzer system. In certain cases it does not correct for errors associated with probe itself. Depending on the measurement frequency and the dielectric constant of the sample, substantial errors may occur. These are due primarily to variations in the fringing field or the fringing capacitance C_f inside the probe tip and due to radiation losses which increase with frequency. As mentioned earlier these losses are partially compensated for by the calibration procedure for conditions near the calibration conditions. Thus if the sample dielectric properties are close to those of the calibration liquid the measured dielectric values will have relatively small errors. These errors increase as the sample properties depart from those of the calibration liquid. In our measurements we have chosen the calibration liquid so that its properties are close to that of the DNA solutions to be measured thus minimizing the errors.

In principle one can eliminate the errors by using an alternate method of calculating the theoretical values for the reflection coefficients which take into account the radiation and fringing field problems. This has been done by Mosig et. al. [12] for the case of a probe which includes an infinite ground plane. In that case it is possible to find solutions for the fields both inside and outside the probe in terms of the dominant incident TEM mode and the higher order TM modes excited by the discontinuity at the probe end. By matching the fields at the boundary according to the appropriate boundary conditions it is possible in principle to obtain the magnitudes of all the contributing modes and in turn the reflection coefficient at the boundary. In practice it is sufficient to match the fields at a few selected points on the boundary and for only the first few possible modes as rapid convergence is generally found. Mosig et. al. wrote a computer program which will calculate the reflection coefficients for arbitrary coaxial dimensions and external dielectric constant. The program was made available to us at a nominal cost. The program can be used to generate the reflection coefficients corresponding to the calibration conditions for the ANA.

In order to take full advantage of this approach it is necessary to be able to solve the inverse problem [13]. That is to calculate the dielectric constant responsible for a measured reflection coefficient. It is possible to employ one of the standard iterative fitting routines in conjunction with the Mosig program to solve this problem. Since the calculations involve complex arithmetic and extensive numerical calculations a mini or larger computer is probably required to perform the calculations in a reasonable time. We were successful in assembling the appropriate routines on a Dec Vax minicomputer.

One of the advantages of the open ended probe measurement method is that the dimensions of the probe are rather small and thus can measure a relatively small sample volume. The Mosig approach assumes an infinite ground plane since that is the only geometry for which mode solutions are available. We thus conducted an investigation to determine the minimum ground plane which could be used to approximate an infinite ground plane. We made measurements with ground planes having diameters as large as 6.5 cm and could not conclude that this was sufficient to approximate an infinite ground plane for all frequencies and sample dielectric values of interest. Even for a measurement range for which such a ground plane was sufficient it is much too large to be used for the measurement of small volume samples. The largest ground plane which would be practical for samples with a volume near 1 ml would be about 9 mm in diameter. The reflection coefficients for a probe having such a small ground plane were significantly different from those measured with the 6.5 cm diameter ground plane and so we conclude that this method is not very useful for small volumes in the frequency range for which we have current interest. It is possible that with a study of the relationship of measured values with and without a ground plane empirical corrections could be found to allow measurement without a ground plane. It was judged that such a study was beyond the scope and needs of our present goals.

3.3 Experimental Results

We examined two samples of the PSASAS plasmid DNA supplied to us by Dr. Thompson. The first was in supercoiled form and the second was linearized. The 260/280 ratio for the samples was 1.8 indicating a low level of protein contamination. The supercoiled form was measured at two DNA concentrations -- 1.72 mg/ml and 0.5 mg/ml. The linear form was measured at a concentration of 0.53 mg/ml. Both samples were in a buffer solutions consisting of 5 mM NaCl, 10 mM Tris-HCl (7.5) and 0.1 mM EDTA. The actual Na content in the solutions was higher than that of the buffer solution. We are not certain of the origin of the excess but assume that it was carried with the DNA solution before the final buffer solution was added to the DNA. Since ionic conductivity contributes to microwave absorption this will be discussed further below.

The samples were measured in the temperature range from 4°C to 34 °C. Sample volumes ranged from 0.3 ml to 1 ml. The typical measurement procedure was as follows. The ANA was allowed to warm up for at least one hour to stabilize. The samples and calibration standard were allowed to equilibrate at the measurement temperature in a bath during this time. The instrument was calibrated using the procedure outlined above over a frequency range from 45 MHz to 18.045 GHz. The reflection coefficient of the calibration liquid was measured by placing the microtube containing the appropriate saline solution in the circulating water jacket. The tube and jacket were then positioned so that the probe was centered in the tube with its tip about 5mm below the surface of the sample. The samples were then measured in the same manner in the same frequency range and the data was stored in the computer for processing.

Typically we examined the dielectric constants as well as the microwave absorption of the samples calculated from the dielectric constants according to equation 5. Since the buffer solution itself contributes to the absorption, we also examined the difference in absorption of the DNA samples and water, the buffer solution or a saline solution with a Na concentration near that of the DNA solution. When plotted, these absorption difference spectra often exhibited what appeared to be resonant absorption peaks as seen in Figure 5. It was soon determined that the magnitude of these peaks could be altered by adjusting the probe position within the sample container indicating that the peaks were not due to the dielectric discontinuity represented by the sample at the probe tip. The peaks were due to some reflection resonance of geometrical origin.

The calibration procedure will correct for spurious reflections such as these as long as certain conditions are met. As proof of this, if we remeasured the calibration liquid immediately after calibration without disturbing either the probe or the sample test tube we would obtain a smooth well behaved absorption coefficient. If, however, the test tube position was moved relative to that of the probe tip by as little as 0.25 mm significant resonant peaks would appear in the reflection spectrum and resultant absorption spectrum. These could be minimized by a careful repositioning of the test tube but only with great difficulty. If we removed the test tube and replaced it with one containing the same or other liquid we always observed substantial resonance peaks. Their magnitude could be changed by adjusting the relative positions of the probe and test tube but in general they could not be eliminated. We could only conclude that the resonances were artifacts due to reflections from discontinuities away from the probe tip. The frequency range of these resonances is in the 2 GHz to 9 GHz range reported by Edwards et al. to be that for the DNA resonances. We concluded that since our measurement arrangement is similar to that of Edwards, it is likely that what he saw was an artifact similar to those we observe.

Our initial measurements indicated that although we did not observe any resonances due to the DNA we did see an excess absorption relative to that of the buffer solutions. We suspected that the ionic content of the solutions might be higher than expected so we had the Na and K contents of the DNA solutions analyzed by our analytical lab. The results of measurements on two separate occasions indicated the concentrations and measurement precision given in Table 1.

Table 1

Sample	Na (mM)	K (mM)
Supercoiled DNA 1.72 mg/ml	64.7 ± 0.7	N/A
Supercoiled DNA 0.5 mg/ml	22.0 ± 0.5	2.0 ± 0.1
Linear DNA 0.53 mg/ml	8.9 ± 0.15	0.3 ± 0.2

It is seen that the Na content is higher than that which was specified for the buffer solution (5 mM Na). The Na contents are self consistent as seen from the fact that the 0.5 mg/ml DNA solution was prepared by diluting 0.3 ml of the 1.72 mg/ml solution with 0.7 ml of the buffer solution. At this point we can only speculate that substantial quantities of Na are attached to the DNA before the storage buffer is added. Since this is the case it appears that we must compare the absorption of the DNA solutions with that of buffer solutions containing the true ionic content of the DNA solutions. At the end of the reporting period for this report we had only begun to make those comparisons. The preliminary results of those comparisons indicated that at least for frequencies below about 9 GHz there was a significant absorption excess in the DNA solutions relative to the appropriate saline solutions. Above about 9 GHz the picture was less clear because at those frequencies the background absorption due to water has become relatively large and small differences in absorption can not be measured easily. There appeared to be a general trend, however, that in the high frequency region the DNA solutions had a lower absorption than the buffer solution indicating the possibility of some relaxation process.

In Figure 6 we show a typical absorption difference spectrum for the 0.5 mg/ml supercoiled DNA sample measured at 23°C. The spurious reflection peaks though not quite as large as those seen

in figure 5 are still quite evident. Between about 0.1 and 7.5 GHz the excess absorption exhibited by the DNA relative to that of the storage buffer is about 30/m. The background water absorption in this frequency range goes from about 10/m to about 500/m. At the lower frequencies the excess absorption associated with the DNA solutions is significantly higher than the water absorption and if one considers the absorption on a per weight basis the DNA excess is very high since it is present at a concentration of 0.5 parts per thousand. The supercoiled DNA was also measured at a concentration of 1.72 mg/ml. The results of the difference spectra for the absorption for this sample is qualitatively the same as for the diluted sample but with the absorption excess being proportionately larger as one would expect from the DNA concentration.

A sample of PSASAS DNA in linear form and at a concentration of 0.53 mg/ml was measured in the same way as the supercoiled DNA. In this case the excess absorption was only about 30% of that found for the Supercoiled DNA at approximately the same concentration as can be seen in Figure 5. Since the conformation of the DNA in linear and supercoiled form are quite different this may shed some light on the nature of the absorption mechanism. The Na content of the linear DNA solution was also lower than that of the supercoiled DNA solutions. There may be some cooperative involvement of the DNA and the Na which contributes to the absorption excess which requires sufficient Na content to be effective.

The microwave absorption spectra were measured at two temperatures in addition to 23°C -- 4°C and 35°C. At this point only qualitative analysis of the data has been made. The results are that the absorption excess as well as the frequency at which the excess seems to disappear increase with temperature. This would be consistent with the presence of a relaxation in the DNA/buffer solution.

At this point we are not prepared to fully explain the observed absorption behavior of the DNA solutions. We are confident that we can preclude the existence of resonant absorption in these materials. We have identified an experimental artifact which causes peaks in the absorption curves which are in the same frequency range as the claimed DNA resonances and have peak to peak magnitudes similar to those reported by Edwards et al. [1,2]. We believe that these artifacts may be the source of the so called resonance absorption. Further we have observed an absorption excess in the DNA solutions below 9 GHz at near room temperature and below 18 GHz at 35°C. Our preliminary evaluation indicates that ionic conductivity due to Na and K, the major mobile ions available, is insufficient to fully explain this absorption. We speculate that the absorption is due to some relaxation process such as that of a DNA counter ion system. To test this hypothesis fully will require further work.

The reflection artifacts must be eliminated from the measurements by improving the probe technique or by using another type of sample cell for measurement. The effect of ionic content in the DNA solutions on the resultant absorption must be determined. Measurements of DNA absorption characteristics as a function of molecule size must be made. Finally when the data is of sufficient quality absorption models must be examined in order to explain the observations.

3.4 High Power Irradiation of DNA

Experiments were conducted in which high power pulsed microwave radiation was directed at samples of supercoiled DNA. The purpose of the experiments was to determine whether large scale damage to the DNA would be observed. The details of the irradiations are given in section 1.5 of this annual report and are summarized here. The irradiations were at near room temperature, at two frequencies (9.37 GHz and 1.25 GHz) and at 78 KW and 200 KW peak powers respectively. The irradiations were for 1 hour. After irradiation the irradiated samples and unirradiated shams were analyzed by gel electrophoresis for damage to the DNA. The results were that no extensive damage to the DNA could be observed. The analysis would only have revealed damage to substantial numbers of DNA molecules (10% or more). If there is direct damage to the DNA a more sensitive test will have to be applied to observe it. Such tests will be considered for future work.

3.5 DNA/Copper/Microwave Interactions

Published work at the FDA [4] indicated that DNA solutions irradiated with microwaves using copper probes resulted in breakage damage to the DNA molecules. It was found that Cu was dissolving and was a possible cause of the resultant damage. We began a study to determine the nature of the Cu dissolution. It was hoped that if the dissolution was a predictable process it could be exploited for some use such as an integrating dosimeter for microwave irradiation. This idea was initially encouraged by preliminary results which indicated that Cu dissolution was proportional to the square root of the microwave power. Subsequent experiments have indicated that the dissolution process is very interesting but much more complicated than initially thought.

Experiments were conducted jointly by the physics and engineering groups. The details of the experiments are given in section 1.7 of this annual report. Initial experiments were done using a coaxial copper probe as both the source of copper and microwaves. In later experiments oriented copper discs within a test tube were irradiated within a waveguide. In general the presence of microwave radiation increased the dissolution of copper. If the electric

fields were oriented parallel to the Cu surfaces which would generate surface currents and heating near the surface it appears that temperature plays the major role in determining the dissolution. When the temperature of the solution was held fixed it was found that there was no microwave effect. The boundary conditions for the electric field outside a conducting surface are such that the tangential field must vanish. If the electric field dominates the microwave effects on dissolution this would explain the absence of nonthermal effects for the cases of tangentially oriented electric fields. Irradiations with the coaxial probe result in electric fields perpendicular to the Cu surfaces. The temperature was not monitored in those experiments and thus although Cu dissolution increased as the square root of the power or equivalently as the electric field strength the results are ambiguous. Additional experiments would be required to isolate the direct microwave effects if any.

During the course of these experiments Dr. Aaron Barkatt who directed the chemical analysis of our solutions, began performing experiments of his own related to the problems of Cu dissolution. He indicated to us that the chemistry of the system was apparently quite complicated and not completely understood. The complexity of the system indicated that a dosimeter would be difficult to produce based on such a system. We decided to suspend the Cu irradiation experiments at least until the chemistry was better understood.

The work that Barkatt has performed on the dissolution of Cu is of general interest for the understanding of dissolution of metals. Several of his results have possible implications for biologists as well. He found that DNA and microwaves both had substantial effects on Cu dissolution. It was found that hydrogen peroxide, which can itself cause biological damage, is formed at a rate proportional to the rate of Cu dissolution. It was found that oxygen is required in the solution to get Cu dissolution. The Cu dissolution rate increases by more than a factor of two as the solution temperature is raised from 10°C to 50°C. Barkatt is continuing to examine the dissolution of Cu in aqueous solutions and expects to publish his results. At a later time we will evaluate his work and determine whether there are any further implications of interest to us in our DNA work.

3.6 References for Chapter 3

1. G. S. Edwards, C. C. Davis, J. D. Saffer, and M. L. Swicord, Phys. Rev. Lett. 53:1284 (1984).

2. G. S. Edwards, C. C. Davis, J. D. Saffer, and M. L. Swicord, Biophys. J. 47:799 (1985).

3. L. L. Van Zandt, Phys. Rev. Lett. 57:2085 (1986).

4. J. L. Sagripanti and M. L. Swicord, Int. J. Radiat. Biol. 50:47 (1986).

5. R. Heckler, M. Colpan, and D. Riesner, J. Chromatogr. 326:251 (1985).

6. M. Colpan and D. Riesner, J. Chromatogr. 296:339 (1984).

7. J. A. Thompson, Biochromatography 1:68(1986).

8. T. W. Athey, M. A. Stuchly and S. S. Stuchly, IEEE Trans. Microwave Theory Tech. MTT-30:82 (1982)

9. M. A. Stuchly, T. W. Athey, G. M. Samaras, and G. E. Taylor, IEEE Trans. Microwave Theory Tech. MTT-30:87 (1982).

10. M. A. Stuchly, M. M. Brady, S. S. Stuchly, and G. Gadja, IEEE Trans. Instrum. Meas. IM-31:116 (1982).

11. A. Stogryn, IEEE Trans. Microwave Theory Tech. MTT-19:733 (1971).

12. J. R. Mosig, J. C. E. Besson, M. Gex-Fabry, and F. E. Gardiol, IEEE Instrum. Meas. IM-30:46 (1981).

13. J. P. Grant, R. N. Clarke, G. T. Symm, and N. M. Spyrou, to be published.

3.7 List of Figures for Chapter 3

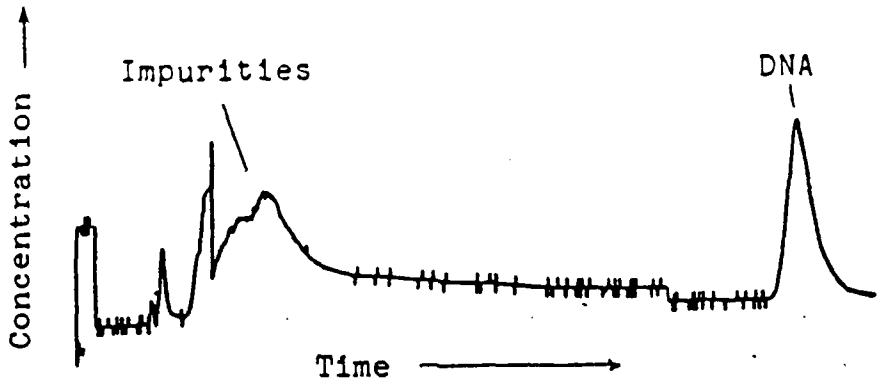

Fig. 1 HPLC trace of a moderately pure plasmid DNA sample.

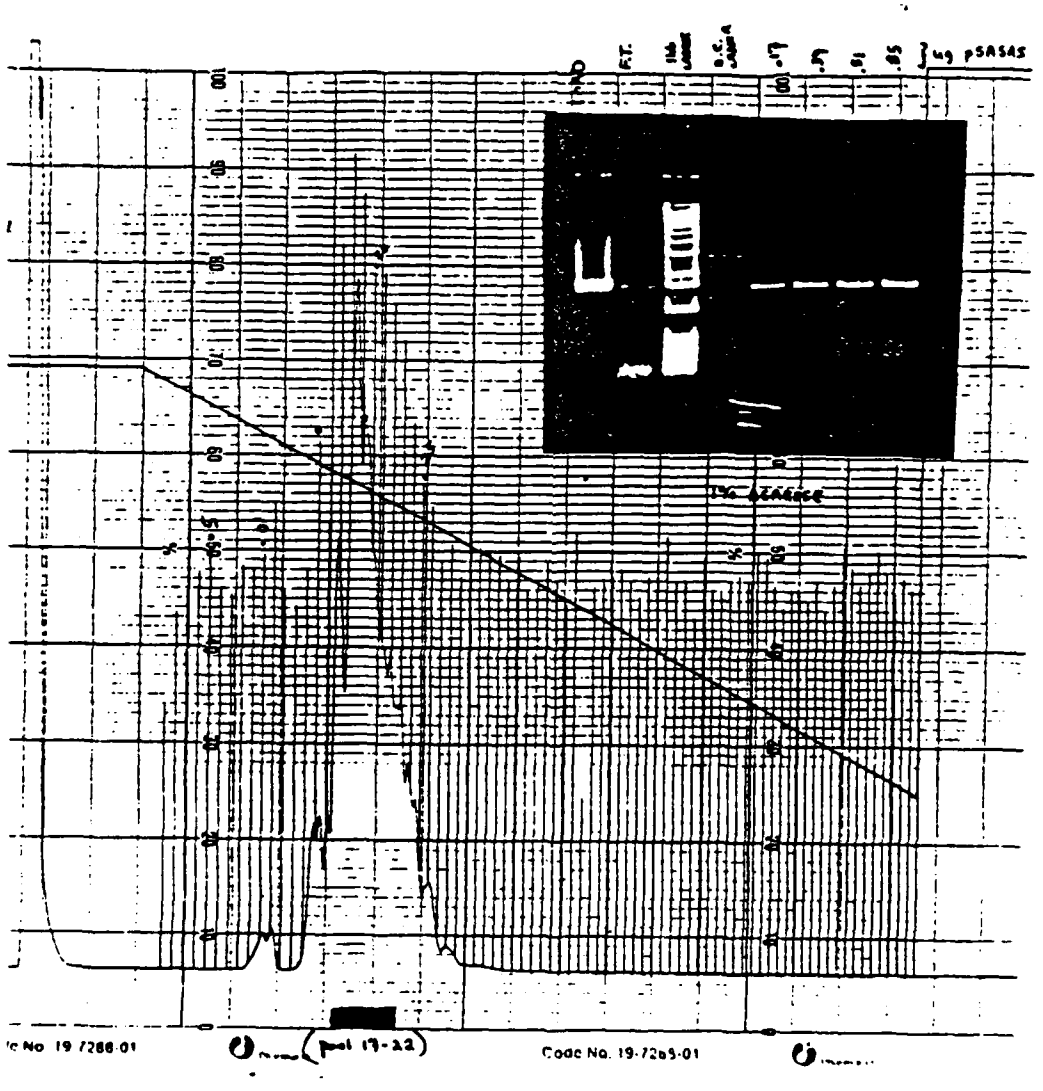

Fig. 2 HPLC trace of a 2668 bp plasmid DNA sample used in the reported absorption measurements. The area indicated as pool represents the collected sample. Also shown is an agarose gel trace showing the sample prior to purification, several calibration ladders, and traces of collected purified DNA.

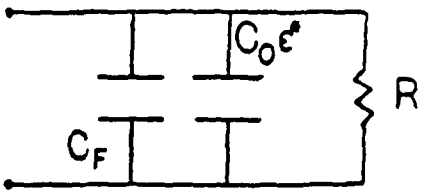

Fig. 3 Equivalent circuit of the open ended probe.

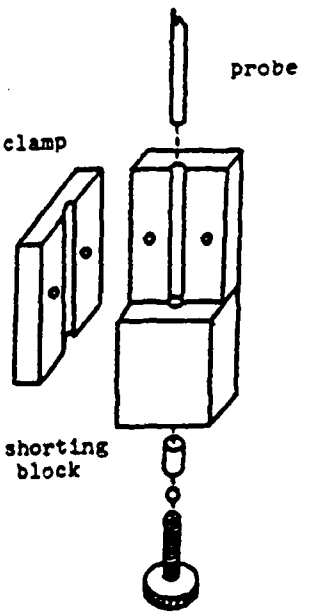

Fig. 4 Exploded view of shorting fixture.

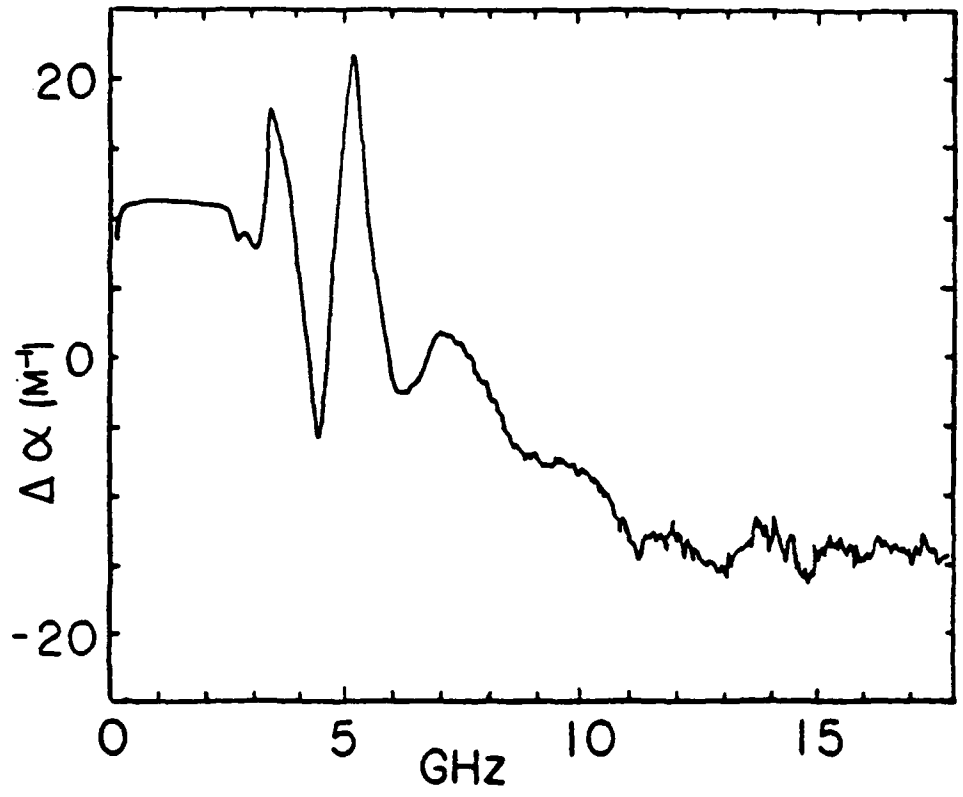

Fig. 5 Absorption difference between Linear DNA (0.53 mg/ml) and water

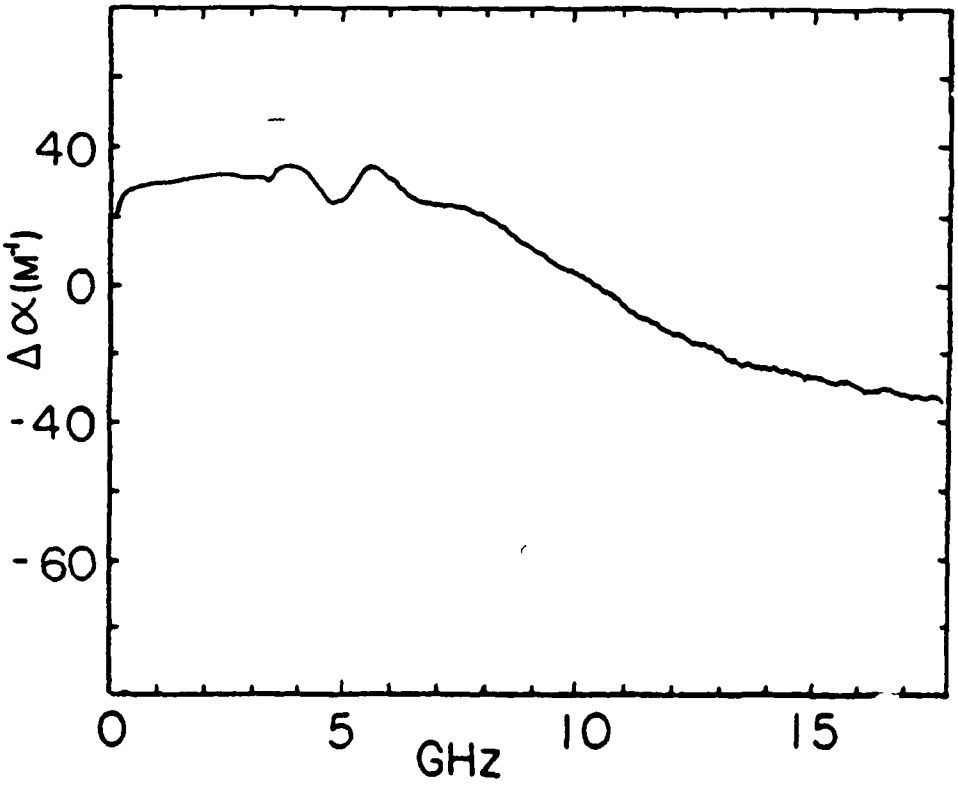

Fig. 6 Absorption difference between Supercoiled DNA (0.5 mg/ml) and storage buffer.

CHAPTER 4

THEORY OF ENHANCED MICROWAVE ABSORPTION OF DNA SOLUTIONS

C. Grosse

Data in the published literature have indicated that microwave absorption of solutions of E. coli DNA and DNase 1 was enhanced when the DNA was shortened by enzyme activity. The interpretation of these results was based on the assumption that DNA molecules could exhibit resonant type absorption whose amplitude and characteristic frequency depended upon chain length. This resonance based argument has been considerably weakened by our work (see Chapter 3) and other published work which have not been able to find any resonance associated with DNA microwave absorption. An important problem does remain unsolved. What is the origin of the enhanced absorption in the E. coli experiment? An often-used explanation is that bound water causes this effect. We consider this explanation below and show that it is inconsistent with the reported data.

Other reports in the literature have attempted to explain the absorption of DNA solutions as being due to the additional brought into the electrolyte buffer by the DNA. Such an interpretation implies that the absorption is only a function of the total number of ions in solution, and does not depend upon how they interact with the biologic species. Because our preliminary data in Chapter 3 does not agree with this hypothesis we have investigated this theoretically in our considerations below. Our results indicate a very important effect of the interaction of the ions with the DNA and suggest that the absorption per unit volume can be over 1000 times greater in the region of the DNA molecule than in the bulk buffer solution.

4.1 Introduction to the Effect of Bound State Water on Microwave Absorption of DNA Solutions

In 1982, Swicord and Davis published microwave absorption data of solutions of E. coli DNA and DNase 1. These measurements showed that the shortening of the DNA molecules due to the enzyme activity, was accompanied by an absorption enhancement which strongly increased in time.

These measurements stand out among other reports of enhanced absorption, in that they show changes occuring at a constant composition of the sample, rather than variations relative to the buffer. Therefore, any argument implying that the enhanced absorption is due to the extra ions added to the solution together with the DNA molecules, is automatically ruled out.

The interpretation of these results provided by the authors, was based on the assumption that DNA molecules could exhibit resonant type absorption with amplitude and characteristic frequency depending on the chain length. This argument was considerably weakened by the recent work of Foster (1987), which was not able to reproduce the resonant absorption data of Edwards (1984), using better experimental equipment.

Another possible explanation of the above results, is based on the assumption that the DNA molecules change the properties of the water surrounding the chains This assumption is supported by the fact that the reported change in the absorption at 10 GHz is of the order of 50%, while the weight fraction of DNA in the solution is of only 0.175%. This suggests that the reported effect is due to a change in the properties of a considerable volume of water, rather than to the tiny amount of DNA. We consider the feasibility of this in the next section.

4.2 Proposed Model For Effect of Bound State Water

We consider that a volume fraction v of the water in the system is "bound" to the DNA molecules. The rotational motion of these molecules is hindered by the interactions with the chain, so that the relaxation time of the "bound" water should be longer than that of normal water.

The absorption of the system is proportional to the total conductivity, which is due to the motion of ions and to the dipolar dispersion of the water molecules. This frequency dependent conductivity can be approximately written as:

$$\sigma(\omega) = \sigma(0) + \epsilon_0 \omega^2 G\left[\frac{(1-v)T_w}{1+\omega^2 T_w^2} + \frac{vT_b}{1+\omega^2 T_b^2}\right] \qquad (1)$$

where $\sigma(0)$ is the static ionic conductivity, ε_0 is the absolute permittivity of free space, w is the angular frequency of the applied field, G is the relaxation amplitude of water, τ_w is the relaxation time of free water, and τ_b is the relaxation time of "bound" water.

Due to the qualitative nature of this discussion, eq. (1) represents the simplest possible expression for the conductivity. The main approximations used in this equation are:

(1) The direct contribution to the absorption due to the DNA molecules is neglected. This is done in view of the very small volume fraction occupied by the DNA, and because the reported initial absorption of the suspension is almost indistinguishable from that of the saline buffer.

(2) The relaxation amplitude of the "bound" water is considered to be the same as that of the free water. This is the highest value which can be taken for this parameter, and it implies that one assumes no irrotationaly bound water to be present.

(3) The relaxation of the "bound" water is represented by a simple Debye term. A Cole-Cole expression would probably be more appropriate, but it would also require an extra unknown parameter, and would not change the final conclusions.

(4) The simplest mixture expression is used, which does not take into account the geometric arrangement of "bound" water surrounding the DNA strands. No suitable expression for this geometry is known, but results obtained with other geometries suggest that for low volume concentrations eq. (1) should provide a satisfactory approximation while slightly overestimating the total conductivity.

The behavior of eq. (1) is represented on Fig 1, which was plotted using the values $v = 0.3$, $\sigma(0) = 1$ S/m, and $G = 75$. This figure shows how the assumption that part of the water has a longer relaxation time broadens the conductivity spectrum, leading to an enhanced absorption over a limited frequency range.

4.3 Comparison With The Amplitude of the Absorption

The data presented by Swicord and Davis (1982), covers a narrow frequency range between 8 and 12 GHz. At 10 GHz, the amplitude of the absorption changes with time from 0.8 mm^{-1} to 1.2 mm^{-1}.

Since 10 GHz is just one half the relaxation frequency of free water, the expression for the conductivity at this frequency can be readily obtained from eq. (1):

$$\sigma(1/4\pi\tau_w) = \sigma(0) + \frac{G\epsilon_0}{\tau_w}\left[\frac{1 - v}{5} + \frac{k\,v}{4 + k^2}\right] \qquad (2)$$

where $k = \tau_b/\tau_w$.

The behavior of eq. (2) is represented in Fig 2. This figure shows the value of the quotient between the absorption (or conductivity) of the heterogeneous system composed of "bound" and free water, and the homogeneous system made up of just free water. The curves correspond to different values of the volume fraction v of free water, and are plotted as functions of the quotient of the two relaxation times. The maximum possible value of the enhancement was considered by taking the ionic contribution to the total conductivity $\sigma(0)$ in eq. (2) equal to zero.

Figure 2 shows that at any volume fraction, the enhancement of the absorption is a peaked function of k. The reason for this behavior can be seen from eq. (1): an increase in the value of τ_b not only shifts the conductivity spectrum of bound water to lower frequencies, but also decreases the amplitude of the conductivity increment.

The maximum enhancement is attained at $k = 2$, but the values obtained at any reasonable volume fraction v (Fig. 2) are insufficient to explain the 50% increase in the absorption reported by Swicord and Davis (1982).

4.4 Comparison With The Frequency Dependence of the Absorption

According to the reported data, the increase of the absorption with time is accompanied by an increase of the slope of the absorption vs. frequency curves. The slope changes from the initial value $1 \cdot 10^{-10}$ $mm^{-1} \cdot Hz^{-1}$, to $3 \cdot 10^{-10}$ $mm^{-1} \cdot Hz^{-1}$.

The value of the slope can be easily calculated from eq. (1). The result obtained for the frequency f = 10 GHz is:

$$\left.\frac{d\sigma}{df}\right|_{1/4\pi\tau_w} = 2\pi\epsilon_0 G \left[\frac{1 - v}{(1 + 1/4)^2} + \frac{k\, v}{(1 + k^2/4)^2} \right] \qquad (3)$$

The behavior of this expression is represented in Fig 3. This figure shows the quotient of the slope of the absorption curve for the heterogeneous system made of bound and free water, divided by the corresponding slope for the homogeneous system. The different curves correspond to different values of the volume concentration v, and are plotted as functions of the quotient of the relaxation times τ_b/τ_w.

It is apparent that at 10 GHz the slope of the heterogeneous system is smaller than for the homogeneous one, in total contradiction with the threefold increase of the slope reported by Swicord and Davis (1982). The decrease of both the slope and the amplitude of the conductivity curve at 10 GHz can also be seen in Fig. 1.

4.5 Conclusions Concerning Bound State Water

A comparison of figures 2 and 3 with the experimental data, shows that the assumption that the enhanced absorption of a DNA solution at 10 Ghz is due to "bound" water must be ruled out.

This conclusion is supported by two arguments:

(1) the maximum possible enhancement is not high enough, and

(2) the slope of the absorption curve should decrease while the absorption increases.

The first argument is all the more important since, in our calculation, all the approximations were such as to increase the absorption value. The second argument seems even more conclusive, in view of its qualitative nature.

4.6 Influence of the Distribution of Ions in the Electrolyte on the Microwave Absorption of DNA

Reports of the enhanced microwave absorption of DNA solutions have been often explained in the recent literature as being due to the additional ions brought into the electrolyte together with the DNA molecules. Such an interpretation implies

that the absorption is only a function of the total number of ions in the system, and does not depend neither on the way they interact with the biologic species, nor on the way they are distributed in space.

In what follows we examine this last assumption, and show that due to ion condensation, the absorption of a DNA solution should be always higher than the absorption of a sample in which the same number of ions were uniformly distributed.

4.7 Proposed Model of the Effect of the Distribution of Ions

For sake of simplicity, we shall first consider a suspension of spherical particles. While this geometry is not appropriate to represent DNA molecules, it is the only one for which complete analytical expressions for the absorption as a function of frequency can be derived. We then calculate the high frequency absorption of rod like particles, and show that the influence of the geometry is surprisingly small.

We consider a volume V of suspension, which contains a total number N of ions, and a volume fraction v of particles. The ions have charges +e or -e, and a mobility μ. Because of the charge of the particles, part of the ions are condensed on their surface, while the remaining ones are uniformly distributed throughout the electrolyte. We designate with p the fraction of condensed ions. The other parameters which characterize the system are the permittivity ε_m of the electrolyte, the permittivity ε_p of the particles, and their radius R.

The permittivities are assumed to be frequency independent, since all the relaxations to be considered occur at frequencies lower than 1 GHz. This assumption does not limit, however, the results to be obtained to low frequencies: at higher frequencies the absorption becomes frequency independent so that its value simply adds up to the absorption due to the frequency dependence of the permittivities of the components.

The conductivity of the electrolyte is determined by the fraction of non-condensed ions:

$$\sigma_m = \frac{(1-p)\, Ne\mu}{(1-v)V} = \sigma_0 \frac{(1-p)}{(1-v)} \qquad (4)$$

where σ_0 is the conductivity that the system would have if all the ions were distributed uniformly throughout its volume, and no particles were present.

At high frequencies, the condensed ions simply behave as a surface conductivity surrounding the particles:

$$\lambda = \frac{NepR\mu}{3Vv} = \sigma_0 \frac{pR}{3v} \qquad (5)$$

4.8 Frequency Dependent Conductivity of a Suspension of Charged Spherical Particles

We shall now write down the expressions for the conductivity of the suspension as a funcion of frequency, since the absorption of electromagnetic energy is proportional to the conductivity.

At high frequencies, this dependence is characterized by a low amplitude single time constant relaxation in the upper MHz range. For small volume fractions, the low frequency limit of this relaxation is:

$$\sigma = \sigma_m \left[1 + 3v \frac{2(\lambda/R) - \sigma_m}{2(\lambda/R) + 2\sigma_m} \right] \qquad (6)$$

while the conductivity increment and relaxation time are:

$$\Delta\sigma = \frac{9v\,[\epsilon_p\sigma_m - 2\epsilon_m(\lambda/R)]^2}{(\epsilon_p + 2\epsilon_m)^2\,(2\lambda/R + \sigma_m)} \qquad (7)$$

and

$$\tau = \frac{\epsilon_0\,(\epsilon_p + 2\epsilon_m)}{2\lambda/R + 2\sigma_m} \qquad (8)$$

where $\epsilon_0 = 8.85 \cdot 10^{-12}$ F·m^{-1} is the absolute permittivity of free space.

The dependence of the conductivity of the suspension on the fraction p of ions which are condensed on the surface of the particles is represented in Fig. 1. The curves were calculated maintaining constant the total number N of ions in the system. This number was determined assuming that the conductivity of the system without the particles but with all the ions is σ_0 = 0.01 S. The values used for the remaining parameters are: v = 0.01, ϵ_m = 80, and ϵ_p = 2.

It is apparent that the conductivity of the suspension strongly depends on how the ions are distributed. The condensation of ions decreases the conductivity at low frequencies, but increases it at high frequencies. Figure 1 shows that with reasonable values for the different parameters, the high

frequency absorption can be about 20% higher than what would be expected if the ions were uniformly distributed throughout the electrolyte.

For $\epsilon_m >> \epsilon_p$ and p different from zero, the limiting expression for the high frequency conductivity is approximately:

$$\sigma(\infty) = \sigma_0 (1 + p/2). \qquad (9)$$

4.9 High Frequency Conductivity of a Suspension of Rod-like Particles

The natural generalization of the model to the case of elongated particles consists in representing each particle surrounded by the layer of condensed ions with two confocal spheroids, since this is the only geometry for which Laplace's equation can be analytically solved.

In such a model, the distance from the inner to the outer boundaries of the volume containing the condensed ions is not constant. The ion layer is extremely thick on the equator of the elongated spheroid, and very thin on its poles, which is an unacceptable representation of the condensed ions on a charged rod like particle in electrolyte solution. Therefore, the above results for the frequency dependent conductivity cannot be simply extended to the case of elongated particles.

Nevertheless, the expression of the conductivity, valid only for high frequencies, can still be deduced. At high frequencies, the field distribution inside the system only depends on the permittivities, and is totally independent of the conductivities. Therefore, the fields can be calculated representing the particles by homogeneous prolate spheroids. The conductivity of the system is then deduced from these fields and the distribution of ions.

The result obtained for rod like particles is:

$$\sigma(\infty) = \sigma_m \left\{ 1 - \frac{v\,[5\epsilon_m\,(2\epsilon_p + \epsilon_m) - 3\epsilon_p^2]}{3(\epsilon_p + \epsilon_m)^2} + \frac{vW\,(\epsilon_p + 5\epsilon_m)}{3\,(\epsilon_p + \epsilon_m)} \right\} \qquad (10)$$

where

$$W = \frac{\lambda \times (\text{Surface area of spheroid})}{\sigma_m \times (\text{Volume of the spheroid})} = \frac{p\,(1-v)}{v\,(1-p)} \qquad (11)$$

For $\varepsilon_m >> \varepsilon_p$ and p different from zero, eq. (10) combined with eq. (4) leads to the following approximate result:

$$\sigma(\infty) = \sigma_0 \ (1 + 2p/3) \qquad (12)$$

When compared to eq. (9), this expression shows that for a given fraction p of condensed ions, the conductivity of the suspension is slightly higher for elongated particles than for spheres.

4.10 Conclusions Concerning Effect of Distribution of Ions in DNA Solutions

We have shown that due to the condensation of ions, the microwave absorption of a suspension of charged particles should be higher than what would be expected from the total number of ions in the sample. This enhancement depends weakly on the shape of the particles, and its magnitude can attain values of the order of 30%.

A direct consequence of this enhancement is that it further increases the inhomogeneous nature of the energy deposition. The first two terms in eq. (10) represent the contribution to the conductivity of the ions uniformly distributed in the electrolyte, while the last term corresponds to the ions condensed on the surface of the particles.

For $\varepsilon_m >> \varepsilon_p$, eq. (10) can be approximately written as:

$$\sigma(\infty) = \sigma_m \left[1 + \frac{5p}{3\,(1-p)} \right] \qquad (13)$$

This result shows that a fraction $5p/(3 + 2p)$ of the total energy absorbed by the system, is disipated in the volume occupied by the particles. For a value p = 3/8, half of the total absorption occurs on the particles, so that the absorption per unit volume on the particles exceeds by a factor 1/v the absorption per unit volume in the electrolyte. Thus for example for a DNA solution of 1 mg/ml of buffer solution the microwave absorption at 1 GHz in the region of the DNA molecule is over 1000 times greater than that in the buffer solution (including the absorption of the water molecules in the buffer).

4.11 List of Figures for Chapter 4

Figure 1

Comparison of the conductivity of a heterogeneous system composed of "bound" and free water, with the conductivity of pure water, according to eq (1). The parameters used are $v = 0.3$, $\sigma(0) = 1$ S/m, $G = 75$, $\tau_w = 8 \cdot 10^{-12}$ sec, and $\tau_b = 8 \cdot 10^{-11}$ sec.

Figure 2

Conductivity (or absorption) of a heterogeneous system composed of "bound" and free water, divided by the conductivity of pure water. The curves correspond to a frequency of 10 GHz, and were drawn as functions of the quotient of the relaxation times of "bound" and free water using eq. (2). The static conductivity $\sigma(0)$ was taken equal to zero, and different values of the volume fraction v of "bound" water were used.

Figure 3

Slope of the absorption versus frequency curve of a heterogeneous system composed of "bound" and free water, divided by the corresponding slope for pure water. The curves correspond to a frequency of 10 GHz, and were drawn as functions of the quotient of the relaxation times of "bound" and free water, using eq. (3). Different values of the volume fraction v of "bound" water were used.

Figure 4

Frequency dependence of the conductivity of a suspension of charged spherical particles in electrolyte solution. The curves correspond to different values of the fraction p of ions condensed on the surface of the particles. They were calculated from eqs. (6)-(8) maintaining constant the total number N of ions in the system. This number was determined assuming that its conductivity, without the particles but with all the ions, is $\sigma_0 = 0.01$ S/m. The values used for the remaining parameters are: $v = 0.01$, $\varepsilon_m = 80$, and $\varepsilon_p = 2$.

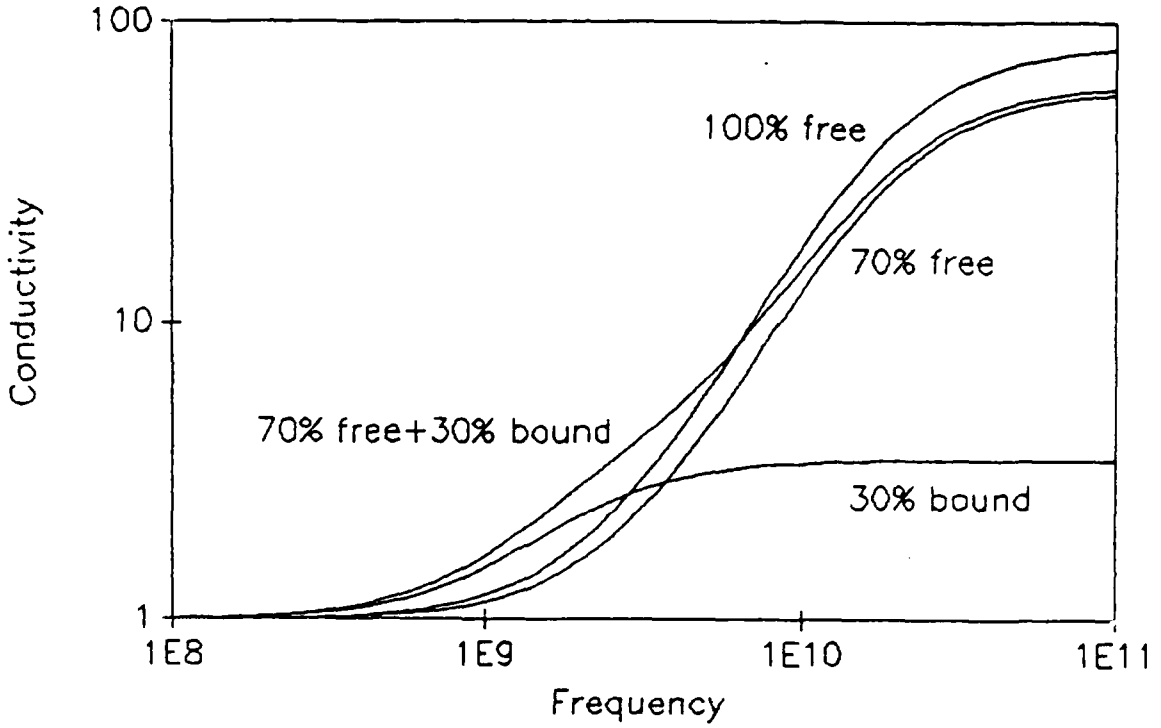

Figure 1. Comparison of the conductivity of a heterogeneous system composed of "bound" and free water, with the conductivity of pure water, according to eq. (1). The parameters used are $v = 0.3$, $\sigma(0) = 1$ S/m, $G = 75$, $\tau_w = 8 \cdot 10^{-12}$ sec, and $\tau_b = 8 \cdot 10^{-11}$ sec.

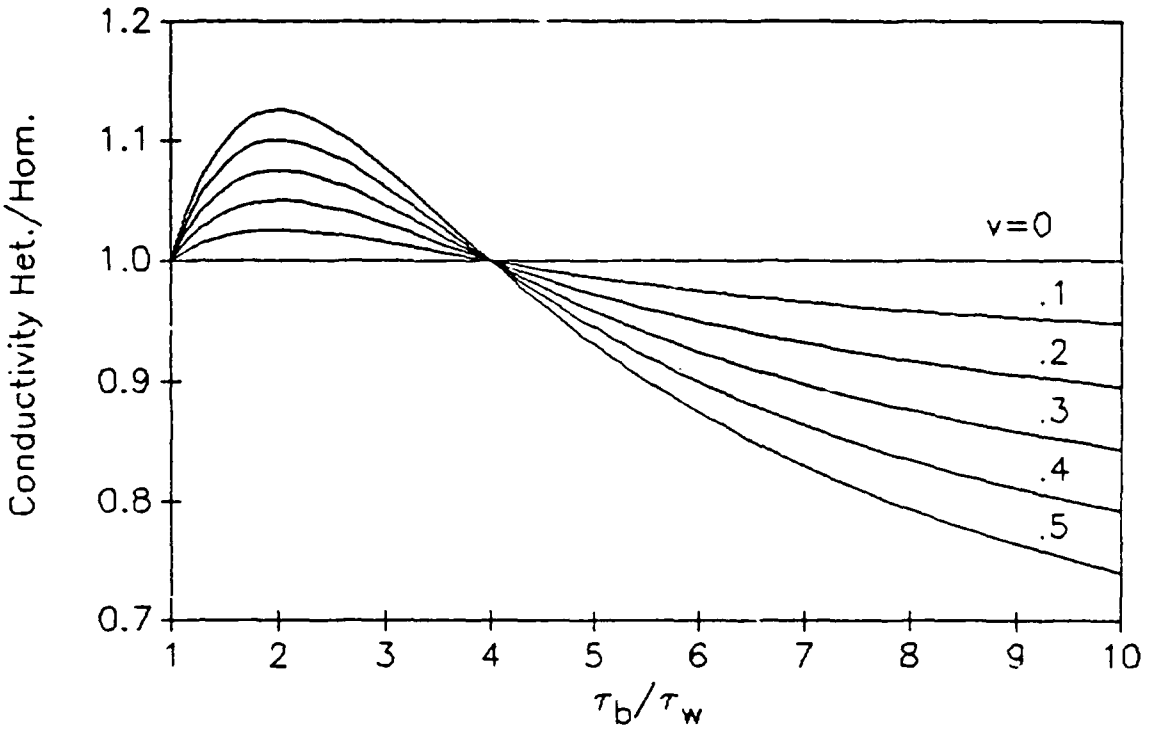

Figure 2. Conductivity (or absorption) of a heterogeneous system composed of "bound" and free water, divided by the conductivity of pure water. The curves correspond to a frequency of 10 GHz, and were drawn as functions of the quotient of the relaxation times of "bound" and free water using eq. (2). The static conductivity $\sigma(0)$ was taken equal to zero, and different values of the volume fraction v of "bound" water were used.

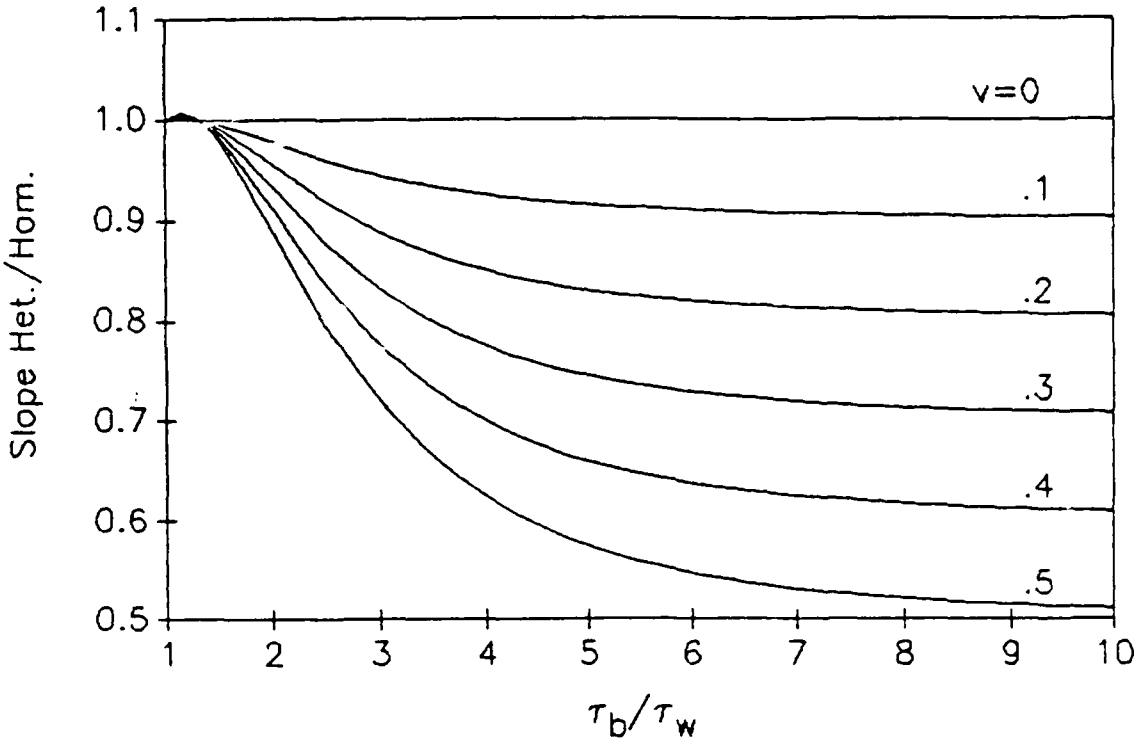

Figure 3. Slope of the absorption versus frequency curve of a heterogeneous system composed of "bound" and free water, divided by the corresponding slope for pure water. The curves correspond to a frequency of 10 GHz, and were drawn as functions of the quotient of the relaxation times of "bound" and free water, using eq. (3). Different values of the volume fraction v of "bound" water were used.

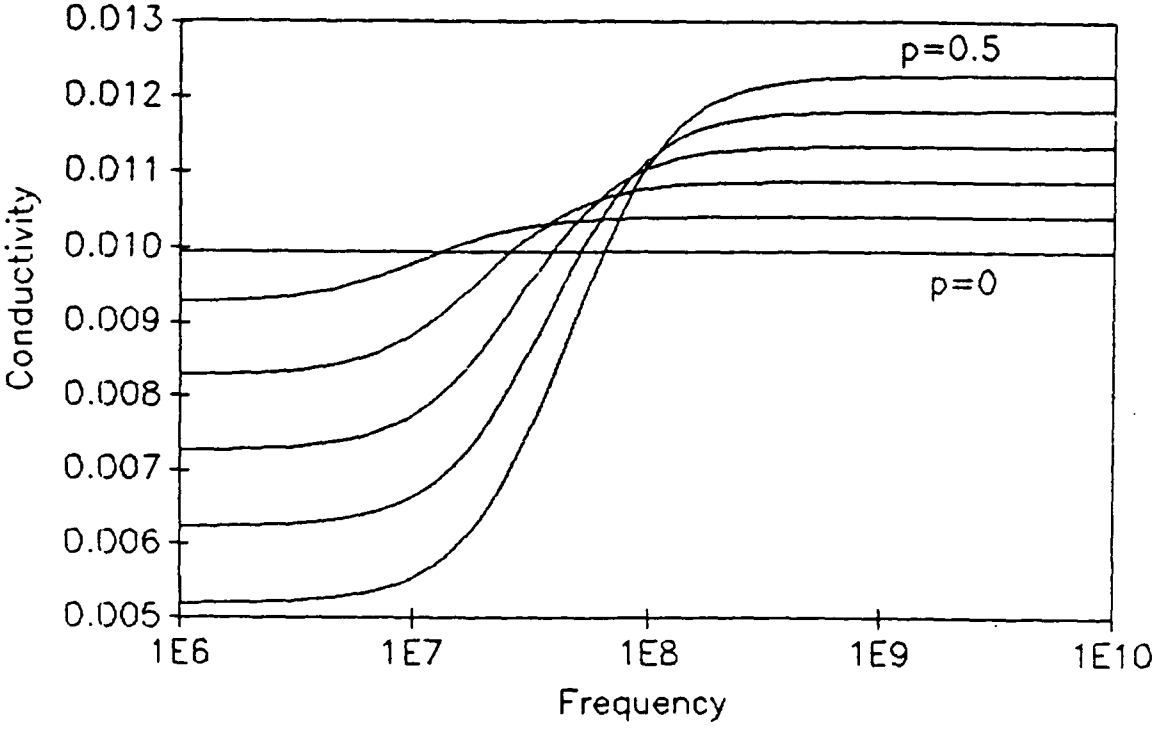

Figure 4. Frequency dependence of the conductivity of a suspension of charged spherical particles in electrolyte solution. The curves correspond to different values of the fraction p of ions condensed on the surface of the particles. They were calculated from eqs. (6)-(8) maintaining constant the total number N of ions in the system. This number was determined assuming that its conductivity, without the particles but with all the ions, is $\sigma_0 = 0.01$ S/m. The values used for the remaining parameters are: $v = 0.01$, $\varepsilon_m = 80$, and $\varepsilon_p = 2$.

CHAPTER 5

MOLECULAR DYNAMICS: THE RESPONSE OF A POLYMER ELECTROLYTE SOLUTION TO SUDDENLY IMPRESSED ELECTRIC FIELDS

J. F. Gumnick, Rocco Mennella and C. J. Montrose

There is a question as to whether there exists any direct, i.e., non-thermal, absorption of microwave energy by biological macromolecules such as DNA. We have hypothesized that such absorption can occur by the non-resonant excitation of internal modes of motion of the molecules through interaction with the field induced motion of counter ions in the immediate neighborhood of the molecule.

The aim of this project is to make use of Molecular Dynamics (MD) computer simulation "experiments" to test this hypothesis and thereby gain some insight into the nature of the response of a polymer electrolyte solution subjected to an external electric field.

To attempt to simulate the behavior of an ionic solution containing biological molecules is certainly beyond the scope of this work; however, testing the essence of the above hypothesis does not demand such a detailed mimicking of the situation. Rather by examining the behavior of the vibrational modes of an electrically charged short-chain polymer in an ionic solution following the sudden application of an electric field, it should be possible to establish whether these modes can be excited by coupling to the ionic atmosphere around the molecule. To ensure that any observed excitation of the molecular vibrations is not due simply to the modes re-equilibrating at a new higher temperature caused by heating the solvent with the ionic current, quasi-isothermal conditions are maintained by continually scaling the solvent atom velocities to maintain a constant total kinetic energy.

To date the results have not been conclusive. What has been established is that there is a coupling of energy between the field-driven motion in the ionic environment and the intramolecular vibrations. However it appears that under certain conditions the effect of the external field is to modify the ionic neighborhood of the polymer molecule such that the internal vibrational energy is actually decreased; under different conditions, the internal vibrations are enhanced.

5.1 INTRODUCTION

Molecular dynamics is a computer simulation technique in which one takes into account the many body nature of the microscopic dynamics by solving the classical equations of motion for the atoms of which a system is composed as a function of time (B. J. Alder and T. E. Wainwright, 1960; A. Rahman, 1964, 1966; L. Verlet 1967, 1968, 1970, 1973). One examines a system under certain given thermodynamic conditions (e.g., volume V, density N/V, total energy E), and assumes some model form(s) for the interactions (taken to be pairwise additive) among the atoms (whose masses are known) comprising the system. Using a finite difference stepwise procedure in which the system configuration (at time t) is updated to a subsequent instant (time t + δ)--in this work the Verlet algorithm was used--one obtains the positions and momenta of all the atoms in the system as a function of time. From this record of the system's path through phase space one can obtain--measure--all the system properties that are amenable to study in conventional experiments as well as many that are not generally accessible (Heyes et al., 1980, 1983). Indeed perhaps the best characterization of an MD simulation is that it is an experiment carried out numerically on a model system.

5.2 THE MODEL SYSTEM

The model system for the study consists of a solution of 894 spherically symmetric solvent atoms, 50 positively charged and 50 negatively charged ions, and a solute polymer in the form of a flexible six-atom chain. The ions and neutral atoms have the same mass and diameter, while the polymer atoms are eight times more massive and 1.5 times larger in diameter. All atoms in the solution interact via a Lennard-Jones 6-12 potential

$$\phi_{LJ}(r) = -4\epsilon\,[(l\sigma/r)^6 - (l\sigma/r)^{12}],$$

where ϵ and σ are parameters describing the strength and range of the interaction, respectively, and l is the arithmetic mean (in units of σ) of the diameters of the interacting particles.

In addition adjacent polymer atoms are bonded to one another via a harmonic potential of ten times the Lennard-Jones strength:

$$\phi_H(r) = -\epsilon_0 + \frac{1}{2} K (r - r_0)^2, \qquad |r-r_0|^2 < 2\epsilon_0/K$$

where ϵ_0 is the the well depth, here taken to be 10ϵ and r_0 is the Lennard-Jones minimum ($\approx 1.6837\ \sigma$). The force constant K was chosen to be $50{,}000\ \epsilon/\sigma^2$.

There is also a coulombic interaction between two polymer atoms, between two ions, and between a polymer atom and an ion given by

$$\phi_C = K' \frac{QQ'}{r^2},$$

where Q and Q' are the charges of the interacting particles (equal to ±1 for the ions and -2 for the polymer units) and K' (=2.5) is the constant of proportionality that fixes the strength of the electric interactions.

All the pair potentials and interparticle forces are truncated smoothly at $2.5l\sigma$. This is accomplished by adding the appropriate constants to the force and to the potential between an interacting pair to make that force vanish at this separation. The intraction potentials between polymer units and solvent atoms and ions is shown in Figure 1.

Each of the polymer units exerts an electrostatic attraction on the positively charged ions, such that a sheath of such ions can be expected to form around the polymer molecule. In the presence of an electric field these counter ions as well as the negatively charged ions will move so as to produce induced dipole moments.

The parameters characterizing the strength of the electrical interactions between the ions and the polymer units were selected using the following:

(1) The polymer-unit/positive-ion attraction from the combined electrostatic and LJ interactions should be about twice the attraction from the LJ force itself (Figure 1).

(2) There should be little interaction (other than an approximately soft-sphere repulsion) between the polymer units and the negative ions (Figure 1).

(3) The total effect of the attraction between polymer units and positive ions is to be such as to develop a cylindrical sheath around the elongated polymer. Figure 2 shows characteristics of the potential between the polymer molecule (in a linear and static configuration) and a neighboring positive ion. The upper curve shows the location (measured as a perpendicular distance from the polymer axis) of the equilibrium position for an ion "trapped" in this sheath. The horizontal axis is the position along the polymer with polymer atom 2 located at position 0.00 and polymer atom 3 at 1.658. This is of course repeated along the length of the polymer. The lower graph shows the actual depth of the attractive potential along this potential-minimum path. The minimum in this graph represents an equilibrium "ring" around the polymer axis halfway between two polymer atoms about one LJ distance unit from the axis.

The remaining things that must be given to complete the specification are the volume V occupied by the system, and its temperature T. The latter is determined by computing the average kinetic energy of an atom and equating this to 3kT/2. The volume was chosen to give a <u>density</u>

$N/V = 0.8442\ \sigma^{-3}$ (the triple point density of the solvent);

and the <u>temperature</u> was held fixed at

$T = 0.722\ \varepsilon/k$ (the triple point temperature of the solvent)

throughout the experiment.

To maintain a constant temperature, the total kinetic energy of the particles comprising the solvent was computed after each updating of the position coordinates. This was then compared with the "desired" value $3N'kT_0$, where N' is the number of solvent particles and T_0 is the desired temperature that one wishes to maintain. The individual particle velocities are then scaled by a factor

$$[T_0/T]^{1/2}$$

before updating to the next time instant. Thus energy is added or removed as required to maintain a constant temperature.

5.3 THE COMPUTER EXPERIMENTS

The solution of Newton's equations of motion to obtain the motion of the "molecules" in time was carried out using a MASSCOMP Model 515 Workstation (speed on the order of a VAX 750).

The major consumer of computer time is the computing of interparticle separations, r_{ij}, for the $\approx N^2/2$ pairs. Thus a major factor limiting the duration of a computation is the number of particles in the system. By maintaining a neighbor table (a list of which particles are in each atom's immediate vicinity) one can save some time since then the number of pairs to be considered is $nN/2$, where n is the average number of atoms in the neighborhood, say within $r \leq R_0$, of a given atom; the important point is that n does not depend upon N. Consequently, the computing time increases as N not as N^2. The neighborhood of a given atom was defined to be just slightly larger than the range of the interaction potential; specifically R_0 was taken to be $2.6\,\sigma$. The neighbor table in this work was updated every ten time steps.

For N=1000, it requires about 30 seconds per position-velocity update. With some allowance for overhead on the machine use (editing, file management and other housekeeping tasks), this amounts to about 2000-2500 updates per day. A "typical" run may require 20,000 or so time steps, and so may last for a week or two.

Once the phase space trajectory is known, one can compute the time dependence of any system property. For example the pressure p(t) is

$$p(t) = P\{\vec{r}_i(t), \vec{v}_i(t)\}$$

$$= (1/V)\left[\sum_{i=1}^{N}[m_i v_i^2 - \sum_{j=i+1}^{N} r_{ij}\,\partial\phi/\partial r_{ij}]\right]$$

as a function of time. From this one can determine the average pressure

$$\langle p\rangle = \frac{1}{M}\sum_{\alpha=1}^{M} p(t_0+\alpha\delta)$$

where t_0 is arbitrary. This gives the equation of state if one performs the computations for systems of varying N, V, and T.

One must also do something to minimize the effects of the boundaries. Because we are dealing with relatively small systems (in a macroscopic sense) the behavior is very strongly influenced by the boundaries of the system. For example in a 1000 atom liquid system, nearly 50% of the atoms lie within a molecular diameter of the boundaries. To minimize the artificial influence of rigid walls, we impose periodic boundary conditions on the system. The MD cell containing the system is a cube of side L ($L^3 = V$), and is assumed to be surrounded by identical replicas of itself.' Thus when a particle leaves, say, through the top of the cell, an image of this particle enters through the bottom. The mass, momentum and energy of the system are conserved.

The last important choice is that of the time step δ. Too large a choice will adversely affect the precision of the algorithm, while too small a choice will result in the consumption of inordinate amounts of computer time. The general rule of thumb is to choose a value of δ such that

distance an atom moves during one time step $\approx (kT/m)^{1/2}\,\delta \ll$ the length over which the potential varies significantly

That is

$$(kT/m)^{1/2}\delta \ll \left|\frac{\phi(r)}{\partial\phi/\partial r}\right|,$$

or

$$-\delta \ll (kT/m)^{-1/2}\left|\frac{\phi(r)}{\partial\phi/\partial r}\right|.$$

For the computations reported here, a step of 1/512 (in LJ units, see below) was used.

All computations are carried out in standard LJ reduced units in which the fundamental units are the atomic mass m (set equal to unity), the LJ energy parameter ϵ, and the LJ length parameter σ. All other units are derived from these. For example, the unit of time is

$$\tau_{LJ} = \sqrt{m\sigma^2/\epsilon}.$$

For reference purposes the characteristic relaxation times of microscopic processes *in the pure solvent* are of the order of 1 LJ unit. Typical vibrational periods of the polymer molecule range from about 0.02 to 0.2 LJ time units; microwave periods are on the order of about 100 LJ units. All quantities discussed in this report will be given in reduced LJ units unless otherwise stated.

Computer graphic codes were developed to enable visualization of the behavior of the polymer and the ions in the box. Elementary animation codes have been written that enable one to view the motion of the polymer and the ions as they move in response to the applied fields. The aim is simply to provide a pictorial representation of the molecular motions so that a "seat-of-the-pants" feeling for the system's dynamical evolution could be developed. It is anticipated that this will assist understanding and facilitate modeling of the motion of a polymer electrolyte and its associated counter-ion sheath.

5.4 RESULTS AND DISCUSSION

Initially an equilbrating run (with no external field on the system) was carried out to allow the system to come to equilibrium at the desired temperature and density. The run was of 15,360 time steps duration which corresponds to 30 reduced LJ time units. The momentum of the system and its average energy were monitored as a guide for determining when thermal equilibrium was achieved. In addition the energy in the polymer's internal degrees of freedom was monitored (as were a number of other system properties) to ensure that the system did not become "trapped" in some pathological metastable state of false equilibrium.

An initial preliminary "experiment" in which the system was exposed to a spatially uniform electric field abruptly switched on at "time equals zero" was carried out. The strength of the field was $E = 1$, so that the force exerted on an ion is roughly the same as that caused by a neighboring ion located at the LJ potential minimum. It corresponds to a field of approximately 2000 V/cm.

The momentum, energy and other system parameters were monitored to guarantee that the program was operating properly. At each time step in the system's evolution, the kinetic energy of the solvent atoms and ions was adjusted to maintain a constant temperature, thereby assuring that only athermal processes will be examined. The graphical display techniques noted above were employed to observe the system's dynamics, in particular, the relative motion of the positive and negative ions in the vicinity of the polymer and the electrophoretic drift of the polymer in the field as it is carried along by it sheath of counter ions.

Initial observations were made concerning the coupling of energy into the excitation of intramolecular vibrations. Within about 12 time units of the electric field being switched on, the average vibrational energy of the molecular bonds has apparently leveled off at a value slightly above the equilibrium value. Although the field is both uniform in space and constant in time, it leads to a flow of charge in the system that, while giving a

uniform and constant average current, exhibits variations in time on a localized scale. The fluctuations show aperiodic oscillations, but, although no detailed analysis of their Fourier spectrum was done, it seemed apparent that the variations contain non-zero components at frequencies in the neighborhood of the lower molecular vibration frequencies. Because of the strong forces that exist between the ions and the polymer units, coupling of this ionic translational energy with the molecular vibrational degrees of freedom should not be considered surprising.

Because these results were of a most preliminary sort, no conclusion as to a mechanism of direct, athermal coupling between a biological molecule and an externally impressed electric field could be reached.

It was decided to repeat the run using a larger electric field value (E = 2) to determine if the intramolecular excitation is enhanced under these more severe conditions. It was observed that there was an initial period during which the vibrational mode energy increased slightly by about the same amount as in the E=1 experiment. After a relatively long time at this energy, there then appeared to be a slight decrease in the excitation of the internal molecular vibrations. The actual data for the equilibrium and E=1 and E=2 experiments are presented in Tables 1 and 2 and are shown in Figure 3. The values presented in the tables for a given time instant t represent a local time average of the values computed for the interval t-1 to t+1; that is, for any property P(t), we report the local average (recall that there are 512 time steps per LJ time unit):

$$\langle P(t) \rangle = \frac{1}{1024} \sum_{\alpha=-511}^{512} P(t+\alpha\delta).$$

In the early studies just described, no restrictions were placed on the angle between adjacent bonds in the polymer molecule. The individual atoms thus enjoyed extraordinary freedom of movement. Especially in the presence of the impressed electric fields, the molecule tended to wrap itself rather tightly around one of the positively charged counter ions, and then to attract a roughly spherical sheath of additional positively charged ions around it. In this configuration the polymer was quite effectively shielded from further interactions with moving ions, the whole assembly simply moving electrophoretically in the impressed field.

To stiffen the polymer backbone so that the polymer will couple more realistically to ionic motions in the surrounding media, we have added a set of constraining forces to the molecule such that the angle between adjacent bonds is maintained. The angle θ_i formed by the bonds between the (i-1)th and the ith polymer atoms and between the ith and (i+1)th atoms is restricted to a narrow range about θ_0 (= 109.47°) by a harmonic potential

$$\phi_A(\theta_i) = \frac{1}{2} K (\theta_i - \theta_0)^2.$$

We have termed this a "shape-constrained polymer" in contrast to the previous unconstrained situation. It was anticipated that this modification would accelerate the exchange of energy between the internal vibrational modes of the polymer molecule and the field-induced dynamics of the surrounding medium. 'Indeed, while this is the case, the results are nevertheless quite surprising. The basic data are shown in Tables 3, 4 and 5.

Focusing on the data shown in Table 5 reveals the surprising observation that switching on the strength = 2 electric field results in a depletion of the molecular vibrational energy. After approximately 15 to 20 time units, both the longitudinal bond vibrational energy and the angular librational energy begin to fall, eventually (by approximately t ≈ 30) reaching steady state values slightly less than half of the equilibrium values. The results are plotted in Figure 4.

The results for the E=4 experiment (shown in Table 5) are plotted in Figure 5. These are more in keeping with one's intuition. There is an increase in the vibrational energy associated with the polymer bonds arising from the coupling of the field energy through the intermediary of the induced motion of the counter ions into the internal modes of the molecule. The increase is bond vibrational energy is nearly 30%, while there is a slight decrease (about 7%) in the librational energy. No obvious explanation of the very different behvior observed for the two different applied fields suggsts itself although there are some clues that are being explored.

In attempting to understand the circumstances that could lead to such differences in behavior we have focused on field-induced changes in the local environment of the polymer molecule. Again examining the data in Tables 4 and 5 it is apparent that the ionic constitution of the molecular environment is radicaly altered inthe strong field case. Indeed, as suggested by the trend toward nearly equal numbers of positive and negative ions in the vicinity of the molecule, it appears that the existence of the counter ion sheath is seriously threatened under very strong field conditions. The electrical attraction of the molecule for positive ions is apparently overwhelmed by the very strong force exerted by the external field. This field dependence of the excitation is to be investigated more fully.

5.5 SUMMARY

The possible existence of direct, non-thermal, absorption of microwave energy by biological macromolecules such as DNA has been investigated using molecular dynmaics computer simulations of the behavior of a short-chain electrically-charged linear polymer subjected to a suddenly applied electric field. We have hypothesized that such absorption could occur by the non-resonant excitation of internal modes of motion of the molecules through interaction with the field induced motion of counter ions in the immediate neighborhood of the molecule.

To date the results, although not conclusive, are highly suggestive. In the presence of the field, a coupling of energy between the field-driven motion in the ionic environment and the intramolecular vibrations is observed. At certaint field strengths, the internal vibrations are enhanced; however it appears that for other field strengths the effect of the external field is to modify the ionic neighborhood of the polymer molecule such that the internal vibrational energy is actually decreased. Further studies under a variety of field strengths and external conditions in which one measures the total energy deposited by the field in all the system's modes are required to clarify the situation.

5.6 REFERENCES FOR CHAPTER 5

Alder, B. J. and Wainwright, T. E. (1960), J. Chem. Phys. 33, 1439.

Heyes, D. M., Kim, J. J., Montrose, C.J. and Litovitz, T. A. (1980), J. Chem. Phys. 73, 3987.

Heyes, D. M., Montrose, C.J. and Litovitz, T. A. (1983), J. Chem. Soc. Faraday Trans. 2 79, 611.

Rahman, A. (1964), Phys. Rev. 136, A405.

Rahman, A. (1966), J. Chem. Phys. 45, 2585.

Verlet, L. (1967), Phys. Rev. 159, 98.

Verlet, L. (1968), Phys. Rev. 165, 201.

Verlet, L. and Levesque, D. (1970), Phys. Rev. A2, 2514.

Verlet, L. and Levesque, D. (1973), Phys. Rev. A7, 1690.

5.7 LIST OF TABLES FOR CHAPTER 5

5.8 LIST OF ILLUSTRATIONS FOR CHAPTER 5

Table 1. Summary of data for the system containing the flexible polymer molecule.

System Property	Electric Field Strength		
	E = 0	E = 1	E = 2
Time duration of the run	30.00	14.06	57.97
Pressure	1.56	1.59	1.57
Vibrational energy of the polymer bonds[1]	1.749	1.857	1.926
Electric current (along field)	0.05	4.64	9.78
Electric current ($\perp$ field)	0.81	0.84	0.76

[1] All data in this table are averages over the duration of the runs.

Table 2. Time dependent data for the experiments on the flexible polymer solution system.

	Electric Field = 1		Electric Field = 2	
Time	Vibrational Energy	Electrophoretic Velocity	Vibrational Energy	Electrophoretic Velocity
1	1.774	0.11	1.765	-0.08
3	1.815	0.13	1.766	0.02
5	1.857	0.06	1.819	-0.03
7	1.879	0.09	1.722	0.03
9	1.879	0.09	1.861	0.22
11	1.887	0.05	1.945	0.13
13	1.911	0.08	1.972	0.08
15			2.028	0.11
17			2.038	0.08
19			2.036	0.17
21			1.991	0.11
23			2.022	0.06
25			1.995	0.13
27			2.003	-0.01
29			1.987	0.23
31			1.969	0.09
33			1.987	0.21
35			2.022	0.15
37			1.971	0.09
39			1.943	0.11
41			1.874	0.11
43			1.803	0.04
45			1.789	0.13
47			1.878	0.19
49			1.928	0.24
51			1.899	0.17
53			1.908	0.19

Table 3. Summary of data for the system containing the shape-constrained polymer molecule.

System Property	Electric Field Strength		
	E = 0	E = 2	E = 4
Time duration of the run	30.00	39.14	24.38
Temperature of the polymer neighborhood[1]	0.729	0.722[2]	0.734[2]
Pressure	1.56	1.62[2]	1.64[2]
Vibrational energy of the polymer bonds	2.29	1.03[2]	2.92[2]
Librational energy of the polymer bonds	0.86	0.45[2]	0.80[2]
Total internal vibrational energy	3.15	1.48[2]	0.72[2]
Positive ions in the polymer neighborhood	19.6	22.5[2]	17.29[2]
Negative ions in the polymer neighborhood	15.6	16.0[2]	19.25[2]
Neutral atoms in the polymer neighborhood	260.8	258.6[2]	262.67[2]
Electric current (along field)	0.33	9.27	19.43
Electric current ($\perp$ field)	0.17	0.92	0.58

[1] The polymer neighborhood is defined as that region within a distance of 3.75 of the center of <u>any</u> polymer atom.

[2] This is the "long-time" steady-state average of the property. It is computed as the average over the final ten time units of the run.

Table 4. Time dependent data for the E = 2 experiments on the shape-constrained polymer solution system.

Time	Polymer Vibrational Energy			Polymer Neighborhood			Electrical
	Bond	Angle	Total	+ ions	- ions	Neutrals	Energy
1	2.199	0.864	3.063	21.22	17.48	262.43	-11.251
3	2.224	0.811	3.035	20.91	15.08	259.13	-11.123
5	2.139	0.789	2.928	20.85	14.96	256.51	-12.527
7	1.911	0.831	2.742	20.17	15.21	255.94	-12.376
9	2.015	0.768	2.783	20.68	15.45	258.66	-12.128
11	2.011	0.741	2.752	19.56	16.11	257.41	-10.918
13	1.879	0.839	2.718	21.14	16.49	254.76	-10.966
15	1.922	0.823	2.745	21.76	13.71	258.36	-8.499
17	1.672	0.971	2.643	21.05	12.79	253.73	-6.827
19	1.361	0.901	2.262	19.61	9.97	259.43	-6.751
21	1.276	0.809	2.085	18.12	11.11	254.14	-5.383
23	1.097	0.721	1.818	19.23	12.57	254.61	-5.846
25	1.009	0.545	1.554	21.53	14.49	256.78	-7.266
27	0.977	0.418	1.395	21.95	14.59	248.27	-8.617
29	1.029	0.432	1.461	22.11	12.84	248.49	-11.302
31	0.975	0.347	1.322	21.98	15.69	252.58	-11.889
33	1.026	0.372	1.398	23.71	16.91	255.51	-9.462
35	1.041	0.421	1.462	23.41	15.53	258.79	-7.813
37	1.039	0.388	1.427	21.59	15.24	262.29	-7.791
39	1.063	0.362	1.425	21.09	16.61	264.04	-10.424

Table 5. Time dependent data for the E = 4 experiments on the shape-constrained polymer solution system.

Time	Polymer Vibrational Energy			Polymer Neighborhood			Electrical
	Bond	Angle	Total	+ ions	- ions	Neutrals	Energy
1	2.211	0.881	3.092	21.31	16.44	259.99	-9.926
3	2.241	0.906	3.147	20.29	14.02	256.13	-8.541
5	2.401	0.928	3.329	21.59	16.59	263.44	-7.273
7	2.906	0.681	3.587	21.35	16.74	262.29	-3.781
9	2.766	0.739	3.505	21.78	16.71	262.47	-6.925
11	2.611	0.724	3.335	20.89	18.68	260.81	-5.547
13	2.629	0.735	3.364	19.46	17.27	268.89	-2.289
15	2.823	0.745	3.568	17.24	18.21	271.69	-0.973
17	2.938	0.774	3.712	17.14	18.27	264.62	-0.694
19	2.978	0.811	3.789	17.11	18.49	261.08	1.008
21	2.969	0.896	3.865	18.56	20.91	256.17	3.444
23	2.889	0.792	3.681	19.53	20.39	259.81	3.568

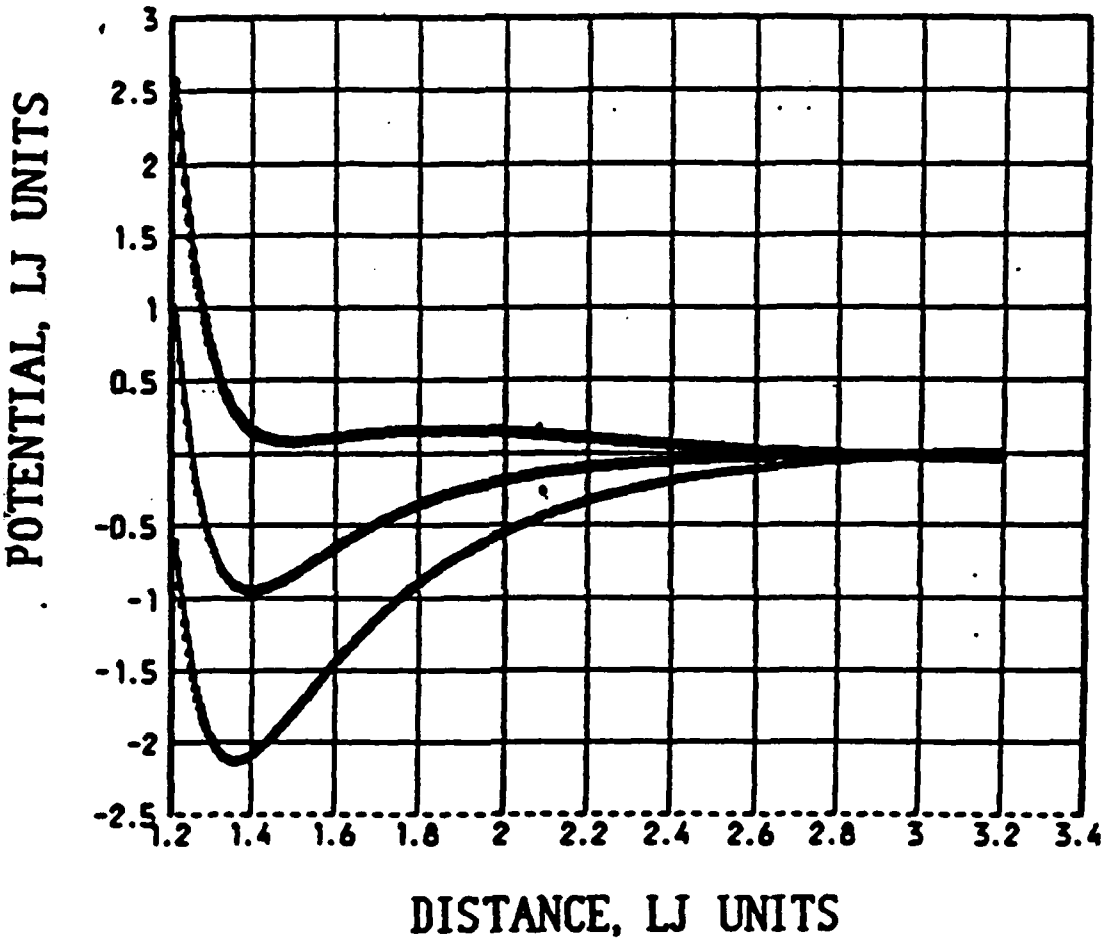

FIGURE 1. The pair interaction potentials between an atom in the polymer chain and a negatively charged ion (upper curve); a neutral solvent atom (middle curve); and a positively charged ion (lower curve).

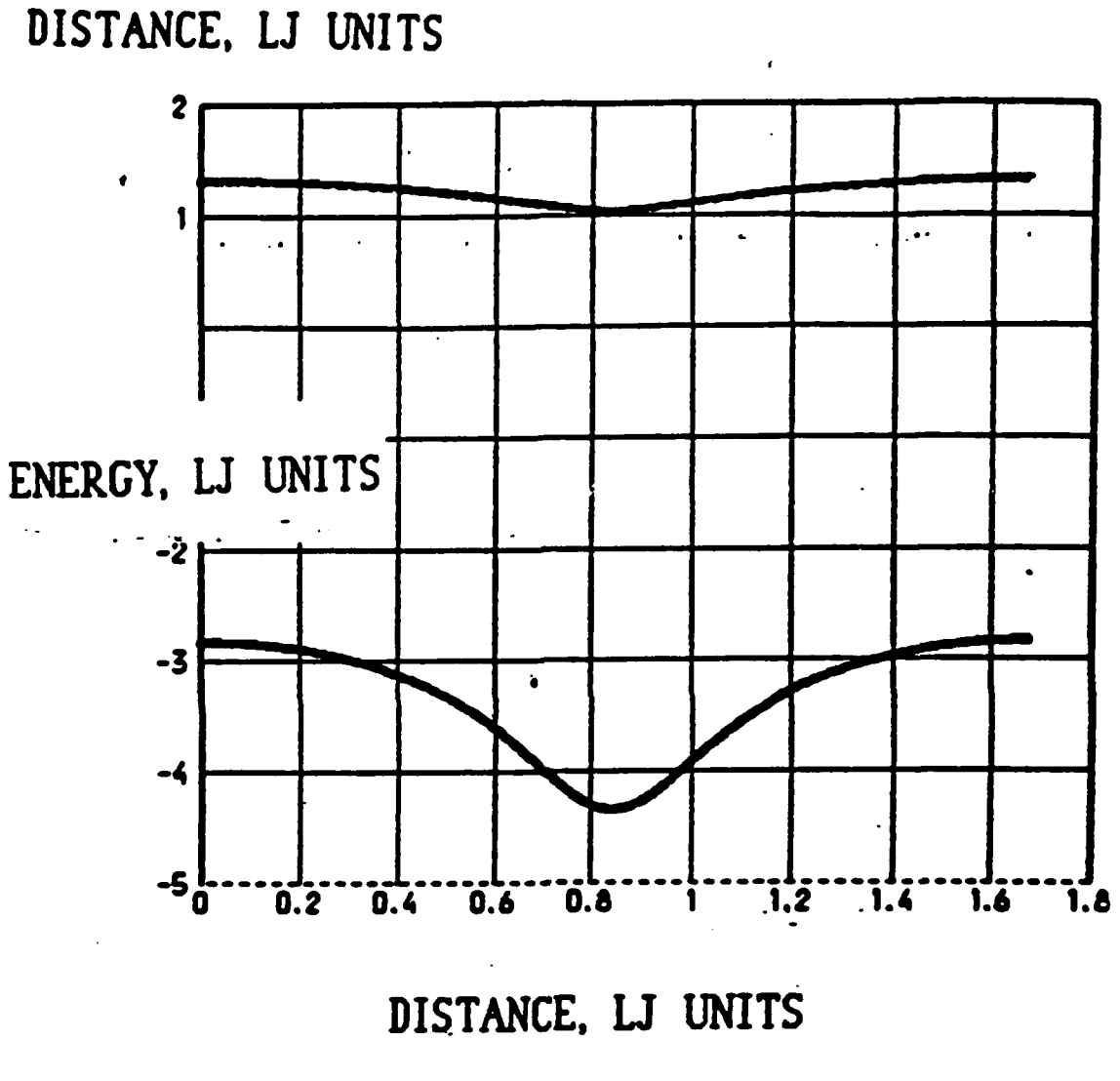

FIGURE 2. Location and depth of potential minima as a function of distance along the polymer axis. The upper curve give the locus of the minima measured as a perpendicular distance from the axis, while the lower curve give the depth of the minima.

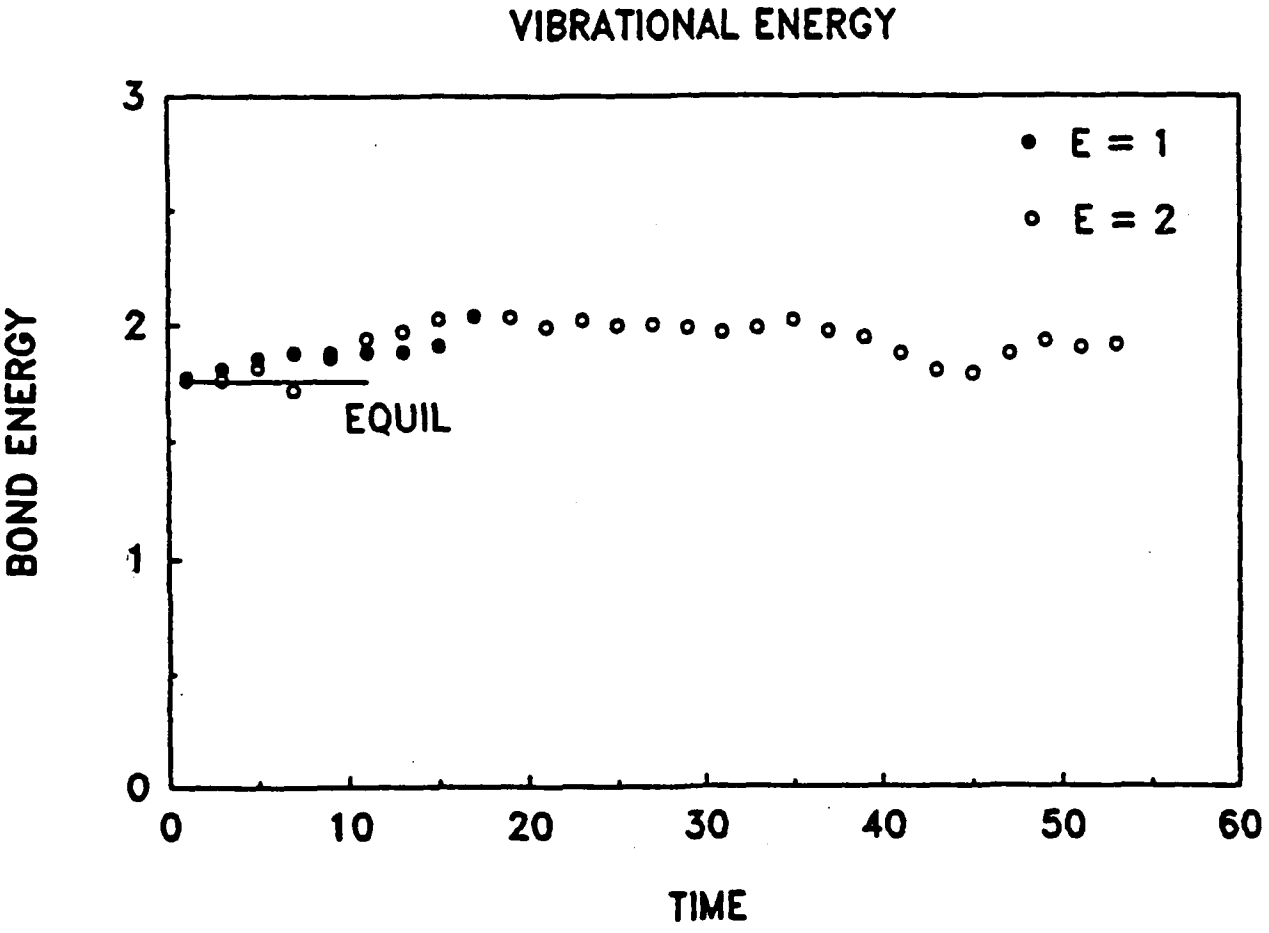

FIGURE 3. The time variation of the energy of the internal vibrational modes of the flexible polymer molecule following the switching on of an electric field at time t = 0.

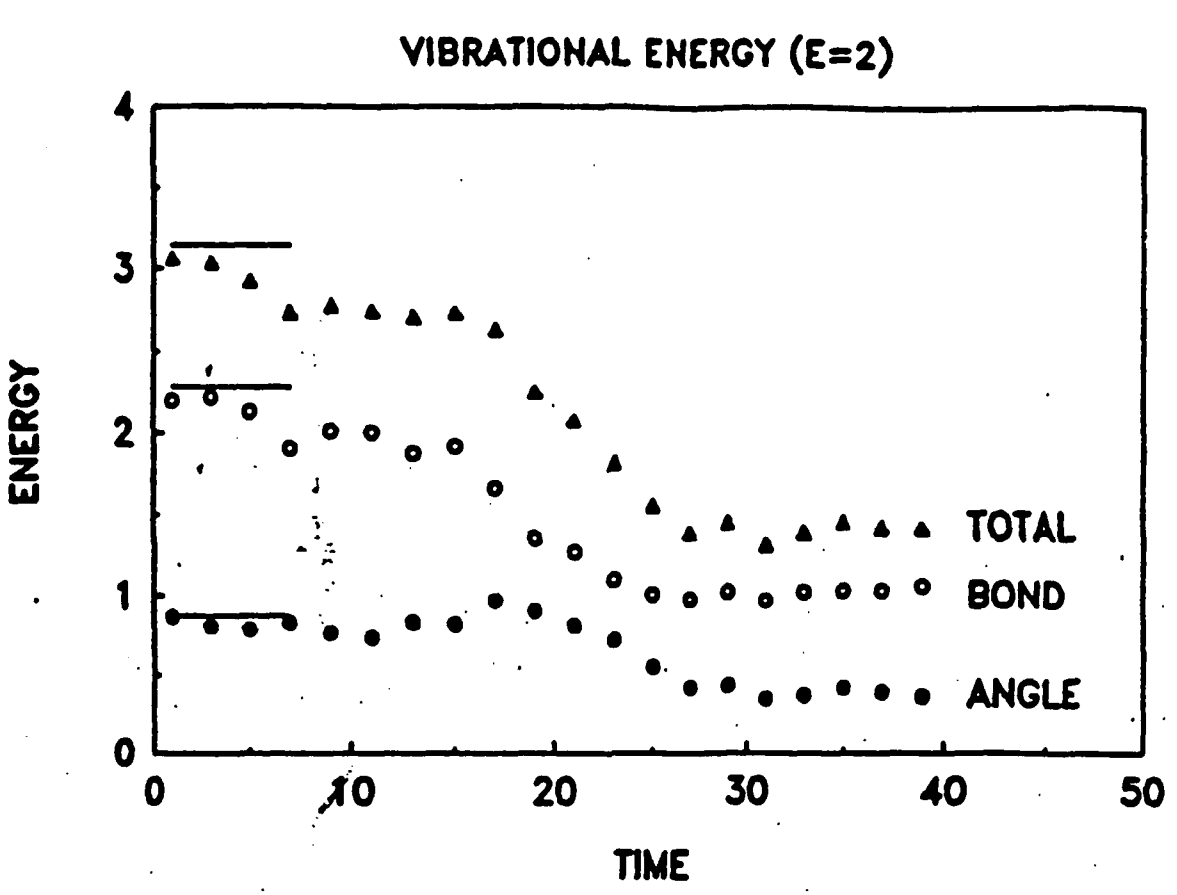

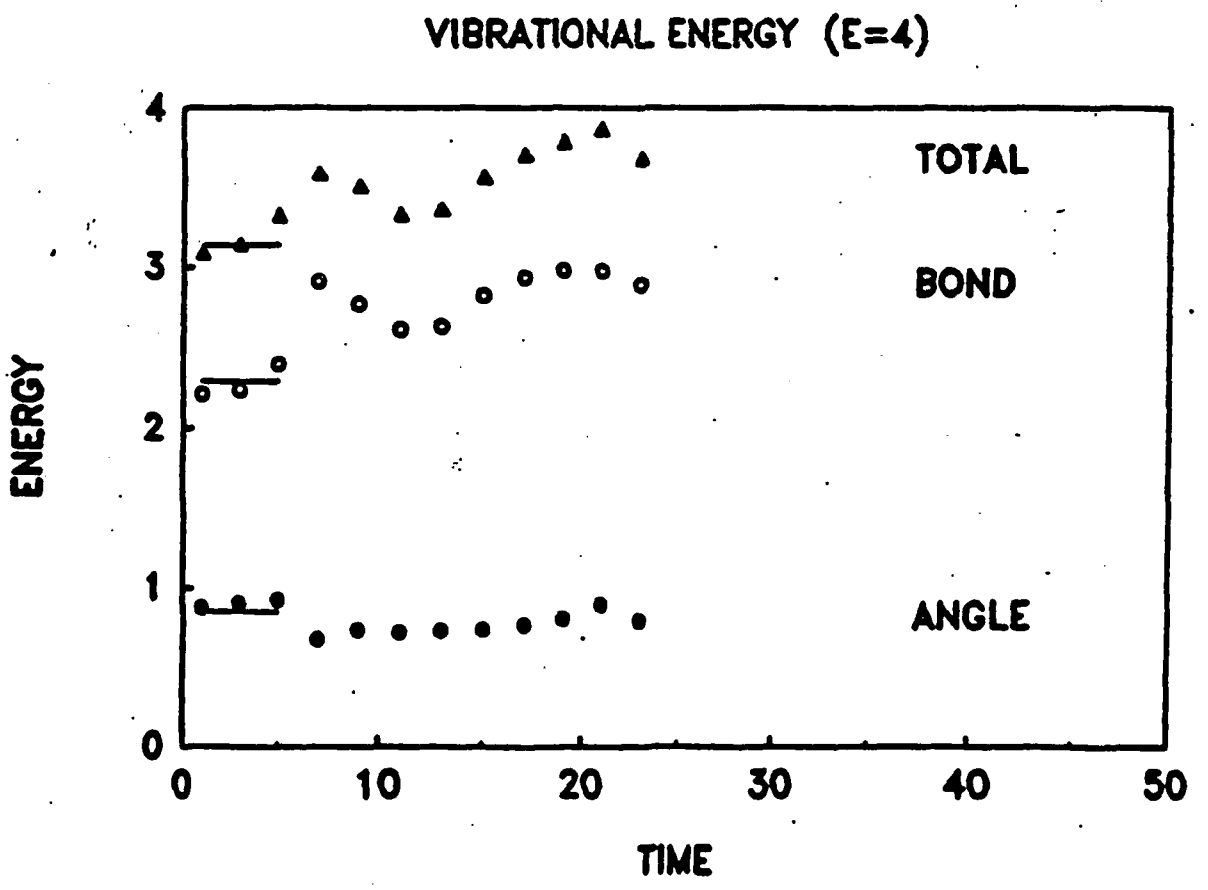

Figures 4 (top) and 5 (bottom). Time variation of the internal vibrational energy of the polymer molecule following the switching on of a field at time t = 0.